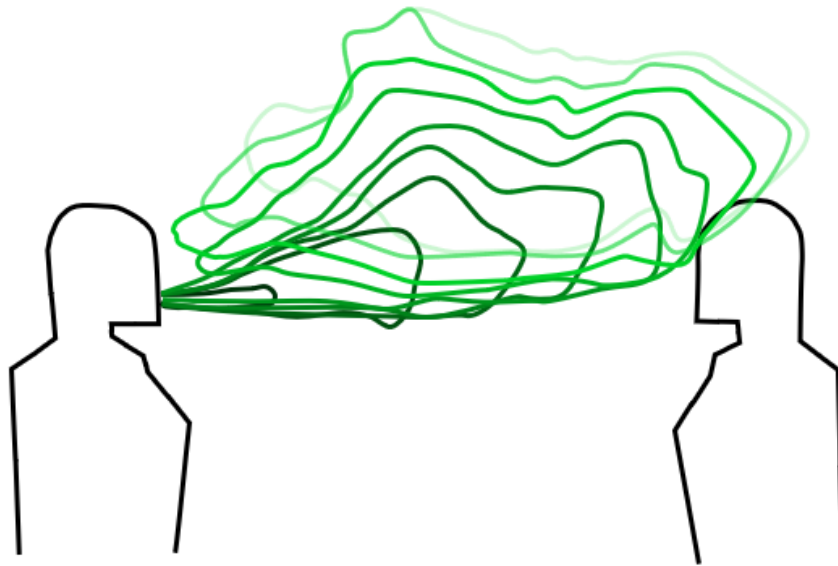


# Experimental investigation of cross infection risk in indoor environments for different respiratory activities

- Master Thesis -



Author:

Simon Madsen

Aalborg Universitet  
Build Department





**AALBORG UNIVERSITY**  
STUDENT REPORT

**Master thesis**  
v/ **Build Department**  
BUILD  
Thomas Manns Vej 23  
9220 Aalborg  
<https://www.build.aau.dk/>

**Title:**

Experimental investigation of cross infection risk in indoor environments for different respiratory activities

**Project:**

Master Thesis

**Projectperiod:**

September 2022 - June 2023

**Attendees:**

Simon Madsen

**Supervisors:**

Chen Zhang  
Peter V. Nielsen

**Number of pages: 115**

**Hand in June 9, 2023**

**Abstract:**

One way to access the cross-infection is the susceptible exposure index. Previous studies have found the susceptible exposure index in many scenarios for breathing and have investigated how different changes affected it. Few have found the exposure for other respiratory activities such as coughing however the comparison to breathing has never been made properly. The susceptible exposure index cannot be compared directly. What the exposure is for a cough and how it can be compared with other respiratory activities is the subject of this study. The exposure is measured for two different activities, breathing and coughing. A full-scale experiment is performed to determine the exposure. To create the necessary conditions thermal manikins are used to replicate a person to the highest possible degree and a machine that can reproduce a cough is designed. The machine was investigated and the cough it generated fitted the theoretical profile well. The exposure was then calculated using tracer gas measurement. It was found that the exposure for a cough remains high at great distances. Further, it was discovered that a comparison between the exposure was not proper and a weighted exposure was calculated instead.

*The content of the report is freely available, but publication (with source reference) may only take place in agreement with the authors.*



# Preface

---

This report has been written by a master thesis semester student of BUILD Department, Indoor Environmental and Energy Engineering. The project was written in the period September 2022 to June 2023.

## Reading Instructions

The main document contains the experimental study made based on the main research question. The main document includes an introduction to the main research question, the methodology, and the results of the experimental study. More information can be found in the appendixes. A scientific article has been made based on the literature review. The article has a separate introduction, conclusion, and bibliography.

References to sources will throughout the report be written with the Harvard method. The references are written in the report as [Last name, year] and refer to the bibliography. When books are referenced the bibliography list the author, title, publisher, edition, and publication year. If a webpage is referenced it will list the author, title, year, and when the webpage was last visited by the author of this master thesis.

Figures and tables are enumerated in relation to the belonging chapter and reading order and have an explaining text below for figures and above for tables. In the scientific article, the figures and tables are enumerated separately after the reading order.

In the report, thousand separators are given with commas, and decimals are divided by a dot.

Special thanks are given to the IV3-300 group, which helped with measurements of the breathing cases, data collection, and testing and calibration of some of the equipment. The group consists of Cille Boldsen Nedergaard, Daniel Dieter Pedersen, Iris Magna Hlynsdottir, Jeppe Høvring Broe, Jonas Lindegaard Mikkelsen, and Sofie Kjølby Niss.

A thanks should also be extended to Chen Zhang and Peter V. Nielsen, the supervisors for this master thesis for their guidance during the project period.

A thanks should also be given to Lars Isbach Poulson who helped in designing and creating the machine to simulate respiratory activities.



# Contents

---

<b>Preface</b>	<b>v</b>
0.1 Introduction . . . . .	1
0.2 Cross infection . . . . .	1
0.2.1 Purpose . . . . .	3
<b>1 Methodology</b>	<b>4</b>
1.1 Measurement plan . . . . .	4
1.2 Experimental setup . . . . .	6
1.2.1 Room setup . . . . .	6
1.2.2 Ventilation system . . . . .	6
1.2.3 Thermal manikins . . . . .	8
1.2.4 Machine for simulation of coughing . . . . .	11
1.3 Setup of sensors for measurements . . . . .	15
1.3.1 Setup of temperature measurements . . . . .	18
1.3.2 Setup of air velocity measurements . . . . .	18
1.3.3 Setup of tracer gas concentration measurements . . . . .	20
1.3.4 Setup of cameras . . . . .	22
<b>2 Results</b>	<b>23</b>
2.1 Breathing . . . . .	23
2.1.1 Conditions during experiment . . . . .	23
2.1.2 Results of smoke measurements . . . . .	25
2.1.3 Results of tracer gas measurements . . . . .	27
2.2 Coughing . . . . .	29
2.2.1 Conditions during experiment . . . . .	29
2.2.2 Results of tracer gas measurements . . . . .	31
2.3 Velocity profiles . . . . .	33
2.3.1 Results . . . . .	34
2.4 Comparison between coughing and breathing . . . . .	35
<b>3 Discussion</b>	<b>37</b>
3.1 Equipment . . . . .	37
3.2 Smoke measurements . . . . .	37
3.3 Conditions during measurement . . . . .	38
3.4 Measurement time . . . . .	38
3.5 Coughing machine . . . . .	39
3.6 Exposure for scenarios with combined respiratory activities . . . . .	39
<b>4 Conclusion</b>	<b>40</b>
<b>Bibliography</b>	<b>42</b>

<b>I</b>	<b>Appendiks</b>	<b>46</b>
<b>A</b>	<b>Scientific Article</b>	<b>48</b>
<b>B</b>	<b>Calculation of boundary conditions for target manikin</b>	<b>76</b>
B.1	Activity level . . . . .	76
B.2	Respiration . . . . .	76
B.3	Correction of manikin exhalation temperature . . . . .	77
B.4	Heat output by thermal manikins . . . . .	78
<b>C</b>	<b>Calibration of temperature sensors</b>	<b>80</b>
C.1	PT100 RTD . . . . .	80
C.1.1	Equipment . . . . .	80
C.1.2	Calibration setup . . . . .	81
C.1.3	Results . . . . .	82
C.1.4	Validation of calibration . . . . .	83
C.2	Thermocouples . . . . .	83
C.2.1	Equipment . . . . .	84
C.2.2	Calibration setup . . . . .	84
C.2.3	Results . . . . .	85
C.2.4	Validation of calibration . . . . .	87
<b>D</b>	<b>F200 Calibration</b>	<b>90</b>
<b>E</b>	<b>Calibration of anemometers</b>	<b>93</b>
E.1	Equipment . . . . .	93
E.2	Calculation of reference air velocity . . . . .	94
E.3	Calibration setup . . . . .	95
E.4	Results . . . . .	96
E.5	Validation . . . . .	97
<b>F</b>	<b>Calibration of tracer gas monitor and sampler</b>	<b>98</b>
F.1	Equipment . . . . .	98
F.2	Zero point calibration . . . . .	100
F.3	Humidity calibration . . . . .	101
F.4	Gas Span Calibration . . . . .	102
<b>G</b>	<b>Compensation for electrical noise generated by Air Handling Unit</b>	<b>104</b>
<b>H</b>	<b>Control of tracer gas concentration in initial cough</b>	<b>106</b>
H.1	Methodology . . . . .	106
H.2	Results . . . . .	107
<b>I</b>	<b>Control test of exhalation temperature</b>	<b>108</b>
I.1	Methodology . . . . .	108
I.2	Results . . . . .	108
<b>J</b>	<b>Technical drawing of coughing machine</b>	<b>110</b>

<b>K Determination of needed measurement period for stable results</b>	<b>114</b>
--	------------



## 0.1 Introduction

During the COVID-19 pandemic, the consequences of airborne disease that infect through airborne transmission became clear. WHO [2021] reported that by inhaling aerosols a person may become infected. The aerosols were found to be produced from the exhalation flow of an already infected source. The aerosols were produced when the source performed various different respiratory activities such as breathing, coughing, or sneezing[WHO, 2021]. The spreading of the disease often occurred in indoor settings and especially in poorly ventilated environments.

## 0.2 Cross infection

Airborne cross-infection has been shown to be a viable transmission path for respiratory viruses such as influenza and recently the COVID-19 (SARS-CoV-2) pandemic[Leung, 2021]. In indoor environments, the airborne transmission of diseases occurs by the generation of droplets and aerosols in an infected person. The droplets and aerosols are then transmitted from the infected subject to the room through the respiratory flow. Other occupants can then be exposed directly by inhalation of droplets or aerosols from the respiratory flow or indirectly by inhalation of the surrounding diluted air [Ai and Melikov, 2018] [Wang et al., 2021]. As we use more of our daily time indoors the importance of understanding the airborne transmission and ensuring good air quality is increased [Cao et al., 2014].

The respiratory flow comes from different respiration activities such as breathing, talking, or violent respiratory events such as coughing and sneezing, all of which can generate thousands of droplets of varying sizes[Duguid, 1946]. Larger droplets will be propelled by the respiratory flow and land on nearby surfaces, however, a majority of droplets will evaporate into aerosols due to evaporation. This evaporation occurs instantaneously for smaller particles with an initial diameter  $\leq 20 \mu\text{m}$ [Nicas et al., 2005]. The total amount of expelled droplets depends on various factors such as the type of respiratory event. Small particles, aerosols, and droplet nuclei weigh very little and can be carried by the air movement in the microenvironment and follow the paths illustrated in figure 0.1. The aerosols can also remain suspended in the air for up to 9 hours if not removed by ventilation posing significant infection risk [Ding et al., 2021].

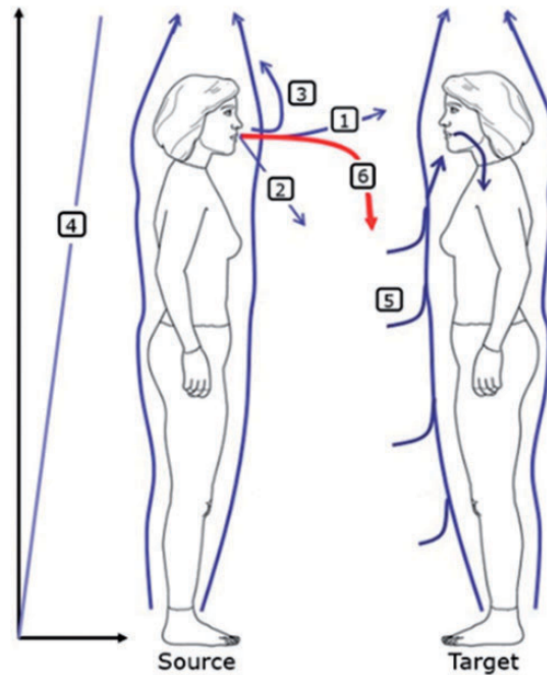


**Figure 0.1** Air paths in the microenvironment. 1 is the exhalation through the mouth, 2 is the exhalation flow through the nose, 3 is the exhalation flow that may occur due to the source's own convective boundary layer, 4 is the temperature gradient in the macro environment, 5 is the entrainment into the targets convective boundary layer and 6 is droplets affected by gravity. [Nielsen and Xu, 2021]

As shown by [Olemdo et al., 2012] factors such as ventilation strategies significantly influence the exposure from an infected person. The parameters influencing the exposure for breathing are summarized in [Nielsen and Xu, 2021] and shown below.

- Distances between persons
- Positions and orientation of persons
- Geometry of mouth and nose
- Breathing process (breathing through the mouth or nose)
- Movement
- Respiratory activity
- Number of persons
- Personal protection equipment (PPE)
- Temperature at face height
- Difference in height of persons
- Activity level of persons
- Virus concentration in surroundings
- Temperature and vertical temperature gradient in the microenvironment around the person
- Air velocity in the microenvironment around persons
- Turbulence level of the air flow in the microenvironment around persons

Coughing and sneezing are some of the most common symptoms of respiratory illnesses and pose a significant cross-infection risk [Leach, 2007]. This was also illustrated by the

COVID-19 pandemic where coughing was one symptom [WHO, 2021]. The conditions for the different respiratory activities have been researched extensively at the mouth and before for the infected person or source, however, how the aerosols move from the source to the target is not well researched and creates challenges when designing indoor environments while trying to reduce the cross-infection risk.

### 0.2.1 Purpose

As mentioned previously cross-infection for different respiratory activities poses challenges for designing indoor environments due to their differences. To identify the challenges with cross-infection in indoor environments a full-scale experiment is set up using thermal manikins and a machine for simulating different respiratory activities. Based on these factors the main research question becomes:

*How does coughing affect the cross-infection risk and how does it compare with the basic respiratory activity of breathing in an indoor environment.*

The research question is answered through a full-scale experiment comparing the respiratory activities of breathing and coughing. To successfully perform the experiment and comparison a series of sub-task arise which are listed below.

- Defining the boundary conditions for an indoor environment in a cross-infection scenario
- Defining boundary conditions for different respiratory activities
- Design of a machine to simulate respiratory activities accurately
  - Control and handling of the machine to provide representative data
  - Characterization of the flow generated by the machine and how it compares with theoretical and experimental data

The main research question and sub-task are answered through various means. A literature review of cross-infection in an indoor environment and boundary conditions for different respiratory activities. The design and characterization of the machine that produces a representative air flow through the use of velocity profiles to investigate the characteristics of the flow. The cross-infection is then evaluated by measuring the exposure for both breathing and coughing in different scenarios. During the measurements, the influence of the air distribution system, the distance, and the flow rate are investigated.

# Methodology 1

---

This chapter focuses on the procedure for the investigation of breathing and coughing as mentioned in the purpose of the report in section 0.2.1. The experiments are built up in different scenarios or cases regarding breathing and coughing where the main parameter investigated is how the exposure develops with regards to distance.

## 1.1 Measurement plan

The measurements are divided into different cases. Two cases are made into breathing in both displacement and mixing ventilation. The measurements from these cases are made by Nedergaard et al. [2022] under the supervision, guidance, and cooperation of the author. They were also involved in the calibration of some of the equipment namely the anemometers. Nedergaard et al. [2022] are not involved in any further measurements.

The goal of the measurements is to investigate the problem given in section 0.2.1. The exposure risk is evaluated based on the susceptible exposure index defined by both Qian and Li [2010] and Liu et al. [2017]. The susceptible exposure index is calculated using equation (1.1).

$$\epsilon_n = \frac{c_n - c_i}{c_r - c_i} \quad (1.1)$$

$\epsilon_n$	Exposure at location n	[-]
$c_n$	Tracer gas concentration at location n	[ppm]
$c_i$	Tracer gas concentration in room ventilation inlet	[ppm]
$c_r$	Tracer gas concentration in room return/exhaust	[ppm]

The cases investigated are shown in table 1.1 with the relevant boundary conditions. Some of the cases are not only tracer gas measurements as smoke measurements were performed in cooperation with the IV group. Furthermore, velocity profiles for the coughing machine are investigated to give an indication of whether the flow type is different compared with breathing.

**Table 1.1** Measurement plan where AC = Air Change Rate,  $T_s$  = Supply temperature,  $T_e$  = Exhalation Temperature, Q = Flow rate, H = Heat production and D = Distance.

Case	Type	Respiratory		Ventilation			Source			Target			D [m]
		activity	Type	AC [ $\text{h}^{-1}$ ]	T [°C]	Q [ $\text{l/s}$ ]	T [°C]	H [W]	Q [ $\text{l/s}$ ]	T [°C]	H [W]		
1	Smoke	Breathing	MV	5.6	20	1.15	37.5	37.3	1.15	37.5	37.3	0.35 & 1	
2	Smoke	Breathing	DV	5.6	16	1.15	37.5	37.3	1.15	37.5	37.3	0.35 & 1	
3	Tracer	Breathing	MV	5.6	20	1.15	37.5	37.3	1.15	37.5	37.3	0.35 & 1	
4	Tracer	Breathing	DV	5.6	16	1.15	37.5	37.3	1.15	37.5	37.3	0.35 & 1	
5	Tracer	Coughing	MV	5.6	20	6.95	20	-	0.58	34	77.8	0.35, 1, 1.5 & 2	
6	Tracer	Coughing	MV	5.6	20	4.68	20	-	0.58	34	77.8	0.35, 1, 1.5 & 2	
7	Velocity	Coughing	MV	-	-	6.95	20	-	-	-	-	0.35, 0.8, 1, 1.25 & 2	

## 1.2 Experimental setup

This section will revolve around the experimental setup with regard to targeted boundary conditions, sensors, and the coughing machine. The setup is generally the same between the coughing cases and the cases made by Nedergaard et al. [2022], however, corrections have been made for more accurate measurements and conformity with Zhang et al. [2022].

### 1.2.1 Room setup

A full-scale setup is used for the measurements in this project. The room is in accordance with the International Energy Agency Annex 20 which is used as a benchmark [Chen et al., 1993]. The test room has the dimensions 4.2 m, 3.6 m, and 2.5 m for the length (North-South), width (East-West), and height respectively. The room and the placement of the manikin, inlet, return/exhaust, and the coughing machine are all shown in figure 1.1. The setup is slightly changed when the distance between the coughing machine and the target manikin is greater than 1.2 m. In cases with a distance greater than 1.2 m symmetry around the inlet cannot be achieved with the shown setup. Therefore the manikin and coughing machine are moved to stand diagonally in the room to ensure symmetry. This will create asymmetry with regard to the return/exhaust. The coughing machine is placed the furthest away from the return/exhaust in those cases.

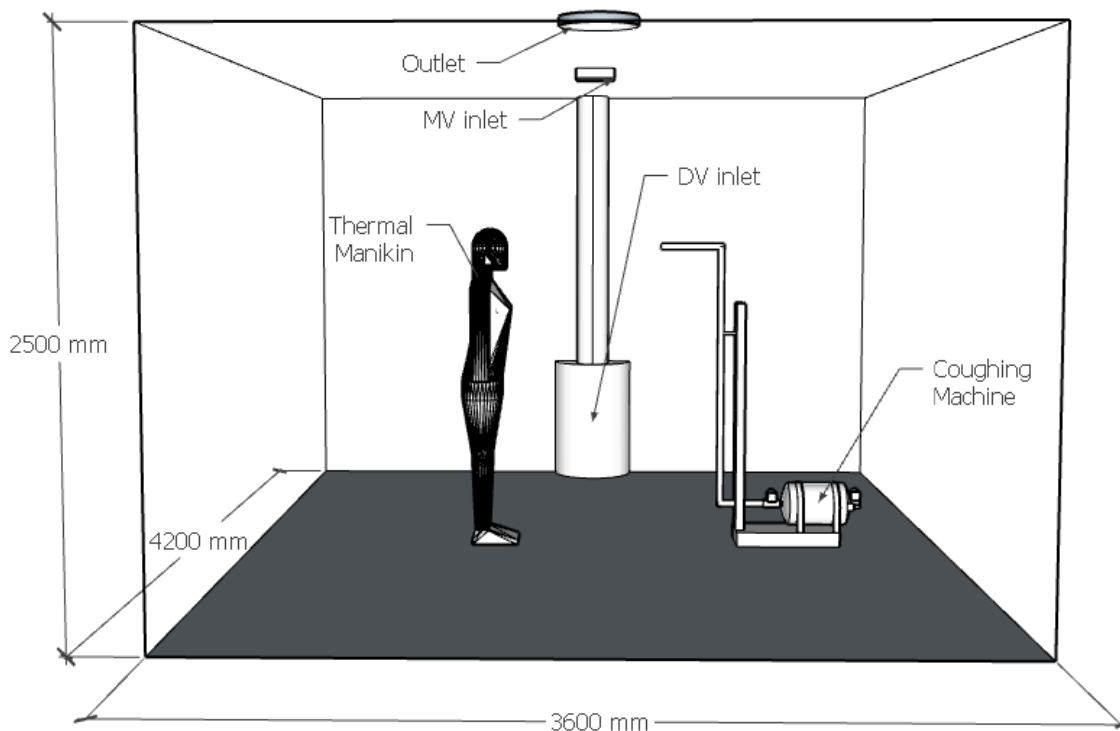


Figure 1.1 3d model of the test room.

### 1.2.2 Ventilation system

The ventilation system plays an integral role in cross-contamination. The test room can be supplied using both mixing ventilation (MV) and displacement ventilation (DV). For

each system, a different diffuser is used. For mixing ventilation a ceiling-mounted swirl diffuser. It is mounted on the ceiling in the middle of the room. The diffuser can be seen in figure 1.2. For displacement ventilation, a wall-mounted 180° semicircular diffuser is used. The diffuser is shown in figure 1.3 and is on the southern wall located opposite the exhaust.



**Figure 1.2** Inlet diffuser for mixing ventilation



**Figure 1.3** Inlet diffuser for displacement ventilation

The return/exhaust location is shown previously in figure 1.1. The return is ceiling mounted in the middle of the northern end of the test room. It is an open ventilation duct with a diameter of 0.16 m. The return is powered by a movable fan placed outside the test room. The fan has a flow of 212 m<sup>3</sup>/h. The return is shown in figure 1.4. The flow is measured by a Lindab UltraLink flow meter which can be seen in figure 1.5.



**Figure 1.4** Return/Exhaust



**Figure 1.5** Flow meter used for both return and AHU.

The system is supplied by an air handling unit (AHU) placed on top of the test room. To avoid fluctuations in temperature the intake air is from the laboratory which then can be cooled in the AHU if needed. The AHU supplies the room with 212 m<sup>3</sup>/h and the ventilation is balanced and measured by a Lindab UltraLink flow meter. The corresponding air change rate in the room is 5.6 h<sup>-1</sup>. The air change rate is selected for conformity with previous studies. The AHU can be seen in figure 1.6



**Figure 1.6** AHU used for ventilation of the room. The intake is under the AHU on the right side.

The temperature of the air supplied by the AHU is normal room temperature unless displacement ventilation is used. The only sources for changes in the room temperature during measurement are the exhalation of the target manikin, the body surface temperature of the manikin, the temperature of flow from the coughing machine, and heat released by the valves on the coughing machine. The temperature of the airflow from the coughing machine is affected by the temperature of the supplied pressurized gas, however, due to non-insulated tubing in plastic materials it is assumed it reaches room conditions, and temperature changes of the supplied tracer gas due to  $\text{CO}_2$  cooling during measurement when moving to a lower pressure.

### 1.2.3 Thermal manikins

This section will describe the thermal manikin both for breathing cases as well as for coughing. A thermal manikin is used to give as realistic conditions as possible for the experiment. The complicated interactions between the human body and the surroundings call for more realistic conditions instead of a simple jet from a hose or pipe [Bjørn, 2000].

#### Geometry

During the measurements, one manikin is used as the target. The manikin has a height of 1.68 m and a body surface area of  $1.44\text{m}^2$ . The torso of the manikins can be heated up. The torso is supplied with a heating element and a fan to distribute the heat within the manikin. The manikin has a circular mouth opening with a diameter of 12 mm and the height to the middle of the mouth is 1.53 m. The manikin has a nose with two nostrils with a diameter of 12 mm each. The nose consists of a singular tube supplying air to a nasal cavity which has two holes. The intervening angle of the nose is  $30^\circ$ . The manikin's geometry can be seen in figure 1.7. The manikin's face can be seen in figure 1.8.

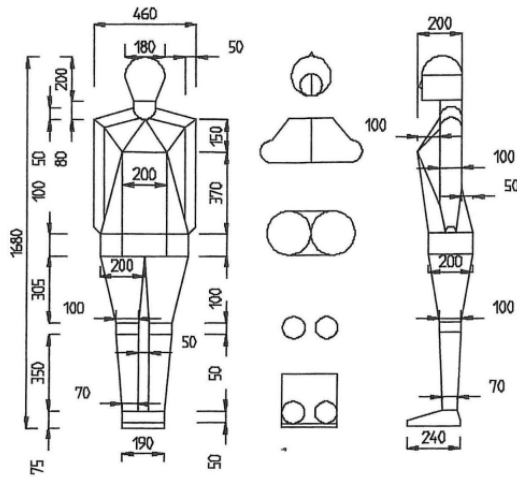


**Figure 1.7** Geometry of the manikin [Bjørn, 2000].



**Figure 1.8** Face of the manikin.

## Respiration

The boundary conditions for the manikin are calculated in appendix B for the coughing cases. The boundary conditions included are activity level, respiration, exhalation temperature, and heat loss. The respiration of the manikin is based on previous studies by Zhang et al. [2022] and ASHRAE [2009]. In appendix B the boundary conditions for the manikin's respiration have been calculated based upon an activity level of 1.4 met corresponding to standing [Hyldgard et al., 1997]. The boundary conditions for the manikin for the coughing cases are shown in table 1.2. The breathing profile is shown for the target manikin during coughing and both manikins during breathing.

**Table 1.2** Boundary conditions for thermal manikin for coughing cases

Parameter	Target manikin
Activity level [met]	1.4
Exhalation flow [l/min]	10.54
Breathing frequency [ $\text{min}^{-1}$ ]	16
Exhalation temperature [ $^{\circ}\text{C}$ ]	34

The setup for delivery of tracer gas to the coughing machine is shown in figure 1.9. The tracer gas is supplied directly into the pressure tank with a flow rate of 6 l/min. The resulting concentration is approximately 73,000 ppm. The test for control of the concentration is in appendix H.

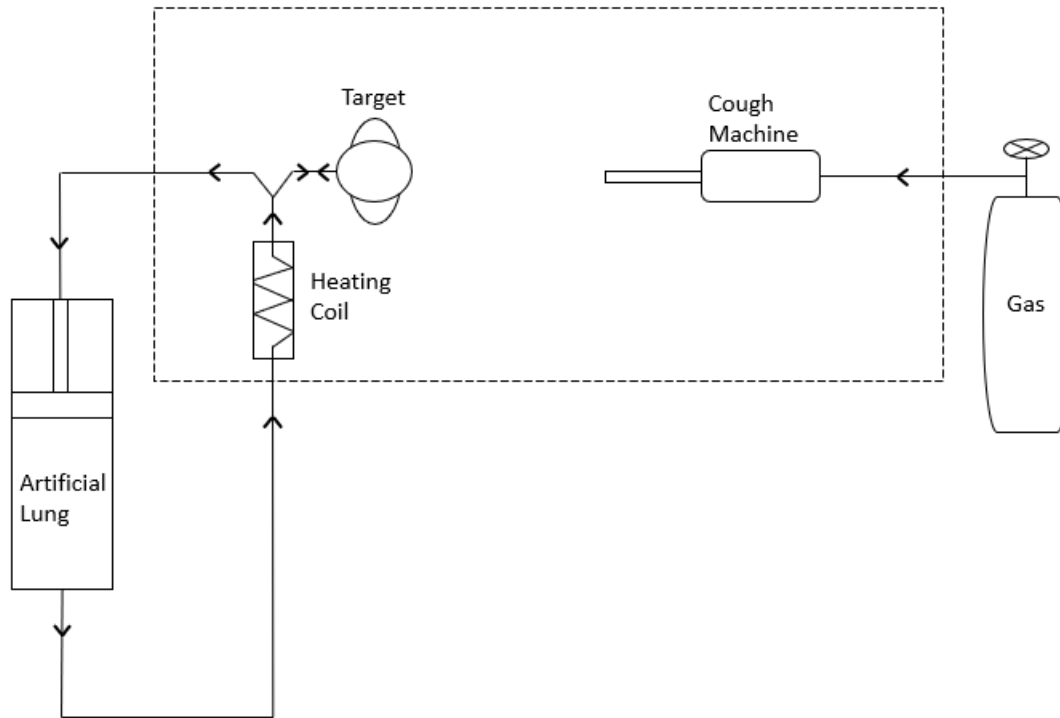


**Figure 1.9** Sketch of the tracer gas system and the artificial lung.

As previously mentioned experiments on breathing were also performed. The boundary conditions for the manikins for the breathing cases were calculated by the IV3 group and are shown in table 1.3. The volumetric airflow is significantly higher than it should be with an activity level of 1.4 met as stated in their report due to calculation errors[Nedergaard et al., 2022]. However, the results are still relevant as their measurements showcase exposure for breathing with a high flow rate. Further error may come from the breathing frequency for both coughing and breathing as the breathing frequency has to be manually timed which may lead to human error. The closest breathing frequency is of  $16 \text{ min}^{-1}$  is therefore used. Furthermore, a correction was made for the density disparity compared with human breathing. To compensate the temperature was set to  $37.5 \text{ }^\circ\text{C}$ . However, an error was made during the initial calculations as the target manikins exhalation temperature should not be corrected as the density of atmospheric air and human breath coincide in the between the temperatures  $32 \text{ }^\circ\text{C}$  to  $34 \text{ }^\circ\text{C}$  [Bjørn, 2000].

**Table 1.3** Boundary conditions for the target and source manikin

Parameter	Target manikin	Source manikin
Activity level [met]	1.4	1.4
Exhalation flow [l/min]	20.08	20.08
Breathing frequency [ $\text{min}^{-1}$ ]	16	16
Exhalation temperature [ $^\circ\text{C}$ ]	37.5	37.5

The breathing profile for both cases is shown on figure 1.10 and is based upon appendix B.

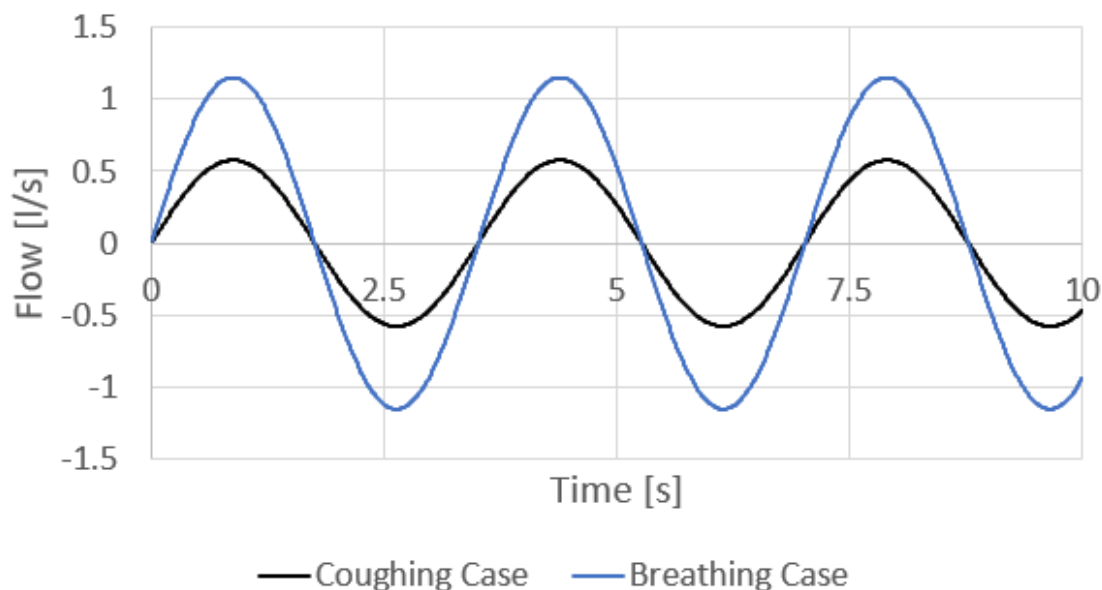


**Figure 1.10** Breathing profile for both source and target manikin during breathing cases and the target manikin during coughing cases.

The setup for tracer gas is different in breathing cases. The air is supplied into the inhalation side of the artificial lung. This principle is shown in Nedergaard et al. [2022]. In breathing cases, the artificial lung has 1 manikin on each of its pistons. The setup is similar to the sketch in figure 1.9. During tracer gas measurements the tracer gas canister is attached before the artificial lung. To avoid damage to the artificial lungs caused by the smoke, the smoke is attached after the artificial lungs. The setup is shown in Nedergaard et al. [2022] report. It should be noticed that compensation for increased flow was not made for those smoke measurements and the smoke container might cause disturbances.

### Temperatures

The temperature or heat output of the manikin should also be calculated in order to reproduce a realistic convective boundary layer around the manikin. The heat output is used at boundary conditions for conformity with previous studies [Zhang et al., 2022]. The heat output of the manikin is calculated based on the activity level. The heat loss due to evaporation is taken into account by removing it from the thermal manikin's heat output. The heat output for an activity level of 1.4 met should thus be 77.8 W for the manikin based on its body surface area. The IV3 group made the assumption during their measurements that the energy used to power the fan inside the manikin would eventually be converted to heat if the manikin was airtight. The power of the fans was 40 W each. For conformity, the power of the fans is not removed from the heat output. The calculation of the boundary conditions of the manikin can be found in appendix B.

#### 1.2.4 Machine for simulation of coughing

This section will revolve around the 'coughing machine'. It will go over the design and principle of the machine, how it is controlled, and the flow profile it generates with regard to coughing. The machine is however also able to produce flow profiles matching other

respiratory activities, the focus of the project however is coughing. A picture of the coughing machine can be seen in figure 1.11.

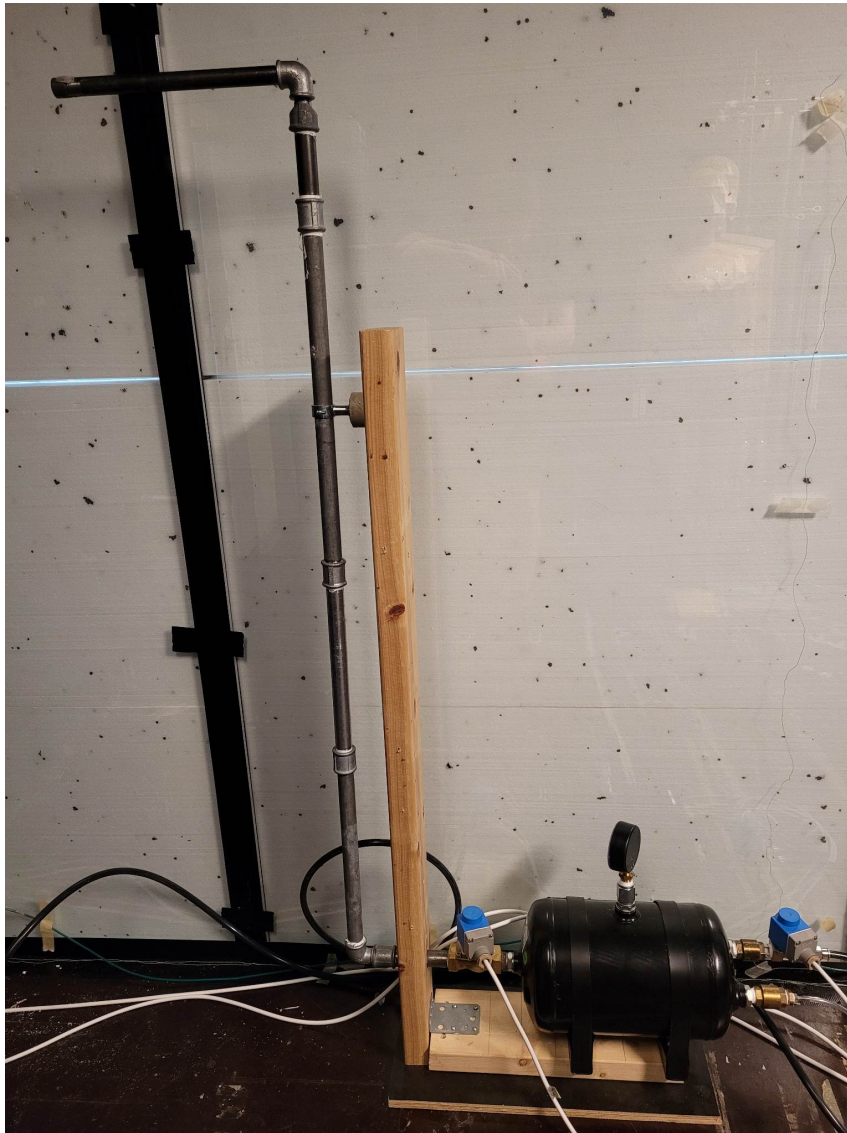


**Figure 1.11** Coughing machine

## Design

As mentioned in the literature review there were two types of machines for simulating respiratory activities. One design is based on pistons and another on pressure. The machine built for this project is based on the principle of pressure. The machine consists of a pressure tank with two inlets and one outlet and is shown in figure 1.12. The outlet goes to what is the mouth opening. The mouth opening has a diameter of 15 mm. One of the inlets is for the supply of the tracer gas which is supplied constantly. The second inlet supplies pressurized air to the tank building up pressure. The outlet and the inlet with pressurized air both have a solenoid valve to control the flow, how they are controlled will be discussed in the next section. Both outlet and inlets are fitted with check valves to avoid backflow. Detailed sketches of the coughing machine can be seen in appendix J.

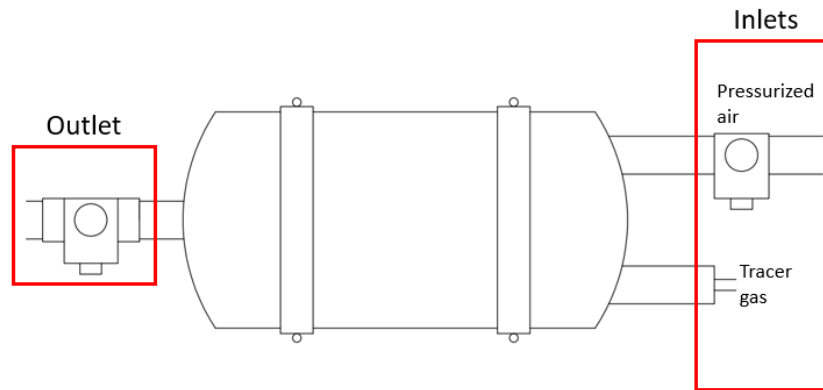


**Figure 1.12** Tank for the coughing machine with inlets and outlets shown.

### Control

The coughing machine is controlled by a relay controlled by the two solenoid valves. The control runs in a cycle starting with a pressure built-up period, of adjustable duration, and a release period, of equal duration. The current control system needs to have an equal duration of the two periods. For a more detailed profile and better control, a new control relay should be used. With this control, the number of coughs over time can be adjusted. For this project a pressure built-up period of 5 s is used with an equal release period of 5 s. The cough duration is however shorter. The cough duration can be seen in figure 1.16 on page 15. The two durations do not match because the valve opens completely and the pressure drops in the tank. This results in a total of 6 coughs each minute as the flow drops quickly after the initial release of pressure. When a specific duration is set the flow rate can be controlled further by adjusting the pressure of supplied air to the pressure tank. Finally, a delay has been enforced on the solenoid valve on the inlet to reduce the risk of backflow and a smaller secondary release/peak. The control setup and relay can be seen in figure 1.13 and the valves can be seen in figure 1.14.



**Figure 1.13** Control system for coughing machine.



**Figure 1.14** Coughing machine seen from the side. The outlet is on the left and the inlet is on the right.

### Profile

The coughing machine generates a very consistent flow profile. The flow profile is therefore measured beforehand. The flow is not measured during the experiments as the equipment

will disturb the airflow significantly. The flow profiles are measured using a Cobra SMARTsense Spirometer from PHYWE. The spirometer can measure in the flow range of  $\pm 10$  l/s with a sampling rate of up to 500 Hz. The spirometer has a resolution of 0.01 l/S with an accuracy of  $\pm 3\%$ . The measurements are done in accordance with Hagen–Poiseuille law [PHYWE, 2023]. The spirometer is placed in connection with the piping from the coughing machine providing a tight seal, see figure 1.15. The measurements are done over a Bluetooth connection from the spirometer to a phone. To operate the spirometer the software provided by PHYWE [2023] is used to get the data in a configurable file format. The software also provided visualized flow profiles used during the tuning of the flow rate. The spirometer is used without the mouthpiece as the coughing machine does not produce any droplets that may damage the spirometer.

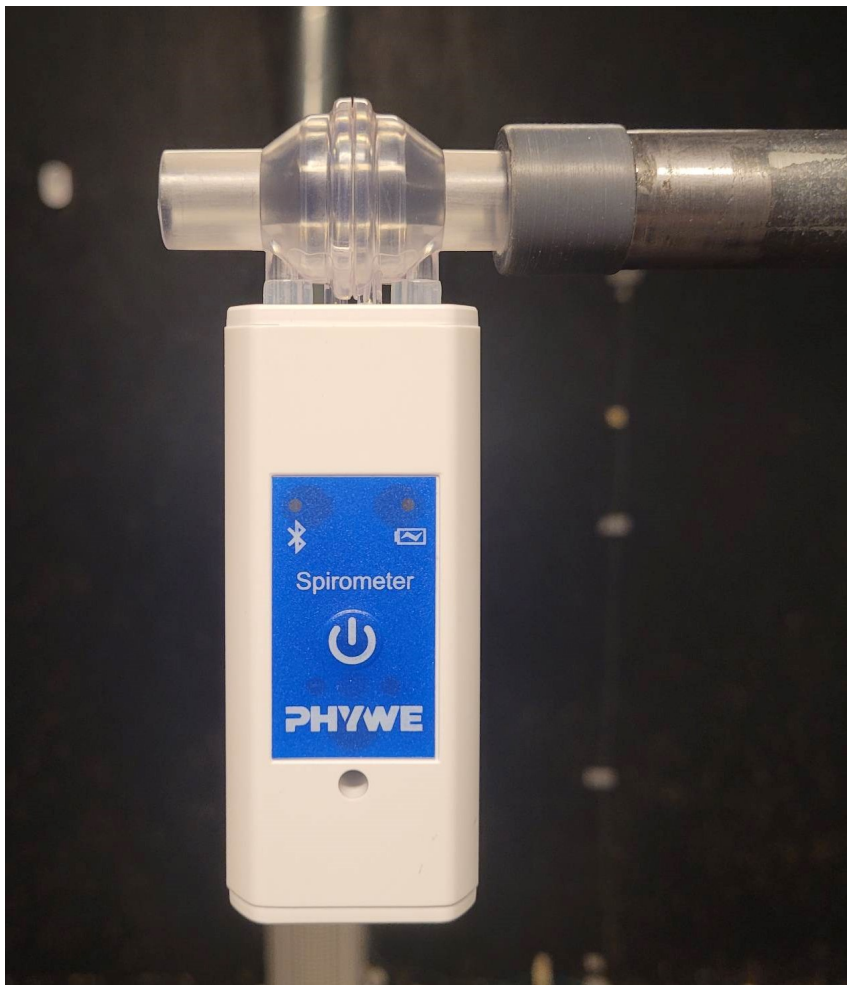


**Figure 1.15** Spirometer used for measurement of flow profiles.

The flow profile generated shown in figure 1.16 is based upon 52 'coughs' from the machine. The machine generates an appropriate initial increase in flow rate, similar to the profiles found in other studies [Gupta et al., 2009][William G. Lindsley et al., 2010]. The peak flow can be adjusted, however, it is chosen to use the average flow rate found by William G. Lindsley et al. [2010] as a reference value. The cough profile used has an average peak flow of 6.95 l/s with a standard deviation of 0.0821/s. The average was taken as the

average value of all the measurements within 10 % of the maximum flow measured which was 7.571/s. The average was taken for all the measurements between 6.811/s to 7.571/s. The volume of expelled air during 1 cough was found to be 1.66l The same was done for cough profile 2 which has an average peak flow of 4.681/s and an expelled volume of 0.91. The flow profiles are shown in figure 1.16 alongside flow profiles obtained using a combined gamma distribution as suggested by Gupta et al. [2009] with different constants. The coughing machine does in general achieve the correct shape of a cough, however, the PVT is approximately 0.05 s shorter. Both the duration and peak flow are consistent with the literature.

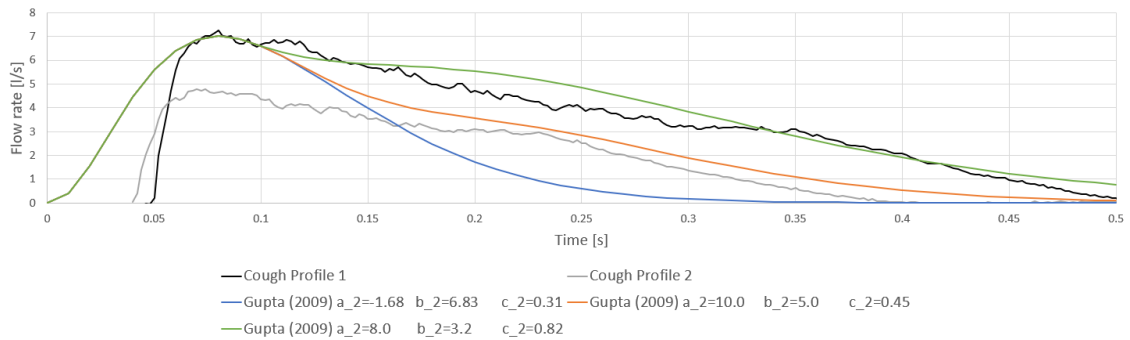


**Figure 1.16** Cough flow profile for the coughing machine case 1 and 2 compared with profiles from literature [Gupta et al., 2009].

### 1.3 Setup of sensors for measurements

During the experiments, three parameters were monitored. The parameters are air velocity, temperature, and tracer gas concentration. The location of the measurement points are shown in figure 1.17 and figure 1.18 viewed from the side and from the top respectively.

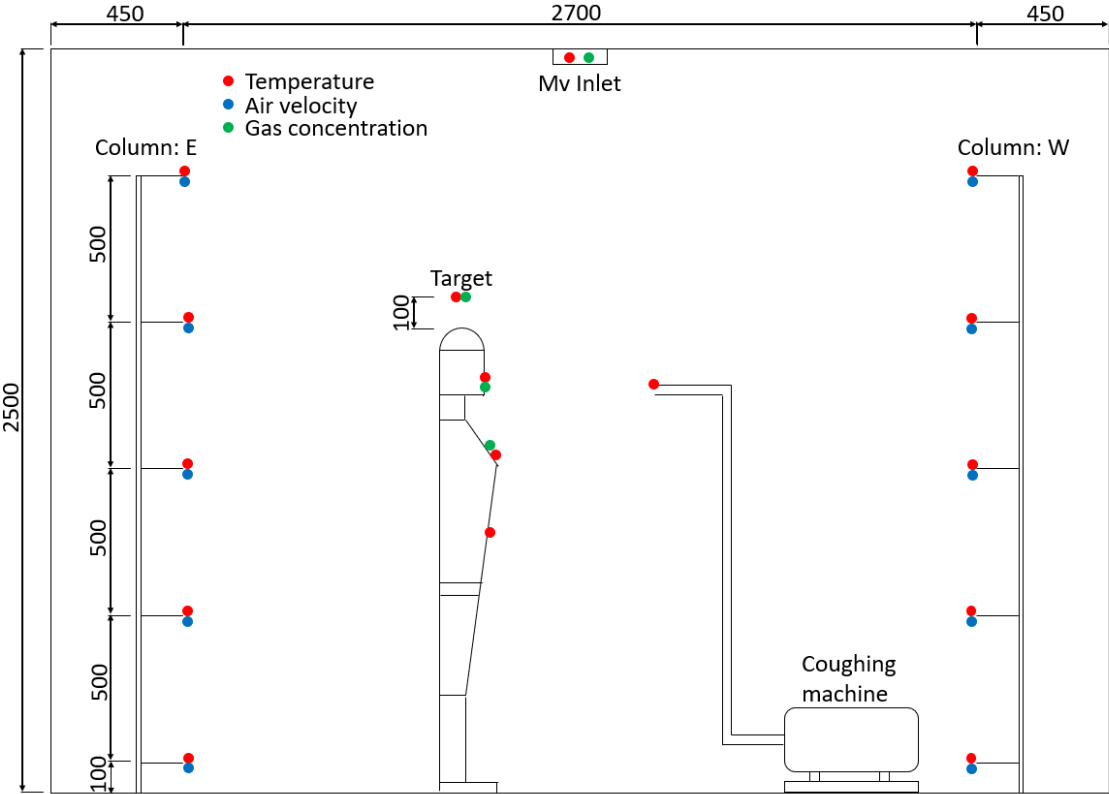
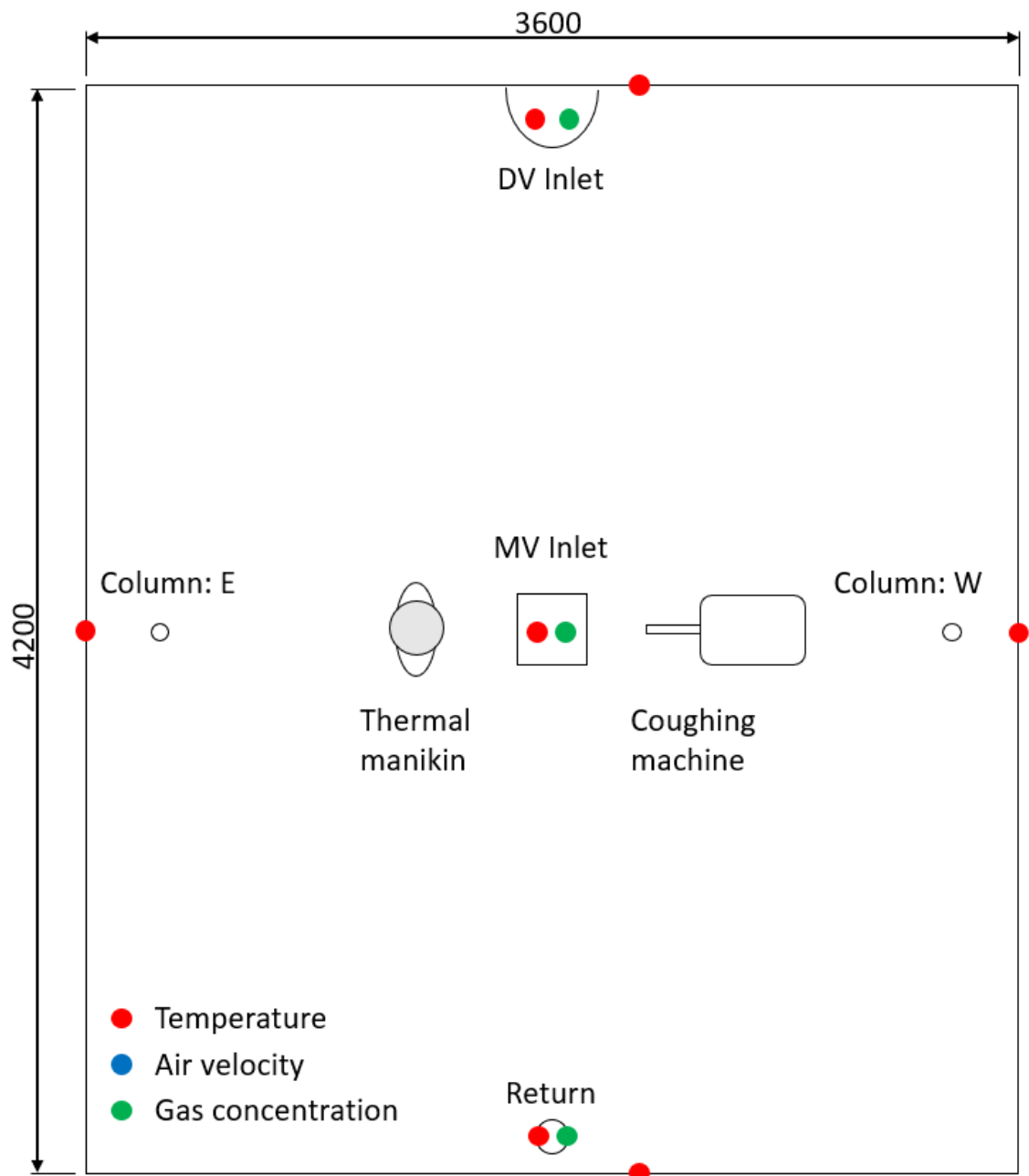


Figure 1.17 Location of measurement points. All measurements are in mm



**Figure 1.18** Location of measurement points. All measurements are in mm

In short, the equipment used to measure the three parameters can be seen in table 1.4. The equipment is explained in greater detail in the following sections.

**Table 1.4** Equipment for generation of boundary conditions and measurement equipment

Equipment	Purpose
Thermal breathing manikin	To largest possible degree represent real human exposure
Artificial lungs	Produce respiration for the manikin
Type K thermocouples	Measures temperatures
PT100	Measures temperatures
Hotwire anemometers	Measures air velocity
1412 Photoacoustic Field Gas-Monitor	Measures the tracer gas concentration
1303 Multipoint Sampler and Doser	Samples the tracer gas at multiple sample points
CO <sub>2</sub> tracer gas	Used for tracer gas
Air handling unit	Ventilation of room
Return/Exhaust	Ventilation of room

### 1.3.1 Setup of temperature measurements

The temperature is measured for three reasons, control of boundary conditions, stable room conditions, and temperature profile. The temperature profile is especially important when displacement ventilation is investigated. The temperature measurements are done using type K thermocouples. The placement of the thermocouples is shown in figure 1.17 and figure 1.18, starting on page 16. The Helios datalogger can be seen in figure 1.19.

**Figure 1.19** Helios datalogger

The calibration of the thermocouples is described in appendix C and compensation for electrical noise is described in appendix G. Both thermocouples and PT100 have been used for measurements, however, due to their larger size the PT100 is used before the experiments commence to be sure of the exhalation temperature as they have a faster sampling rate. For a detailed description of the equipment see appendix C. The temperature was measured every 3.5s due to limitations of the Helios datalogger.

### 1.3.2 Setup of air velocity measurements

As the air velocity is measured differently between cases both situations are described in this section.

### Air velocity sensors during tracer gas measurements

The air velocity is measured in a set of columns behind and beside both the target manikin and the coughing machine. During breathing measurements, they are placed directly behind both manikins. The anemometers are used to ensure that the air velocity in the room due to ventilation does not exceed 0.2 m/s which may disturb the target manikins micro-environment [Stampe, 2000]. The anemometers performed the measurements with a sampling rate of 10 Hz and averaged the values every 1 s. The calibration for the anemometers can be found in appendix E. The datalogger is shown in figure 1.20 and the anemometer is shown in figure 1.21.



**Figure 1.20** Danvak datalogger for anemometers



**Figure 1.21** Danvak 54R102 thermal comfort probe

The anemometers are hot wire anemometers and the setup is also described in E. The location of the measuring points can be seen in figure 1.17 and figure 1.18, starting on page 16.

### Setup of air velocity sensors during measurements of velocity profiles

The sensors are moved during the measuring of the velocity profiles. Instead of two poles a single pole with 9 anemometers is used. The anemometers are spaced with 10 cm between each. The middle anemometer is 1.56 m from the ground centering it at the opening of the coughing machine. The positioning of the anemometers is shown in table 1.5. The pole can be seen in figure 1.22 and the setup can be seen in figure 1.23. The pole is placed directly in front of the coughing machine during measurements. During measurements, all other equipment except thermocouples is moved away and turned off including the manikin and ventilation.

**Table 1.5** Positioning of anemometers. The distance is the vertical distance between the anemometer and the opening of the coughing machine

Anemometer	Vertical distance [m]
A-10	0.4
A-11	0.3
A-12	0.2
A-13	0.1
A-2	0.0
A-15	-0.1
A-5	-0.2
A-6	-0.3
A-7	-0.4



**Figure 1.22** Position of anemometers during measurements of the velocity profile.



**Figure 1.23** Velocity profile setup seen from the side.

### 1.3.3 Setup of tracer gas concentration measurements

The tracer gas concentration is measured using a tracer gas analyzer, which determines the concentration, and a sampler which enables the gas analyzer to measure at multiple locations. The field gas monitor and multipoint sampler used in the measurements are shown in figure 1.24.



**Figure 1.24** Photoacoustic field gas monitor and multipoint sampler and doser.

The measurement points are shown in figure 1.17 and figure 1.18, starting on page 16, and is described in table 1.6. The measurement point 0.1 m above the head of the manikin (1.78 m) gives insight into what the exposure would be if there is a height difference between the source and the target. The measurement point at the manikin's chest gives insight into what the exposure from inspiration is as the inhaled air for a real person is from this region. The measurement point at the mouth of the target is placed directly at/beside the mouth and measures the direct exposure.

**Table 1.6** Measurement points for gas concentration

Channel	Location
1	Return/Exhaust
2	Inlet
3	0.1 m above target head
4	Targets chest
5	Targets mouth

For a detailed description of the equipment and how the equipment is calibrated see appendix F. Two gas monitors are used due to problems with receiving data from the 1412. The 1412 is used for the breathing cases described later in this chapter and the 1302 is used for coughing cases.

### 1.3.4 Setup of cameras

To be able to capture how the flow moves during smoke measurements cameras are placed inside the test room. The cameras allow videotaping of the test room without creating any disturbance that might affect the measurements. Two cameras are used to capture both the vertical and horizontal spread of the flow. The cameras are placed directly in the middle of the room on the floor to capture the horizontal spread and of the ventilation duct to the diffuser for displacement ventilation on the southern wall. The camera is placed at a height of 1.53 m, the same height as the mouth opening of the manikins and coughing machine. The camera used is shown in figure 1.25. The camera is a Logitech C920 HD Pro Webcam. The camera record in 1080p resolution in 30 fps.



**Figure 1.25** Video camera used for smoke measurements.

# Results 2

This chapter contains the results of the measurements described in chapter 1. The results obtained for the breathing scenario are made in cooperation with group IV3. The IV3 group helped with both smoke and tracer gas measurements for the breathing cases which will be presented first.

## 2.1 Breathing

This section revolves around the results found for the breathing scenario. The breathing process is a normal breathing process but with an increased flow rate. For breathing both mixing and displacement ventilation were investigated with both exposure and smoke measurements. For all cases, different distances were investigated. The breathing cases were done by the IV3 group with the guidance and supervision of the author.

### 2.1.1 Conditions during experiment

The conditions of the setup are controlled to investigate if the targeted boundary conditions have been reached during the measurements. Both the ventilation and temperature parameters are investigated.

#### Ventilation

As previously mentioned the air velocity should be below 0.2 m/s. In figure 2.1 and figure 2.2 the air velocity behind the target and source respectively, are measured during the tracer gas measurements for breathing. The figure shows that the velocities are below the requirements. The data from the anemometers for a distance of 1.0 m with displacement ventilation was corrupted and thus are not provided. Further, the velocity was not checked during the smoke cases.

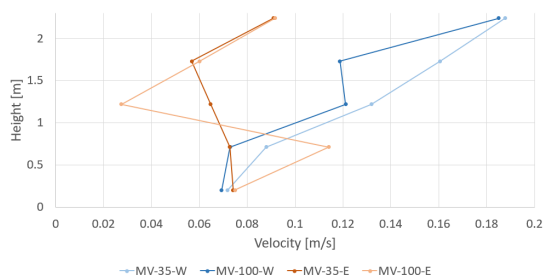


**Figure 2.1** Air velocity for the mixing ventilation cases during the tracer gas measurements

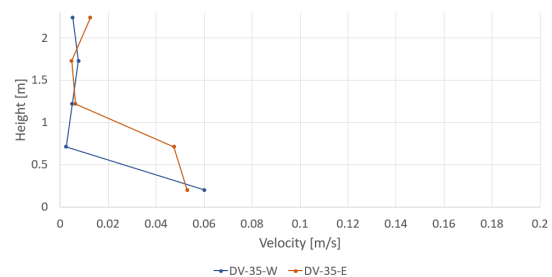


**Figure 2.2** Air velocity for the displacement ventilation cases during the tracer gas measurements.

## Temperatures

The temperatures have been measured to ensure that the target boundary conditions are met. The temperature for the exhalation and body surface is listed in table 2.1. The table shows that the body surface temperature is significantly lower than expected. The exhalation temperature is measured using thermocouples however the thermocouples sampling rate is not fast enough to measure the exhalation so a large data set is required, and the thermocouples may disturb the flow during measurements. The target's exhalation temperature does not reach the targeted temperature of 34 °C either. The wire inside the target's heating coil was found to be defective which was fixed for coughing. The temperature gradient can be seen in figure 2.3 for the smoke measurements.

**Table 2.1** Temperature conditions for the target and source manikin. TET= Target exhalation temperature, SET= Source exhalation temperature, TST= Target surface temperature, and SST= Source surface temperature.

Distance [m]	Case	Type	TET [°C]	SET [°C]	TST [°C]	SST [°C]
0.35	Smoke	MV	25.6	35.5	25.8	25.9
1.00	Smoke	MV	25.0	35.5	25.4	25.5
0.35	Smoke	DV	23.9	35.6	23.5	23.6
1.00	Smoke	DV	22.8	35.8	23.5	23.5
0.35	Tracer	MV	24.7	35.6	25.0	25.1
1.00	Tracer	MV	25.0	36.5	25.7	25.7
0.35	Tracer	DV	23.9	35.6	23.5	23.6
1.00	Tracer	DV	22.8	35.8	23.5	23.5

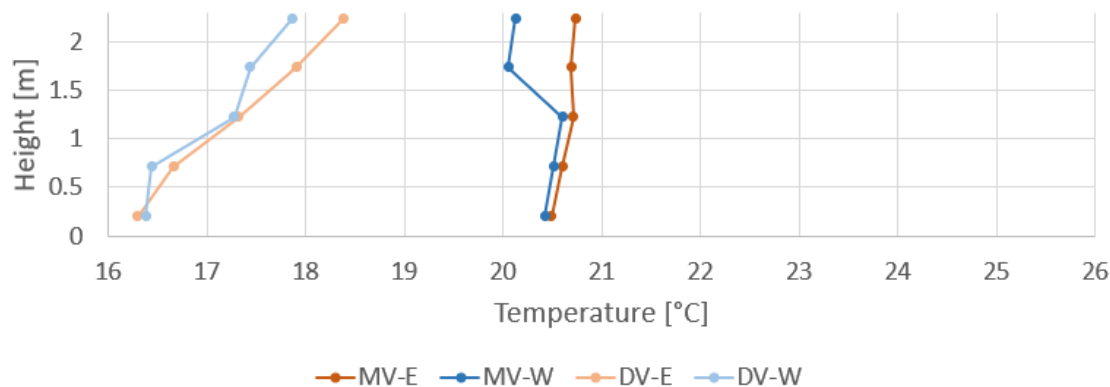


**Figure 2.3** Temperature gradient for smoke measurement. Both poles were placed 0.45 m from the wall directly behind both the target and source. The distance between the manikins was 1 m.

The temperature gradient for the tracer gas measurements is shown in figure 2.4 and figure 2.5 for the cases with mixing ventilation and displacement ventilation respectively

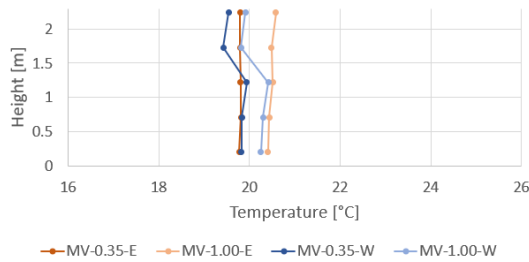


**Figure 2.4** Temperature gradients for the mixing ventilation cases during the tracer gas measurements

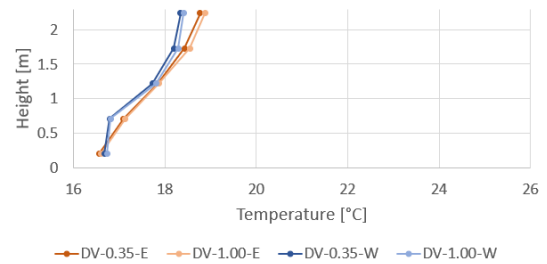


**Figure 2.5** Temperature gradients for the displacement ventilation cases during the tracer gas measurements.

### 2.1.2 Results of smoke measurements

In this section, the results of the smoke measurements are presented. The smoke measurements were performed at both 0.35 m and 1 m. In figure 2.6 the outline of the smoke cloud is shown at different intervals for mixing ventilation. The same method is used for the case with displacement ventilation which is shown in figure 2.7. The interval between the outlines is chosen based on the frame rate of the video. The video of the smoke measurements is in 30 fps and an interval of 10 frames are chosen which correlates to  $1/3$  s. The flow during mixing ventilation is more upwards and at 1 m it barely reaches the target manikin. For displacement, the flow is centered and begins to rise when it has reached the target manikin and thus travels further into the room.

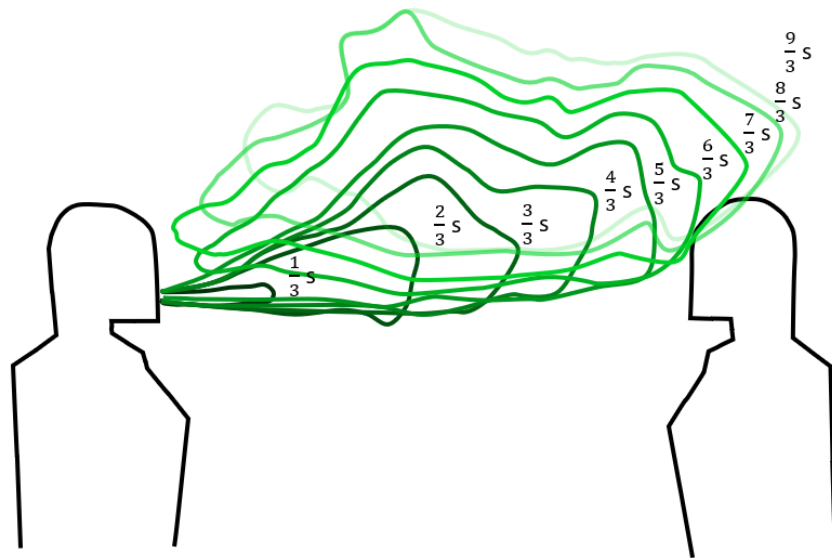


**Figure 2.6** Outline of smoke clouds from the smoke measurements at a consistent interval for mixing ventilation. The target manikin is on the right.

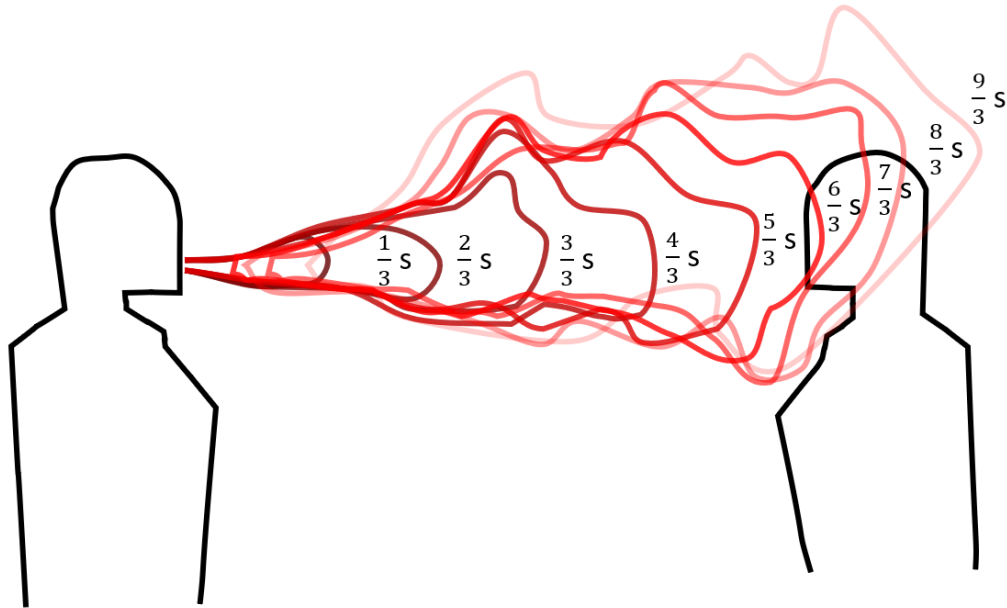


**Figure 2.7** Outline of smoke clouds from the smoke measurements at a consistent interval for displacement ventilation. The target manikin is on the right.

The smoke photos are shown in figure 2.8 and figure 2.9 for a distance of 0.35 m and 1 m respectively.

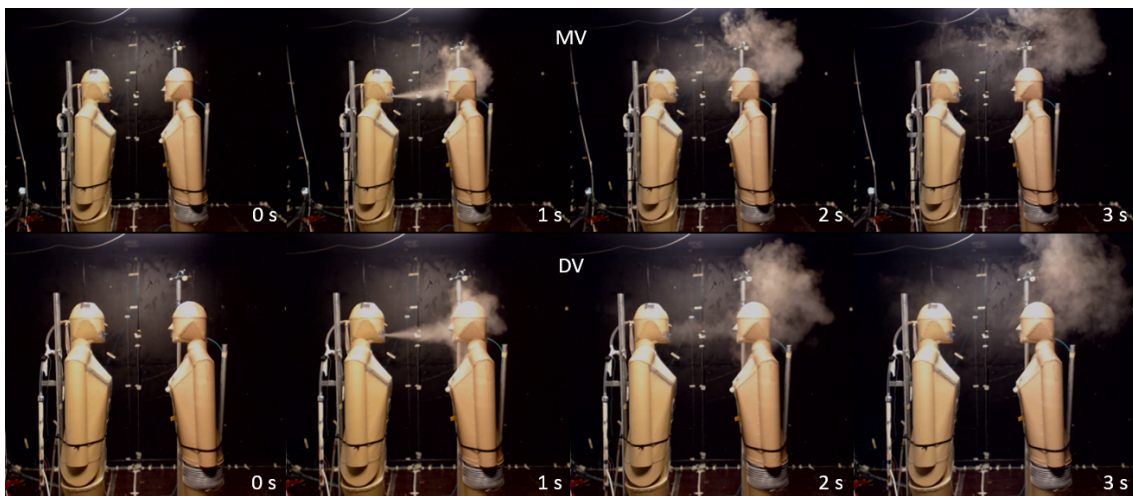


**Figure 2.8** Smoke photos for mixing and displacement ventilation at a distance of 0.35 m at an interval of 1 s.

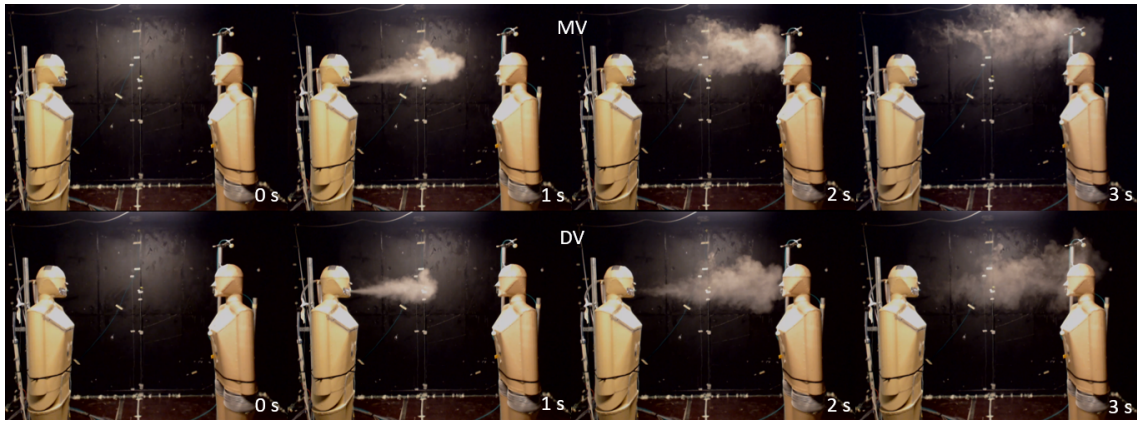


**Figure 2.9** Smoke photos for mixing and displacement ventilation at a distance of 1.00 m at an interval of 1 s.

### 2.1.3 Results of tracer gas measurements

The result of the tracer gas measurements is shown in figure 2.10 for the exhalation zone for both mixing and displacement ventilation. The exposure in the displacement case is double the exposure found for mixing.

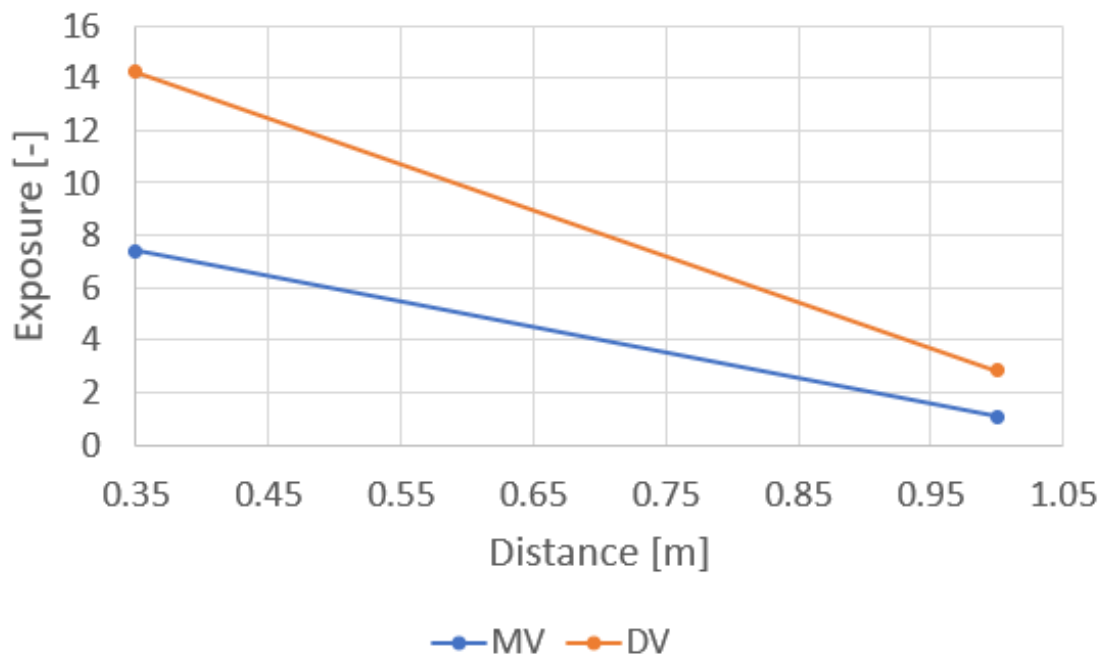


**Figure 2.10** Exposure for the exhalation zone of the target for both mixing and displacement ventilation

The exposure was also measured at the target's chest and 10 cm above the head. These results are shown in figure 2.11 for mixing ventilation. At 0.35 m the exposure at the mouth area is clearly the highest. The exposure at the chest area does not experience any increased exposure. At 1 m the exposure at the mouth area has been significantly reduced. The exposure above the head is the highest at a distance of 1.0 m.

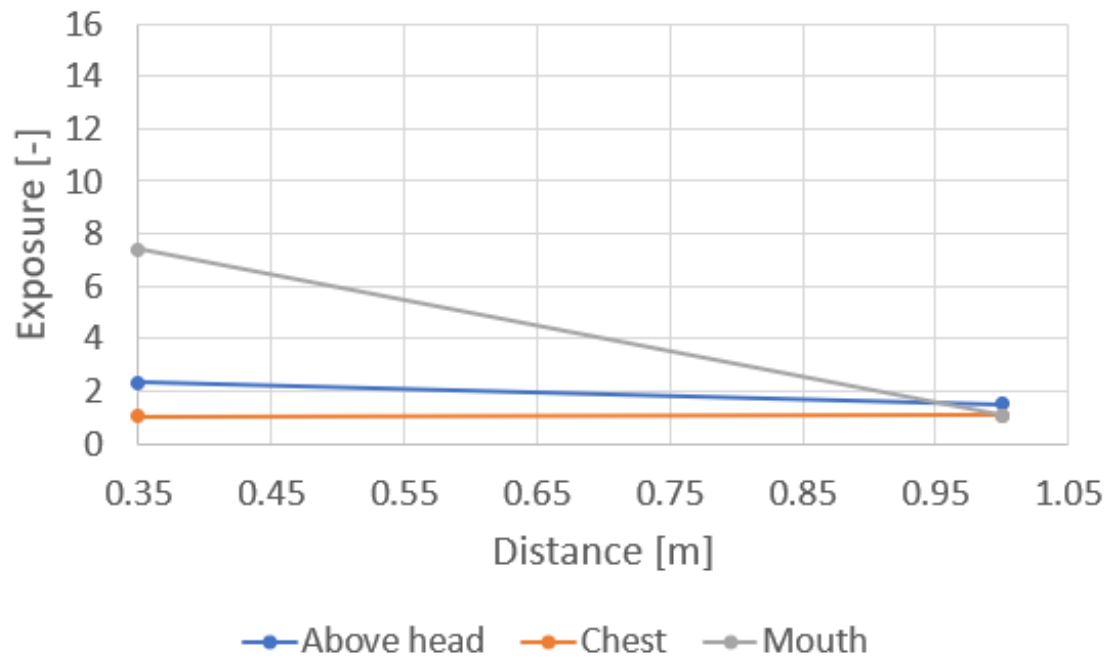


**Figure 2.11** Exposure at the target manikin for mixing ventilation.

The same measurements have been done during displacement. The results are shown in figure 2.12. In cases with displacement ventilation, the lower zone has cleaner air. This is caused by stratification. The figure suggests that the chest area is in the clean zone as the exposure is almost 0. As in mixing ventilation, the exposure for short distances dominates. Above the head experience a slight rise with distance.

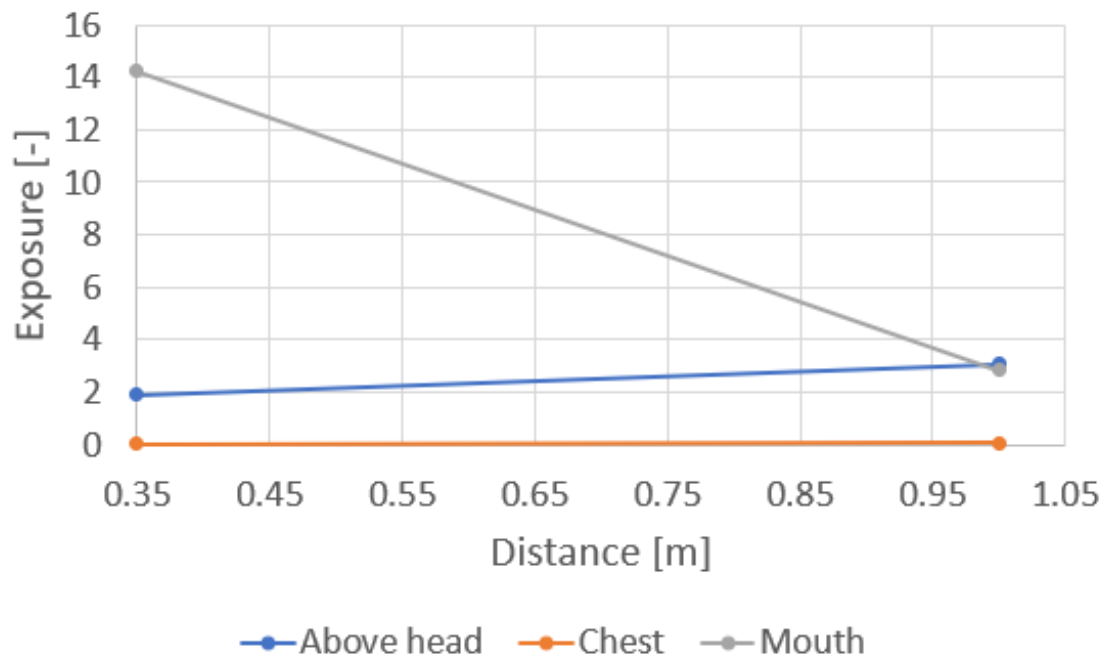


**Figure 2.12** Exposure at the target manikin for displacement ventilation.

## 2.2 Coughing

This section contains the tracer gas results of the measurements performed on coughing as described in chapter 1. The section will describe the conditions during the experiment and the results of the tracer gas measurements.

### 2.2.1 Conditions during experiment

In order to ensure that the measurements are done under the conditions described in chapter 1 the boundary conditions are monitored. Both the ventilation and temperature parameters have been measured during the experiments. As mentioned previously some boundary conditions such as the supply and exhaust flow rate and the exhalation temperature were measured beforehand so as to not disturb the measurements. Furthermore both the supply and exhaust flow rates have not been adjusted between measurements. The surface temperature on the manikin is measured to evaluate what the temperature is during the measurements since the heat output was chosen as the boundary condition. The boundary conditions for the gas were measured beforehand and are shown in appendix H. The value should be seen as an estimate as the flow of CO<sub>2</sub> varied with both the pressure in the tank and the gas canister.

### Ventilation

The airflow behind the manikin and the coughing machine is monitored to ensure that air velocity does not go above 0.2 m/s to ensure that the ventilation does not disturb the microenvironment. Furthermore, it is used to see if the ventilation in the room has reached steady state conditions before the measurement begins. Due to limited space behind the manikin and coughing machine, the air velocity measurements were done behind and to the side of the manikin and coughing machine. The air velocity can be seen in figure 2.13 and figure 2.14 for pole W and pole E respectively for cough case 1. The air velocity for pole W and pole E respectively for cough case 2 is shown in figure 2.15 and figure 2.16. The air velocity shown is the average at each position over the entire measuring period.

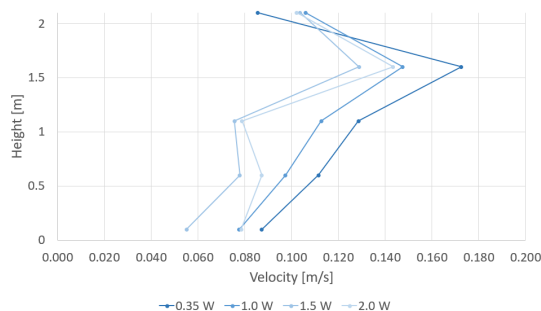


**Figure 2.13** Air velocity for pole W for cough case 1.

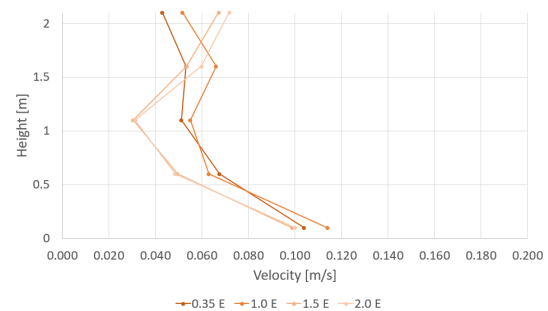


**Figure 2.14** Air velocity for pole E for cough case 1.

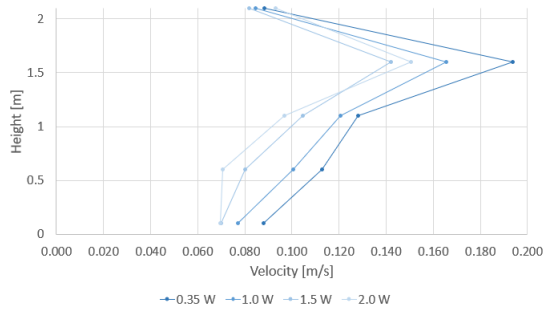


**Figure 2.15** Air velocity for pole W for cough case 2.

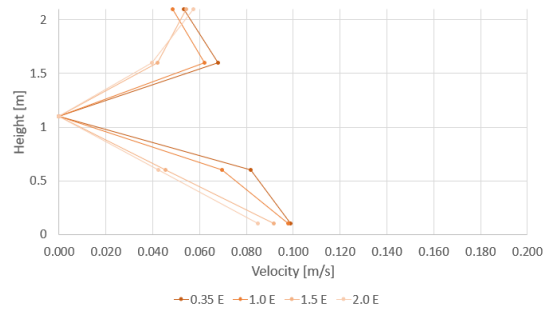


**Figure 2.16** Air velocity for pole E for cough case 2. One anemometer stopped working during measurements.

As mentioned previously many of the boundary conditions are monitored before the measurements begin and are not adjusted further. The ventilation system is one of those boundary conditions. Related boundary conditions are shown in table 2.2.

**Table 2.2** Boundary conditions for the target and source manikin

Parameter	Target value
Air change [ $\text{h}^{-1}$ ]	5.6
Supply flow rate [ $\text{m}^3/\text{h}$ ]	212
Exhaust flow rate [ $\text{m}^3/\text{h}$ ]	212

## Temperatures

The target boundary conditions have previously been described in chapter 1. The boundary conditions related to the temperature are summarized in table 2.3 below. The target room temperature is the same as the temperature in the laboratory to reduce convective flow along the walls of the room. The temperature in the laboratory varies but is usually between 20 °C and 23 °C.

**Table 2.3** Boundary conditions for the target and source manikin

Parameter	Target value
Exhalation temperature [°C]	34
Heat output of manikin [ $\text{W}/\text{m}^2$ ]	54.0
Room temperature [°C]	$T_{\text{lab}}$
Inlet temperature [°C]	$T_{\text{lab}}$

How the exhalation temperature is achieved is described in appendix I. The exhalation temperature was measured beforehand using PT100 as the main equipment that would not disturb the flow did not sample quickly enough. The heat output for the heating coil is then kept constant between measurements.

During the measurements, the room temperature, inlet temperature, and body surface temperature were measured. The results of these measurements are shown in table 2.4.

The temperature gradient in the room is shown in figure 2.17 and figure 2.18 for pole W and pole E respectively for cough profile 1 and figure 2.19 and figure 2.20 for pole W and pole E respectively for cough profile 2.

**Table 2.4** Temperature conditions in the room.

Distance [m]	Room temperature [°C]	Inlet temperature [°C]	Surface temperature [°C]
Cough case 1			
0.35	22.8	22.6	31.7
1.00	23.1	22.7	31.7
1.50	22.9	22.6	31.5
2.00	23.0	22.6	31.8
Cough case 2			
0.35	22.94	22.69	31.78
1.00	22.83	22.63	31.66
1.50	22.77	22.42	31.75
2.00	22.93	22.63	31.91

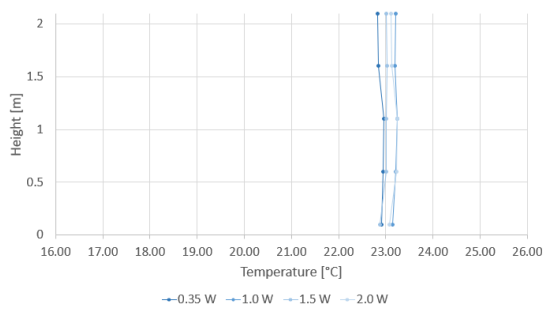


**Figure 2.17** Temperature for pole W for cough case 1

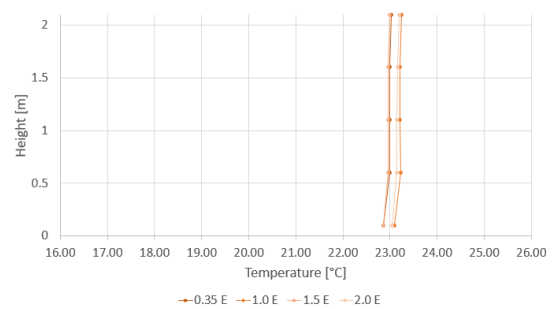


**Figure 2.18** Temperature for pole E for cough case 1

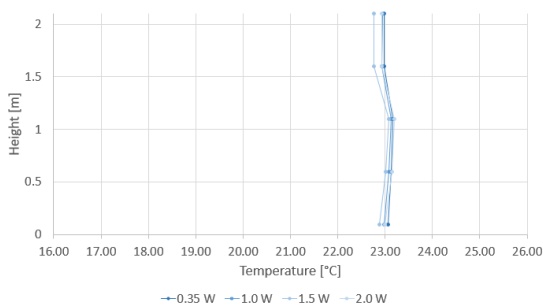


**Figure 2.19** Temperature for pole W for cough case 2

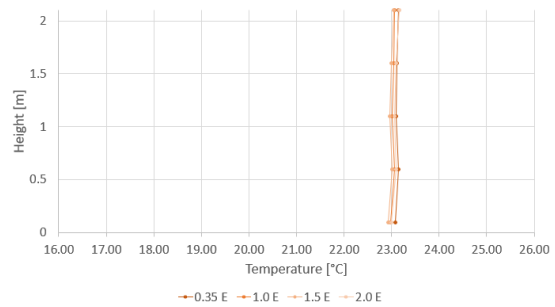


**Figure 2.20** Temperature for pole E for cough case 2

## 2.2.2 Results of tracer gas measurements

The result of the tracer gas experiment is shown as previously mentioned in chapter 1 using the susceptible exposure index. The exposure is shown in figure 2.21 for both cough

profiles. It can be seen that at close distances the low-flow case has a considerably higher exposure. However after 1 m they are the same. The exposure remains higher than the room until a distance of 2 m. This seems to suggest that a short measurement period was used for the short distances especially.

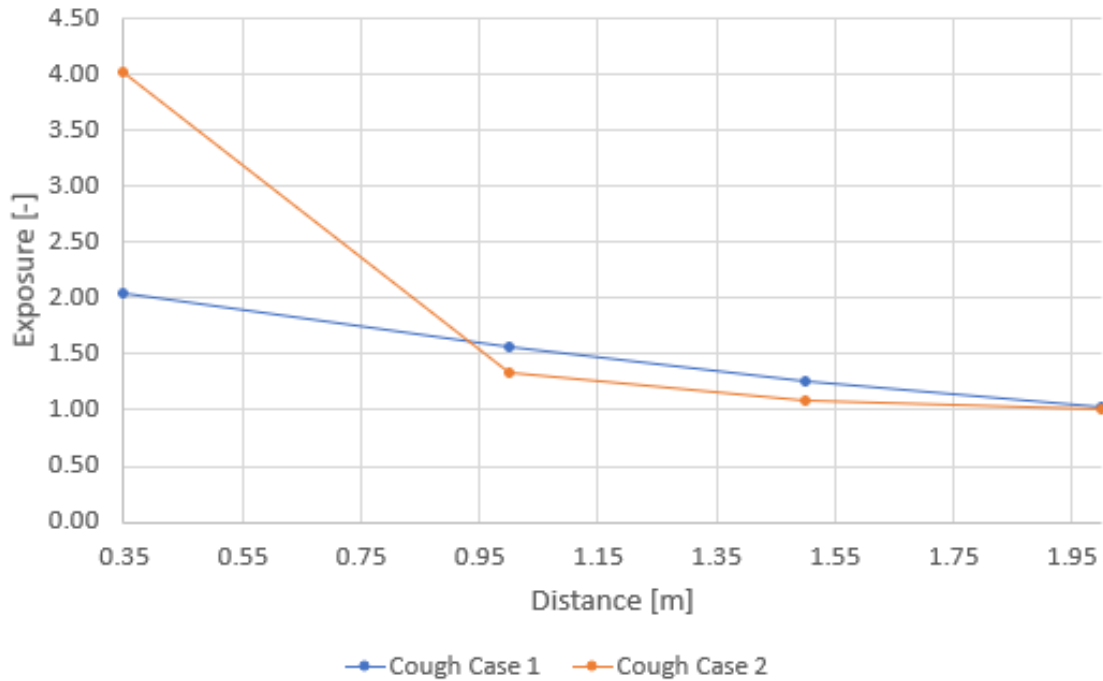


**Figure 2.21** Susceptible exposure index for coughing measured at the exhalation zone of the target manikin for cough profiles 1 and 2.

In figure 2.22 and figure 2.23 the exposure is shown for the other sampling points for cough profiles 1 and 2 respectively. At close distances, the exposure is highest in the mouth area (exhalation zone). As the distance grows a reduction in the exposure can be observed for the mouth. The exposure above the head grows to be the highest exposure experienced at a distance of 1 m where after it drops off and becomes stable around an exposure of 1.3. The exposure at the chest (inhalation zone) is the lowest at all distances and drops to an exposure of approximately 1.1 at a distance of 1 m. The exposure is constant for the inhalation zone after 1 m. The exposure measured both above the head and at the chest level seems to be very similar between the two cases.

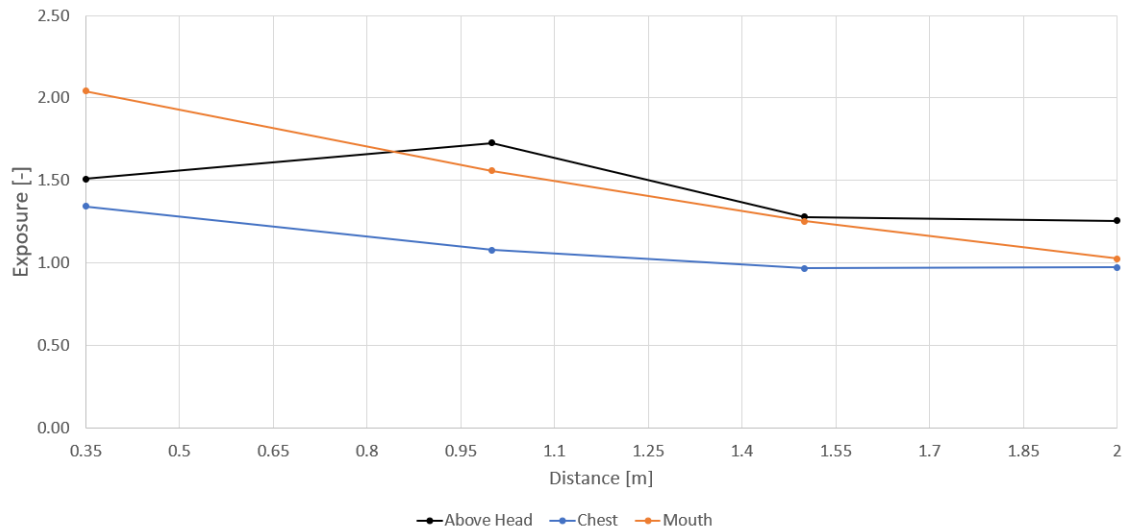


**Figure 2.22** Susceptible exposure index for coughing measured at the exhalation zone of the target manikin, at the chest of the manikin and 10 cm above the head of the manikin for cough profile 1

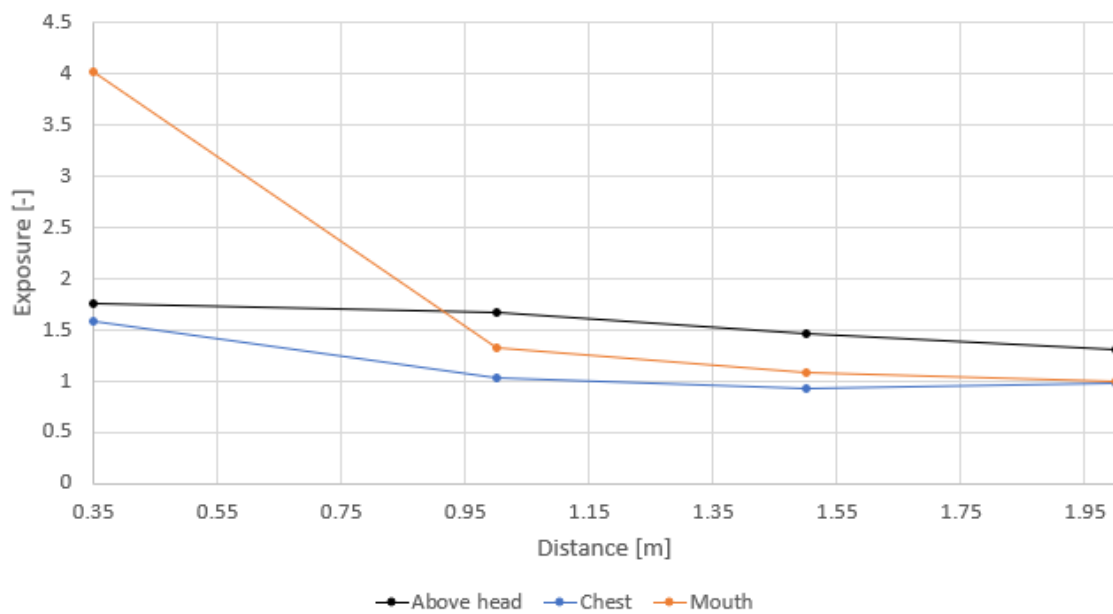


**Figure 2.23** Susceptible exposure index for coughing measured at the exhalation zone of the target manikin, at the chest of the manikin and 10 cm above the head of the manikin for cough profile 2

## 2.3 Velocity profiles

This section describes the velocity profiles generated. The velocity is measured using anemometers in the setup described in section 1.3.2 on page 18.

## Ventilation

During the measurements, the ventilation and manikin were turned off so as to not disturb the cough. The manikin is moved out into a corner to remove any influence the geometry might have on the flow. The flow rate for both inlet and return are  $0 \text{ m}^3/\text{h}$ .

## Temperatures

Despite no changes in temperature are expected the temperature is measured to investigate the room temperature and gradient. The temperature is measured in the same positions as the air velocity. The room temperature is described in table 2.5 and the temperature profile generated is shown in figure 2.24. The room temperature during the measurements are approximately  $21^\circ\text{C}$  for all distances. The temperature profile shows that the cough is slightly cooler than the surrounding air however only slightly.

**Table 2.5** Boundary conditions for the target and source manikin

Distance [m]	Room [ $^\circ\text{C}$ ]
0.50	21.5
0.80	21.4
1.00	21.3
1.25	21.1
1.50	20.9

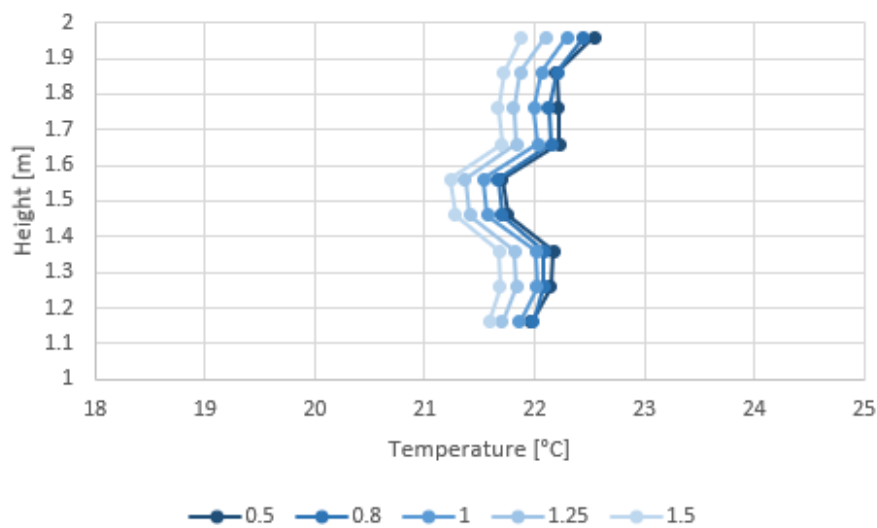


**Figure 2.24** Temperature profile during measurements of velocity profile

### 2.3.1 Results

The profile is shown for multiple distances and heights. The highest velocities are experienced in the center and are reduced as both the vertical and horizontal distance increase. The velocity profiles are shown in figure 2.25. The velocity in the centerline reduces gradually over time however the velocity of the edge zone increase with distance as the cough spreads vertically. From the figure, it can clearly be seen that the coughing

machine produces a cough with vortex flow. This is clearly shown at a distance of 1 m and 1.25 m at the bottom edge. When viewing the bottom half of the velocity profile two distinct peaks can be seen one in the centerline of the cough and another near 1.2 m in height. It seems that the generated flow resembles a vortex flow. A decay in velocities could be observed for the center line however the decay was not as present in the outer edges of the profile where vortices were observed. After 1.5 m the vortices could no longer be observed.

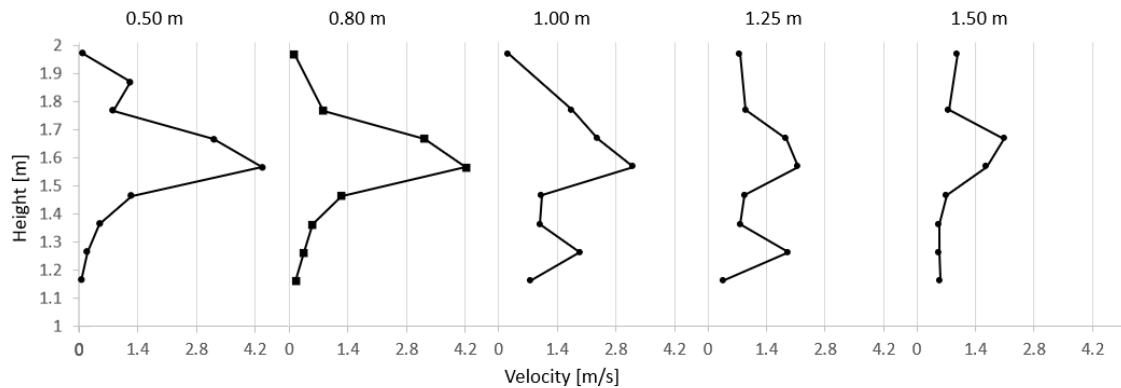


**Figure 2.25** Velocity profile for the average peak velocity for the coughing machine.

## 2.4 Comparison between coughing and breathing

The exposure may seem to be lower for coughing however the basis for the two respiratory activities is different meaning they cannot be directly compared. If we look at a scenario where a person is coughing once and then breathing, then in order to predict the actual exposure for the scenario viral load and expelled volume into account as well as the exposure for each respiratory activity in that scenario. The scenarios are showcased on figure 2.26.

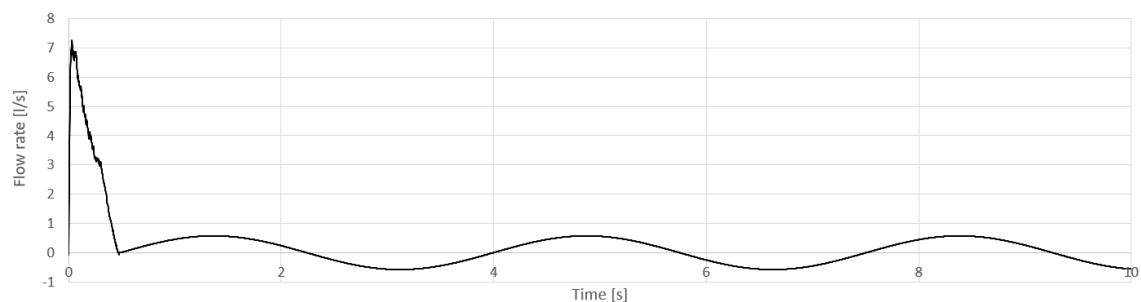


**Figure 2.26** Respiratory scenario for comparison between coughing and breathing.

If this is done then the exposure can be weighted for the different activities to provide the exposure. For this to be done a few assumptions have to be made. The profile is consistent and does not change with time. The measured exposure does not change when the number of coughs is reduced or increased. Since the exposure is relative it can be assumed that the exposure does not change with a change in the number of coughs as both the concentration at in the inhalation zone and the room would change accordingly. The inhalation does not

incur on the expelled air by the source and does not change the characteristic of said flow. The particle type and size are the same for both coughing and breathing. If they are not the exposure should be used as done in previous studies and the activities should be separated. These assumptions should be studied more in-depth to validate them. The exposure can then be calculated using equation (2.1). The equation gives a weighted exposure that can be used to investigate different combinations of respiratory activities as it also works for sneezing, for instance, the above-mentioned profile will in a distance of 0.35 m and under the boundary conditions during the measurements give an exposure of 7.24 when using a 40,000 ppm concentration for both coughing and breathing. Adjustments do have to be made to the equation must be made when using it with speech. Using the exposure different conditions can then be investigated with a combination of respiratory activities. How each activity compares to another depends on the boundary conditions used in the equation. The equation can be combined with aerosol concentrations found in other studies to provide more precise results for different scenarios.

$$\epsilon_{\text{comb}} = \frac{\epsilon_{\text{cough}} \cdot CEV \cdot n_{\text{cough}} \cdot c_{\text{cough}} + \epsilon_{\text{breath}} \cdot V_{\text{breath}} \cdot (BF^{\frac{60-t_{\text{cough}} \cdot n_{\text{cough}}}{60}}) \cdot c_{\text{breath}}}{CEV \cdot n_{\text{cough}} \cdot c_{\text{cough}} + V_{\text{breath}} \cdot (BF^{\frac{60-t_{\text{cough}} \cdot n_{\text{cough}}}{60}}) \cdot c_{\text{breath}}} \quad (2.1)$$

$\epsilon_{\text{comb}}$	Weighted exposure	[-]
$\epsilon_{\text{cough}}$	Exposure for cough	[-]
$\epsilon_{\text{breath}}$	Exposure for breathing	[-]
CEV	Cough expired volume	[l]
$V_{\text{breath}}$	Volume of a single exhalation	[l]
$n_{\text{cough}}$	Coughing frequency	[min <sup>-1</sup> ]
BF	Breathing frequency	[min <sup>-1</sup> ]
$t_{\text{cough}}$	Duration of a singular cough	[s]
$c_{\text{cough}}$	Viral concentration in the cough	[ppm]
$c_{\text{breath}}$	Viral concentration in breathing	[ppm]

# Discussion 3

---

This chapter focuses on the results of the experiments, its limitations and future work.

## 3.1 Equipment

The full-scale experiments of the cross-infection focuses primarily on the exposure. Air-velocity sensors, temperature sensors and gas sensors are used to investigate the experiments. The sensors were calibrated and verified in appendix E, C and F. All the sensors are deemed to have acceptable deviations for the measurements. However the tracer gas analyzer is not deemed precise enough to give accurate measurements of the tracer gas concentration in the exhalation flow with the current calibration. A single point calibration was performed which gives is a range of 15,000 ppm. The range covers the measurements on the target manikin and in the ventilation system but with a targeted concentration of 40,000 ppm any measurement of the exhalation concentration should be viewed as an estimate.

During tracer gas measurement the flow supplied to both the source manikin and the coughing machine varied due to loss in tank pressure over time. The variation was further amplified by the fluctuations in pressure in the coughing machine. To prevent large discrepancies between measurements the flow was set to a specific value which was measured at a specific time in the coughing profile. Since the result of the experiments are a relative number it can be argued that lesser fluctuations in the supply flow rate of tracer gas would result in a corresponding increase of tracer gas in the room. The fluctuations are not deemed to have a significant influence on the final result.

During the measurements of the velocity profiles a single anemometer stopped responding resulting in the upper half of the velocity profiles not capturing the full profile. At the shortest distance of 0.5 m sign of a vortex flow was observed in the upper half of the profiles, however after 0.5 m the anemometer at a height of 1.86 m stopped responding. The vortex flow was however also observed in the lower half of the profile at a greater distance.

## 3.2 Smoke measurements

During the smoke measurements performed by IV3, proper compensation for the disturbance of the flow was not made. The way the smoke measurements were performed was not ideal as a container was filled with smoke and then connected to the respiration system. When the container is connected the artificial lung cannot maintain the flow into the room resulting in a disturbance of the steady state conditions. An improved method

would be to connect the smoke machine directly to the respiration system and make a compensation for the increased flow rate.

### 3.3 Conditions during measurement

The conditions during the experiments influenced the results significantly. The conditions affected multiple cases and are discussed for each.

For the cases with breathing significant deviations were observed from the targeted boundary conditions which affected the results. The main conditions that were not reached were the body surface temperature of both manikins and the exhalation temperature of the target manikin. The body surface area for both the source and target manikin was between 23.5 °C and 25.9 °C. The targeted body surface temperature was 33.5 °C. The heat output of the manikin was chosen as the boundary condition instead of the body surface temperature so a slight deviation was expected. The deviation however is large enough that the convective boundary layer is weakened compared to the targeted conditions. The effect was shown in the smoke measurements where the flow from the source manikin was centered until it was behind the target manikin. The reason for the error was an assumption made by the group regarding the ventilator inside the manikin. The error was corrected for measurements of the coughing machine.

The exhalation temperature deviated slightly for the source manikin and significantly for the target manikin. The exhalation of the source manikin was determined to be 37.5 °C to compensate for the disparity in density due to the humidity difference between the respiratory tract and atmospheric air and to compensate for a tracer gas concentration of 4%. During the measurements the exhalation temperature varied between 35.5 °C to 36.5 °C. The deviation is small however it might have created some uncertainty. The exhalation temperature of the target manikin deviated significantly more. The exhalation temperature varied between 22.8 °C to 25.6 °C. The targeted temperature was 34 °C. The uncertainty caused by the deviation is deemed small compared to other deviations such as the surface temperature.

When the breathing measurements were started a calculation error was made when the artificial lung. The airflow from the lungs was double the targeted value which was 10.5l/min. The increased flow rate and the surface temperature are deemed the main reason for the deviation from the exposure measured by Zhang et al. [2022].

### 3.4 Measurement time

In general, the measurement period was long enough to achieve stable results for most cases. The calculated value depends on the size of the data set and how many peaks are present. In appendix K it was found that the average should be calculated over a minimum of 2 hours to reduce the relative error below 10%. A large enough data set was acquired for most cases, however, the tracer gas measurements for cough profile 1 with a distance of 1.5 m had a smaller data set. The expected error is therefore expected to be.

Furthermore, the low exposure found from cough profile 1 compared with cough profile

2 may suggest that the measurement period should be even longer to get stable results. As described in K the average time does not seem to be long enough especially in short distances. For more precise exposure the measurements should be carried out for a period of more than 4 hours for the short distances to determine the exposure more precisely.

### **3.5 Coughing machine**

The coughing machine was built to match the manikins. This includes the height to the mouth opening. For the thermal manikins, the height to the mouth opening is 1.54 m. The height to the opening of the coughing machine is 1.56 m. The centerline of the cough starts above the mouth opening. Identifying the influence of this discrepancy is however difficult as there exists a lack of comparable measurements for coughing. The height should be adjusted for further studies to remove the uncertainty.

Exposure for coughing has not been investigated thoroughly as opposed to breathing. Identifying which parameters influence the exposure for a cough is paramount to understand how to prevent cross-infection from coughs. The factors investigated in the breathing scenario to reduce cross-infection should also be performed for coughing. This includes but is not limited to orientation, ambient temperature, the geometry of the mouth and the other parameters listed by Nielsen and Xu [2021]. To investigate these parameters further improvements would have to be made on the coughing machine. It should be made possible to adjust the temperature of the cough. To give a better understanding of the generated flow, the machine should be able to perform smoke measurements. It is currently not possible due to the pressure in the tank.

### **3.6 Exposure for scenarios with combined respiratory activities**

The equation presented earlier to calculate the exposure for a combined scenario with multiple respiratory activities needs to be studied further. The assumptions work in the traditional cases where exposure has been calculated however further research has to be made. The exposure for a cough should also be investigated in the same scenarios as breathing. When a database of different exposures can be made combined scenarios can easily be calculated following the assumptions. The assumption should be investigated further to ensure when they are valid or adjustments must be made to take them into account.

# Conclusion 4

---

The main purpose of the master thesis was to investigate how coughing affects the cross-infection risk in an indoor environment. To do this several sub-tasks needed to be investigated beforehand for the main purpose to be answered in the experimental study.

The boundary for the indoor environment was investigated and determined based on previous studies to ensure conformity. Furthermore, the results of this master thesis can be used together with previous studies for exposure in different settings. Among these were the ventilation rate. The ambient temperature was only monitored during the study and was on average between 22°C to 23°C. The ambient temperature influence has been investigated previously for breathing but not for coughing.

In the literature review, a detailed description of boundary conditions was given. The conclusion of the literary review revealed that further studies were needed for all boundary conditions to be defined and validated. For this study most of the boundary conditions were provided through the literature however the mouth opening area used in the study was not the same as that found in the literature review. For future studies, the effect of the mouth opening area and cavity should be investigated to determine its influence on the exposure.

The coughing machine was designed to build pressure using pressurized gas and release it in a short burst. The machine was able to reproduce the flow profile of a theoretical cough from the literature review. The CPF<sub>R</sub> of the coughing machine was adjustable so different flow rates could be measured. The machine managed to follow the decay of theoretical profiles. The PVT of the machine was measured along the CPF<sub>R</sub> and it was found that the PVT was shorter for the machine compared to theoretical models. This discrepancy was reduced with reductions in the flow rate however due to the design of the machine no further adjustment could be made. The velocity profiles showed signs of a vortex flow from the machine with the given mouth opening. A clear decay in velocity was measured for the center line. It was observed that the decay in velocity in the vortexes was slow compared with the center line until 1.5 m.

The main research purpose was to investigate the cross infection for a cough. The experimental study determined exposure for two similar cough profiles after 1 m. At the shortest distance of 0.35 m a significant contrast could be seen between the two profiles. The case with the lowest flow, cough profile 2, had the highest exposure of 4 while the case with the highest flow rate, cough profile 1, had the lowest exposure of 2. The reasoning was discussed and determined to be that the measurement period for the exposure at short distances was not long enough and should be more than 4 hours. The study found that the exposure was significant until a distance of 2 m.

When comparing with breathing it was found that the best way to compare different respiratory activities exposure was to calculate a weighted exposure. This calculated weighted the exposure with regards to the volume of each activity, the frequency of the activity, and the initial concentration. The combined exposure was found to provide a way how investigating new cases with combined respiratory activities given the exposure under the same boundary conditions has been measured for each individual activity.

The general conclusion for the master thesis is that a person can be exposed over large distances under the conditions of the experiment and that the exposure between the different respiratory activities cannot easily be compared but should rather be weighed against each other at the basic characterization of the airflow is different between each activity.

# Bibliography

---

- Ai and Melikov, 2018.** Z.T. Ai and A.K. Melikov. *Airborne spread of expiratory droplet nuclei between occupants of indoor environments: A review*. Indoor Air, 28, p. 500–524, 2018.
- Artman et al., 2008.** Nikolai Artman, R. Vonbank and Rasmus Lund Jensen. *Temperature Measurements Using Type K Thermocouples and the Fluke Helios Plus 2287A Datalogger*. Dept. of Civil Engineering. Aalborg University, Technical Reports No. 52, 2008.
- ASHRAE, 2009.** ASHRAE. *ASHRAE HANDBOOK: FUNDAMENTALS*. ASHRAE, 2009. ISBN 978-1-933742-55-7.
- ASL, 2022.** ASL. *Precision Thermometer F200 Series*, 2022. URL <https://www.instrumart.com/assets/ASL-f200-datasheet.pdf>. Visited: 01-11-2022.
- Bjørn, 2000.** Erik Bjørn. *Simulation of Human Respiration with Breathing Thermal Manikin*. Dept. of Building Technology and Structural Engineering, Aalborg University. Indoor Environmental Engineering, R9944, 2000.
- Cao et al., 2014.** Guangyu Cao, Peter V. Nielsen, Chunwen Xu and Rasmus Lund Jensen. *Experimental Study of the Cross-infection Risk due to the Cross-flow of Exhaled Airflows and a Plane Jet with Protected Occupied Zone Ventilation*. ASHRAE 2014 Annual Conference, 2014.
- Chen et al., 1993.** Q. Chen, M. Evert, J. Heikkinen, C. Inard, A. Moser, P.V. Nielsen and G. Whittle. *Room Air and Contaminant Flow, Evaluation of Computational Methods Annex 20: Air Flow Patterns within Buildings*, International Energy Agency, 1993.
- Ding et al., 2021.** Shirun Ding, Zhen Wei Teo, Man Pun Wan and Bing Feng Ng. *Aerosols from speaking can linger in the air for up to nine hours*. Building and Environment, 205, 2021.
- Duguid, 1946.** J.P. Duguid. *The size and the duration of air-carriage of respiratory droplets and droplet-nuclei*. J Hyg (Lond), 44, 471–479, 1946.
- Engen, 1985.** Hans Engen. *Forureningsfordeling i ventilerede lokaler*, Institut for Bygningsteknik, Aalborg Universitetscenter, 1985. URL [https://vbn.aau.dk/ws/portalfiles/portal/198758309/Forureningsfodeling\\_i\\_ventilerede\\_lokaler.pdf](https://vbn.aau.dk/ws/portalfiles/portal/198758309/Forureningsfodeling_i_ventilerede_lokaler.pdf).
- Engineering, 2022.** Omega Engineering. *What is a type K Thermocouple?*, 2022. URL <https://www.omega.com/en-us/resources/k-type-thermocouples>. Visited: 01-12-2022.

- Group, 2018.** BMI Group. *Icopal Handbook 9*, 2018. URL <https://bmigroupdanmark.dk/losningar/digitale-varktojer/icopal-handbog/11-tabeller-og-diagrammer>. Visited: 01-02-2022.
- Gupta et al., 2009.** Jitendra K. Gupta, Chao-Hsin Lin and Qingyan Chen. *Flow Dynamics and Characterization of a Cough*. *Indoor Air*, 19, 517–525, 2009.
- Hansen et al., 2013.** H.E. Hansen, P. Kjerulf-Jensen and Ole B. Stampe. *Varme og klimateknik*. Danvak ApS, 2013. ISBN 978-87-982652-0-7.
- Hyldgard et al., 1997.** Carl Erik Hyldgard, E. J. Funch and M. Steen-Thøde and. *Grundlæggende Klimateknik og Bygningsfysik*. Paperback. Aalborg Universitet, 1997. ISBN 1395-8232 U9714.
- Instruments, 2022.** National Instruments. *NI-9216 Specifications*, 2022. URL <https://www.ni.com/docs/en-US/bundle/ni-9216-specs/page/overview.html>. Visited: 01-11-2022.
- Isotech, 2022.** Isotech. *Isocal-6 Venus Plus 2140*, 2022. URL [http://www.isotechna.com/v/vspfiles/product\\_manuals/Isotech/Venus%202140.pdf](http://www.isotechna.com/v/vspfiles/product_manuals/Isotech/Venus%202140.pdf). Visited: 01-11-2022.
- Johra, 2020.** Hischam Johra. *Assembling temperature sensors: thermocouples and resistance temperature detectors RTD (Pt100)*. Dept. of Civil Engineering. Aalborg University, DCE Lecture Notes No. 78, 2020.
- Kristensen et al., 2015.** Martin Heine Kristensen, Jakob Søland and Rasmus Lund Jensen. *Air Temperature Measurements Using Dantec Draught Probes*, Dept. of Civil Engineering. Aalborg University, 2015. URL <https://vbn.aau.dk/en/publications/air-temperature-measurements-using-dantec-draught-probes>.
- Leach, 2007.** Richard M Leach. *Symptoms and signs of respiratory disease*. *Medicine*, 36, 2007.
- Leung, 2021.** Nancy H.L. Leung. *Transmissibility and transmission of respiratory viruses*. *Nature Reviews*, 19, p. 528–545, 2021.
- Liu et al., 2017.** L. Liu, Y. Li, P.V. Nielsen, J. Wei and R.L. Jensen. *Short-range airborne transmission of expiratory droplets between two people*. *Indoor Air*, 27, 2017.
- LumaSense, 2017.** LumaSense. *Innova Multi-Gas Monitoring Instruments*, 2017. URL <https://innova.lumasenseinc.com/manuals/1412i/>.
- LumaSense, 2016.** LumaSense. *1412i Photoacoustic Gas Monitor*, 2016.
- LumaSense, 2008.** LumaSense. *1303 Multipoint Sampler and Doser*, 2008.
- Mensor.com, 2005.** Mensor.com. *Operation Manual Digital Pressure Gauge Series 2100*, 2005.
- Nedergaard et al., 2022.** Cille Boldsen Nedergaard, Daniel Dieter Pedersen, Iris Magnea Hlynsdottir, Jeppe Høvring Broe, Jonas Lindegaard Mikkelsen and Sofie Kjølby Niss. *Airborne transmission and cross-infection*, Aalborg University, 2022.

- Nicas et al., 2005.** Mark Nicas, William W. Nazaroff and Alan Hubbard. *Toward Understanding the Risk of Secondary Airborne Infection: Emission of Respirable Pathogens*. Journal of Occupational and Environmental Hygiene, 2, 143–154, 2005.
- Nielsen and Xu, 2021.** Peter V. Nielsen and Chunwen Xu. *Multiple airflow patterns in human microenvironment and the influence on short-distance airborne cross-infection - A review*. Indoor and Build Environment, 31, 2021.
- Nielsen et al., 2011.** Peter V. Nielsen, Inés Olmedo, Manual Ruiz de Adana, Piotr Grzelecki and Rasmus Lund Jensen. *Airborne Cross-Infection Risk Between Two People in a Displacement Ventilated Room*. ASHRAE, 2011.
- Olemdo et al., 2012.** I. Olemdo, P.V. Nielsen, M. Ruiz de Adana, R.L. Jensen and P. Grzelecki. *Distribution of exhaled contaminants and personal exposure in a room using three different air distribution strategies*. Indoor Air, 22, 64–76, 2012.
- PHYWE, 2023.** PHYWE. *Cobra SMARTsense spirometer operating instructions*, 2023. URL <https://www.phywe.com/equipment-accessories/measurement-devices/physiology-measuring-instruments/cobra-smartsense-spirometer-sensor-for-measuring-the-respiratory-volume-10-l-s-bluetooth-2052/>. Visited: 01-05-2023.
- Qian and Li, 2010.** H. Qian and Y. Li. *Removal of exhaled particles by ventilation and deposition in a multibed airborne infection isolation room*. Indoor Air, 10, 2010.
- Sensirion, 2015.** Sensirion. *Datasheet evaluation Kit EK-H4*, 2015.
- Stampe, 2000.** Ole B. Stampe. *Danvak Ventilationsteknik*. Hardback. Danvak ApS, 2000. ISBN 87-987995-0-9.
- Toolbox, 2023a.** Engineering Toolbox. *Universal and Individual Gas constant*, 2023a. URL [https://www.engineeringtoolbox.com/individual-universal-gas-constant-d\\_588.html](https://www.engineeringtoolbox.com/individual-universal-gas-constant-d_588.html).
- Toolbox, 2023b.** Engineering Toolbox. *Air - Composition and Molecular weight*, 2023b. URL [https://www.engineeringtoolbox.com/air-composition-d\\_212.html](https://www.engineeringtoolbox.com/air-composition-d_212.html).
- Wang et al., 2021.** Chia C. Wang, Kimberly A. Prather, Josué Sznitman, Seema S. Lakdawala, Zeynep Tufekci and Lindsey C. Marr. *Airborne transmission of respiratory viruses*. Science, 373, 2021.
- WHO, 2021.** WHO. *Coronavirus disease (COVID-19): How is it transmitted?*, 2021. URL [https://www.who.int/emergencies/diseases/novel-coronavirus-2019/question-and-answers-hub/q-a-detail/coronavirus-disease-covid-19-how-is-it-transmitted?gclid=CjwKCAjw-IWkBhBTEiwA2exyO9astEBXDuwWbFLLYCaImujuBzvEYIqHAeptJ-AifzMIhRssbahARoC1xcQAvD\\_BwE](https://www.who.int/emergencies/diseases/novel-coronavirus-2019/question-and-answers-hub/q-a-detail/coronavirus-disease-covid-19-how-is-it-transmitted?gclid=CjwKCAjw-IWkBhBTEiwA2exyO9astEBXDuwWbFLLYCaImujuBzvEYIqHAeptJ-AifzMIhRssbahARoC1xcQAvD_BwE). Visited: 01-06-2023.
- William G. Lindsley et al., 2010.** Françoise M. Blachere William G. Lindsley, Robert E. Thewlis, Abhishek Vishnu, Kristana A. Davis, Gang Cao, Jan E. Palmer, Karen E. Clark, Melanie A. Fisher, Rashida Khakoo and Donald H. Beezhold.

*Measurements of Airborne Influenza Virus in Aerosol Particles from Human Coughs.*  
Plos One, 5, 2010.

**Zhang et al., 2022.** Chen Zhang, Peter V. Nielsen, Li Liu, Emilie Tranegaard Sigmer, Sarah Ghoreishi Mikkelsen and Rasmus L. Jensen. *The source control effect of personal protection equipment and physical barrier on short-range airborne transmission.* Building and Environment, 211, 2022.

Part I

Appendiks

# Scientific Article A

## Cross infection risk in indoor environments for different respiratory activities: A review

Simon Madsen<sup>a</sup>

<sup>a</sup>*Department of the Built Environment, Aalborg University, Denmark*

---

### Abstract

This article reviews cross-infection between people in indoor environments. The review focuses on different respiratory activities and sets up boundary conditions for experiments and numerical studies. Attention is made to how these activities can be reproduced in an experimental setup. For the respiratory activities the origin, mouth opening area, droplet profile, flow profile, and direction of flow are described.

---

### Cross-infection risk

Cross-infection between two persons can occur in multiple ways and from different types of contaminants such as viruses, bacteria, and more. One way of cross-infection is through inhaling contaminants. Airborne transmission often occurs indoors by the generation and spread of infectious droplets nuclei from an infected person[Tang et al., 2006]. The droplets are then inhaled by an exposed person for the airborne transmission to be successful. Each inhalation of contaminated air has an inherent risk of infection and can be evaluated based on a critical dose, which is the amount of infectious material needed to be infected. The critical dose is lower for more infectious diseases[Riediker et al., 2022]. The airborne transmission comes from droplets expelled during respiratory activities infected with pathogens that are small enough or evaporate to become small enough to be carried with the air-

flow from the respiratory activity and the air flows in the room. The spread of droplet nuclei and aerosols is affected by the interaction between ventilation flows, human boundary layer flow, and respiratory flow[Ai and Melikov, 2018]. Ventilation is especially important as the aerosols can linger for up to nine hours if not removed. The half-life of aerosols in stagnant air is 87.2 minutes. Therefore a person can be infected by an infected person long after the initial release of the aerosols[Ding et al., 2021].

### Microenvironment

The human microenvironment around our body affects our breathing and thermal sensation directly. The flow patterns in the microenvironment affect cross-contamination significantly. The main flow patterns are the exhalation, inhalation, and the thermal boundary layer [Nielsen and Xu, 2021]. Both Nielsen [2009] and Melikov [2004] indicated that

Simon Madsen

for aerosol transmission in short ranges, the interaction of the airflow patterns in the human microenvironment is crucial. For short ranges, the air flows in the microenvironment heavily affect the route of airborne transmission. For longer distances, the air flows affect the exposure [Nielsen and Xu, 2021].

The thermal boundary layer is a zone surrounding the human body. The boundary layer is a result of the convective flow induced by the heat loss along the human body. The temperature gradient between the surface of the human body and the surrounding cooler air is what generates this upward convective flow. The boundary layer ens above the head where the convective flow develops into a thermal plume[Licina et al., 2015]. The thermal boundary layer does however not protect us against all cross-infection. In the scenario of two people standing in front of each other and one of them being contaminated is considered then the infected individual can still infect the other. There are mainly two modes of cross-infection with aerosolized particles, directly or indirectly. Direct cross-infection occurs when the airflow from the infected person is strong enough to penetrate the breathing zone of an opposing person. The indirect route comes from the entrainment into the thermal boundary layer from the surrounding air, especially in the lower regions of the room[Bjørn and Nielsen [2002]. The contaminants that get entrained are then carried along the convective flow to the breathing region[Licina et al., 2015]. The convective boundary layer is shown in figure 1



**Figure 1** Convective boundary layer of a human. The thermal plume can be seen above the head.[Craven and Settles, 2006]

Nielsen and Xu [2021] summarized the parameters that influence the cross-infection risk between two people with a short distance between them. The parameters are listed below.

- Distance between people
- Orientation and position of people
- Mouth and Nose geometry
- Breathing process
- Movement
- Respiratory activity
- Number of people
- Face mask
- Temperature at head height
- Difference in height of people
- Activity level
- Virus concentration in the surroundings
- Temperature and temperature gradient in the microenvironment
- Air velocity
- Turbulence level

These are the parameters as listed by Nielsen and Xu [2021], that affect cross-infection risk in microenvironment. The cross-infection risk at longer distances is

also affected by the macro-environment such as ventilation among others [Bjørn and Nielsen, 2002].

### Macroenvironment

The macro-environment also affects the cross infection. The main parameters within the macroenvironment that affects the cross-infection are the ventilation and the ambient temperature.

### Ventilation

Ventilation is considered one of the most influential parameters for reducing airborne cross-infection. Personalized ventilation and exhaust have also shown great effect in reducing airborne transmission [Ai and Melikov, 2018]. Studies have been inconsistent with which ventilation principle is better for reducing cross-infection as they are efficient at different times. Which ventilation principle is the most effective depends on many parameters such as the distance between the persons. Displacement ventilation was found to be more effective by some studies noting the vertical diluting as the main reason. Other studies found that mixing ventilation was better as it reduced the travel distance of the aerosols. The studies also noted that displacement ventilation comes with the risk of the aerosols being trapped due to stratification [Ai and Melikov, 2018]. No matter the system the air change rate is an important factor to reduce the cross-infection. It was found by Ding et al. [2021] that the half-life of aerosols could be reduced from 87.2 minutes to just 4-6 minutes with a higher air change. Much effort has been used on finding the exposure for breathing in different ventilation scenarios however only a few studies

have done the same for other respiratory activities.

### Temperatures

The temperature gradient in the room has already been described to have the ability to reduce the cross-infection risk through the effectiveness of displacement ventilation. However, the ambient temperature also affects the cross-infection risk. In rooms with mixing ventilation, so no temperature gradient, it has been shown that the ambient temperature can both reduce and increase the cross-infection risk. When the ambient air temperature is colder the cross-infection risk is reduced as the centerline from human exhalation is moved upwards due to the temperature differences. In warmer temperatures, it was found to be the direct opposite where the centerline moved downwards. When the ambient temperature and the exhalation temperature were identical it was found that the exhalation stratified [Nielsen et al., 2022]. The effect of the ambient temperature is shown in figure 2 on page 4.

### Definition of respiratory activity and origin

The respiratory system is comprised of many parts. In this report, the respiratory system will be divided into 3 modes or systems based on where the droplets originate. The 3 modes are listed below [Johnson et al., 2011].

1. Bronchiolar Mode
2. Laryngeal Mode
3. Oral Mode

The Bronchiolar Mode is associated with breathing and occurs in the lower respiratory tract (lower airway). The Laryn-

Simon Madsen

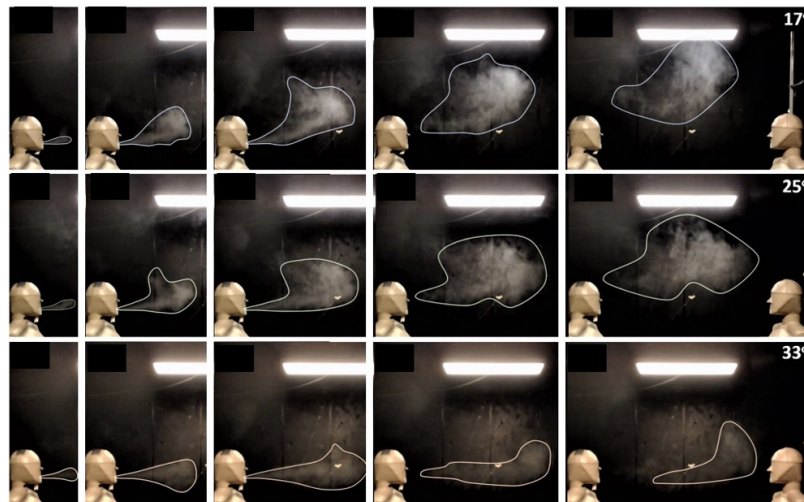


**Figure 2** The movement of exhaled air during breathing cycle at different ambient temperatures.[Nielsen et al., 2022]

geal mode is associated with vocalization and occurs in the region around the larynx. The Oral Mode is mainly associated with speech and occurs in the upper respiratory tract including the oral cavity [Johnson et al., 2011]. Respiratory activities are generally associated with one or more modes and will be explored in-depth for breathing, coughing, sneezing, and speech in the following sections. The origin and how the respiratory activity is generated is important knowledge when evaluating cross-infection, as the origin of the activity often determines the size of the droplets released during expiration.

### Breathing

Breathing is the simplest respiratory activity. Breathing comes from the movement of the expansion and deflation of the lungs. Breathing consists of two activities, inspiration (inhalation) and expiration (exhalation). During inspira-

tion, the thorax is expanding resulting in a lower pressure inside the lungs compared with the surrounding atmospheric air. Due to the lower pressure air is sucked into the lungs. The pressure is afterward increased by decreasing the size of the thorax resulting which result in expiration[Thomas et al., 2023]. Breathing is associated with the Bronchiolar mode, as the process occurs in the lower respiratory tract[Johnson et al., 2011]. During breathing the larynx does not affect the breathing process significantly. In the larynx, the vocal cords are abducted to allow airflow through. In the upper respiratory system, the main event during breathing is whether the soft palate arches upwards against the top of the pharynx or not. If the soft palate arches towards the pharynx breathing is through the mouth. When the soft palate is relaxed breathing occurs through the nose[Thomas et al.,

2023]. Normal quiet breathing normally occurs through the nose unless blocked. During periods where a higher airflow is required, periods with high metabolic rates such as exercise, the breathing occurs through the mouth.

#### **Coughing**

Coughing consists of three phases, an inspiratory, a compressive phase, and an expulsive phase which is associated with the Laryngeal and Oral modes. The inspiratory phase is generally short and is an inspiration of air [Fontana, 2008]. The second phase is a force expiratory effort against adducted vocal cords [Thomas et al., 2023]. The vocal cords are however only adducted initially as they are actively opened in the third and final phase resulting in a rapid expiration flow [Fontana, 2008]. A cough is different from the expiration reflex. The cough has a preparatory inspiration which the expiration reflex does not. They also differ in their purpose. The expiration reflex is to prevent aspiration into the lungs (clearing the airways from foreign debris like food) while a cough clears the lower airways from debris and mucus. A cough is rarely in an isolated form and often consists of both cough and expiration reflexes [Fontana, 2008].

#### **Sneezing**

Sneezing is like a cough a defense mechanism. Sneezing is not associated with a specific mode, however, looking at the bimodal droplet distribution found by Han et al. [2013] and it can be assumed that a sneeze consists of multiple modes. Han et al. [2013] shows a clear indication that a sneeze is associated with both the laryngeal and oral modes. A sneeze is a

response to irritants in the upper airways specifically the nasal cavity. It has been found that sneezing can also occur due to more abnormal reasons such as bright light. A sneeze, like coughing, consists of two distinct phases, an inspiration phase and a violent expiration phase [Özlem Önerci Celbi and Önerci, 2023]. During sneezing the abdominal muscles contract and pushes the abdomen against the diaphragm, forcing it up into the chest resulting in the expulsion of air from the lungs. These muscles are especially active during sneezing and coughing compared to normal breathing [Thomas et al., 2023].

#### **Speech**

Speech is a complicated respiratory activity. Speech is a combination of phonation, articulation, and resonance. Phonation occurs in the larynx by the vibration of the vocal cords. Phonation is the source of speech. Articulation is what shapes the sound/voice from phonation into speech. Articulation is the process of moving elements to join them, in the production of speech an example would be the movement of the tongue or lips to articulate a specific sound. The articulatory system consists of both immobile and mobile articulators that exist in the oral cavity, the pharynx, and the nasal cavity. How the articulatory system produces a specific sound is due to the resonant frequency. We use the mobile parts of the articulatory system to change the resonant frequency to produce a specific sound. The following sections describe both the importance of the vocals used for the study of speech and how loudness also should be considered [Seikel et al., 2019].

Simon Madsen

### Vocals

As mentioned above the articulatory system moves to change the resonant frequency. This also changes the resulting flow. Different articulations/syllables/phrases result in a different airflow from the mouth. The difference can be seen in figure 3 on page 7, which shows the difference in the air velocity at the mouth opening for different syllables. The vocals pronounced do therefore influence the conditions of the flow from our mouth. Therefore the contaminants people spread are dependent on what is articulated. From this, it can be assumed that for a short burst of speech, a large variation in flow characteristics can be observed, but would move to an average value for a phrase as it consists of many different vocals [Han et al., 2021].

The literature used to produce the flow profiles uses different vocals for their data. The vocals known are counting from 1 through 10 and pronouncing different letters of the alphabet. The vocalization of sounds is important for the flow rate that needs to be used. Counting from 1 through 10 is often used in the study of speech, whereas phrases often vary between studies.

### Loudness of voice

The loudness of the voice during vocalization is also an influencing factor on the particles emitted during speech. The number of particles emitted per second is linearly correlated with the root mean square amplitude ( $A_{rms}$ ). The increase in particles was present in the vocalization of a single vowel and for a phrase. Figure 4 shows the correlation between the particle emission and  $A_{rms}$ , where

$A_{rms}$  of 0.45 roughly corresponds to a loudness of 98 dB. The particle emission rate should not be considered an absolute value and should be perceived in relative terms due to limitations [Asadi et al., 2019]. The same study by Asadi et al. [2019] also found that the droplet distribution remained despite the loudness of the voice, The study also found that no matter the voice loudness, certain test subjects could be considered super emitters as they produced significantly higher particle emission rates than the other subjects at the same voice amplitude.

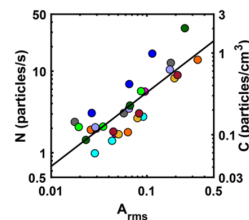


**Figure 4** Particle emission rate with regards to loudness for 10 subjects. The graph is color coded after participants and the solid line is a power law fit with a correlation coefficient of  $p = 0.865$  [Asadi et al., 2019].

### Mouth opening area

The mouth opening area significantly affects the results of some of the literature and can be used to link the measured initial peak velocities and peak flow. Many studies use a PIV system to measure the instantaneous velocity, but provide little to no information about the mouth opening area or the peak flow rate. To ensure conformity between the literature it is important that mouth opening area and how it varies between different respiratory activities. The mouth opening area is mentioned in very few studies and

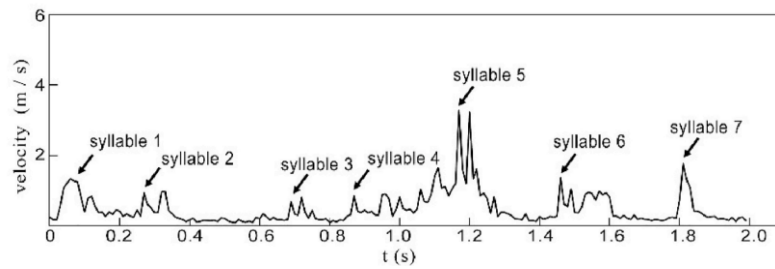


Figure 3 Velocity for speech at the mouth opening [Han et al., 2021].

is often based on only a few subjects. In general, Gupta et al. [2009] and Gupta et al. [2010] are used for many numerical studies and have a large data set, however, they do not mention the mouth opening area for sneezes. This is a clear lack in the literature and can affect the results significantly if new and more reliable data is found.

#### Mouth opening area during breathing

The mouth opening area during breathing is similar between the gender, with small variance. The mouth opening area is shown below for both gender and the variance between the subjects. The opening area is the average based upon 8 male and 8 female subjects during a study for breathing and coughing. The same study found that the opening area is independent of the body surface area for both the mouth opening as well as the nose opening. The nose opening is also shown for the breathing process. The below statements give the mouth and nose opening areas with 95% confidence [Gupta et al., 2010].

Mouth opening area:

- Mouth opening area=  $1.20 \pm 0.52$  cm<sup>2</sup> for male

- Mouth opening area=  $1.16 \pm 0.67$  cm<sup>2</sup> for female

Nose opening area:

- Nose opening area=  $0.71 \pm 0.23$  cm<sup>2</sup> for male
- Nose opening area=  $0.56 \pm 0.10$  cm<sup>2</sup> for female

#### Mouth opening area during coughing

The mouth opening area expands for a cough. The opening area is different for males and females and is shown below. It was shown that the mouth opening area is independent of the height of the subject. The opening area has a large variation however the opening area was larger than for both breathing and sneezing for all subjects during the measurements [Gupta et al., 2009]. Another study is consistent with Gupta et al. [2009], however, it is an estimate of only 1 subject [Bourouiba et al., 2014].

- Mouth opening area=  $4.00 \pm 0.95$  cm<sup>2</sup> for male
- Mouth opening area=  $3.370 \pm 1.4$  cm<sup>2</sup> for female

How the opening area develops during a cough is also shown in figure 5 from the same study.

Simon Madsen

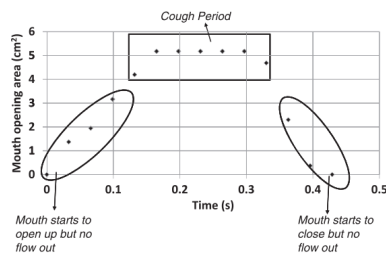


**Figure 5** Mouth opening area during a cough [Gupta et al., 2009].

**Mouth opening area during sneezing**

The mouth opening area for sneezing is similar to that of breathing. The mouth opening does not expand during the event as it does during a cough which produces higher velocities but a smaller flow rate. The mouth opening area during a sneeze is approximately 1.3 cm<sup>2</sup> based on 1 subject. The area of the mouth is visualized in figure 6 from Busco et al. [2020]. Both a cough and a sneeze are considered violent respiratory events, however, since the mouth area is smaller the flow rate is also smaller for a sneeze.

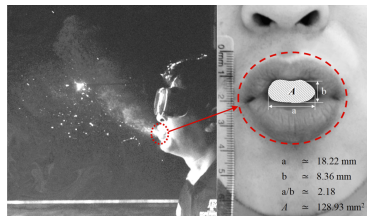


**Figure 6** Mouth opening area during sneezing [Busco et al., 2020].

**Mouth opening area during speech**

During speech, the mouth opening is one of the factors that determine the produced sound. The mouth opening area varies for different syllables. The mouth

opening area is shown for the numbers 1 through 10. The variation is shown in figure 7 and shows a clear difference, however, normal speech is continuous and the variation of the mouth opening area would be a sequence of the individual vocals of the pronounced phrase. It would then be more accurate to use the average mouth opening area for all the vocals. The figure shows the numbers 1 to 10 as an example and argues it could be used as a representation of the mouth opening area during speech [Gupta et al., 2010]. The average opening area for the numbers is 1.8 cm<sup>2</sup>[Gupta et al., 2010].

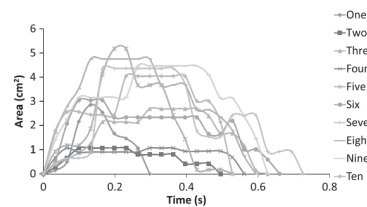


**Figure 7** Mouth opening area during speech [Gupta et al., 2010].

**Droplet and aerosol profile**

The droplet size distribution is an important factor when evaluating the exposure and cross-infection risk. As mentioned above there are three distinct modes associated with respiratory events. The active modes determine the droplet distribution and the origin is therefore important. In the following sections, the droplet distributions will be discussed for breathing, coughing, sneezing, and talking. Some respiratory activities are associated with multiple modes creating complicated profiles such as coughing [Johnson et al., 2011]. The general droplet distribution for the three modes is shown in

figure 8.

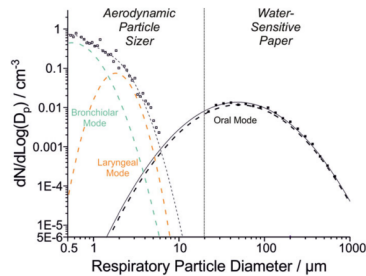


**Figure 8** General droplet distribution associated with the three modes in the respiratory tract [Harrison et al., 2023]. The split in the middle comes from the use of different methods to cover a bigger range of droplet sizes.

### Breathing

As described earlier breathing is associated with the bronchiolar mode. The bronchiolar mode does produce smaller droplets and aerosols compared to the other modes. The bronchiolar mode happens deep in the respiratory tract. The particles from the bronchiolar mode are in general the smallest type of aerosols, generally  $\leq 1 \mu\text{m}$ . The droplet distribution is shown in figure 8 in green. Breathing is not a violent respiratory activity and does not create significant movement or vibration in the respiratory system to release larger droplets [Harrison et al., 2023]. This is in good agreement with both Johnson et al. [2011] and Gregson et al. [2021].

### Coughing

Coughing is associated with multiple modes resulting in a varied distribution of particle size. A study has found that the highest count of droplets in coughing is under  $0.6 \mu\text{m}$  [Papineni and Rosenthal, 1997]. Using the same method

it was found that 82% of the droplets was centered in the range of  $0.74\text{-}2.12 \mu\text{m}$  [Yang et al., 2007]. The results found by Chao et al. [2009] is similar to that found by Duguid [1946] despite using different methods. Duguid [1946] used a collection media and microscopic analysis to determine the size class of the droplets. In the upper ranges, the most common particle was in the size  $4\text{-}8 \mu\text{m}$ . The distribution shown in table 1 on page 1 is the droplet count aggregated across 50 coughs [Chao et al., 2009]. Later studies such as Papineni and Rosenthal [1997] and Yang et al. [2007] used sampling-based optical counters, however, these studies do not provide the immediate droplets at the mouth and were influenced by factors such as evaporation and dilution [Chao et al., 2009]. The study by Chao et al. [2009] had a lower detection limit of  $2 \mu\text{m}$  which suggest that a large portion of the particles might have been left out. Johnson et al. [2011] found that the most particles was in the range of  $1\text{-}2 \mu\text{m}$ . Their method used both the aerodynamic particle sizer and a droplet deposition analysis for larger droplets while Harrison et al. [2023] found similar results. Figure 9 on page 9 shows the size distribution of droplets for a cough.

Simon Madsen

**Table 1** Droplets distribution for coughing [Chao et al., 2009]

Range [ $\mu\text{m}$ ]	Size class [ $\mu\text{m}$ ]	Average droplet number count	SD
2-4	3	4.0	3.46
4-8	6	55.0	15.88
8-16	12	20.4	15.44
16-24	20	6.7	4.60
24-32	28	2.5	2.42
32-40	36	2.4	2.37
40-50	45	2.0	2.67
50-75	62.5	2.0	1.41
75-100	87.5	1.4	1.84
100-125	112.5	1.7	1.77
125-150	137.5	1.6	1.84
150-200	175	4.4	2.80
200-250	225	2.5	1.84
250-500	375	2.1	1.20
500-1000	750	1.4	0.97
1000-2000	1500	0.0	0.00

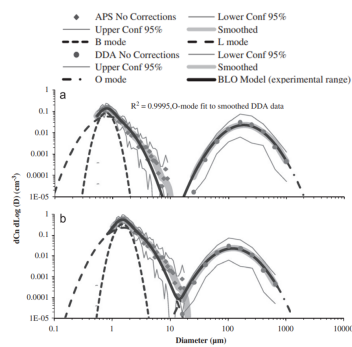


**Figure 9** Particle size distribution, where (a) is the uncorrected data and (b) is the corrected data [Johnson et al., 2011].

Despite the lower number of droplets in the larger ranges, they are not insignificant. If looking at the volume concentration the larger droplets have a significantly large influence than the smaller droplets despite the number difference [Johnson et al., 2011].

### Sneezing

During a sneeze, a larger droplet distribution can be found when compared to

other respiratory activities. This might be due to the effect more unique effect of being able to clear the nasal cavity of irritants compared with other respiratory activities. Duguid [1946] showed a distribution where the most common droplets were in the range of 4-8  $\mu\text{m}$ . The study however used a solid impaction method which was inaccurate because of the collection device [Gralton et al., 2010]. Han et al. [2013] found using a more precise particle size analyzer a significantly larger size distribution. The measurement was also done immediately at the mouth. The most common droplet size of 31.2% was in the range 80-100  $\mu\text{m}$ . The size distribution was found to be similar to that of coughing with two distinct peaks, however, the droplets were in general larger. The peaks found by Han et al. [2013] had a geometric mean of 386.2  $\mu\text{m}$  and 72.0  $\mu\text{m}$  with a geometric standard deviation of 1.5 and 1.7 respectively. The distribution found by Han et al. [2013] was made based using volume % and not the number count of droplets indicating that the number of

aerosolized particles might be higher.

### Speech

In speech the most common droplet size found by Chao et al. [2009] is in size class  $6\ \mu\text{m}$ . The average count of droplets falls off quickly as the second highest count is 9.2 of size class  $12\ \mu\text{m}$ . In table 2 on page 12 the distribution of droplet count is shown for an 11 subject study. The results count is immediately after the mouth opening at a distance of 10 mm. The results are aggregated across counting from 1-100 10 times [Chao et al., 2009]. As with coughing the results are similar to that reported by Duguid [1946]. As the results from the study are based upon a count from 1-100 the average value can be used for more general speech as suggested earlier as it covers a large number of pronunciations.

As with coughing another study by Papineni and Rosenthal [1997] found that the majority of particles was smaller than  $0.6\ \mu\text{m}$ . Another study by Pan et al. [2022] found that 50% of droplets were smaller than  $1.037\ \mu\text{m}$  and 80% was smaller than  $2.642\ \mu\text{m}$ . The study used an aerodynamic particle sizer instead. The study by Chao et al. [2009] had a lower detection limit of  $2\ \mu\text{m}$  suggesting that a large portion of particles might be outside the detection range. As for coughing Johnson et al. [2011] found similar results to both studies. The distribution found by Johnson et al. [2011] is shown in figure 10 on page 11, and suggests that the droplet concentration is highest for smaller particles but the majority of the volume and mass may be caused by larger particles as in coughing [Johnson et al., 2011].

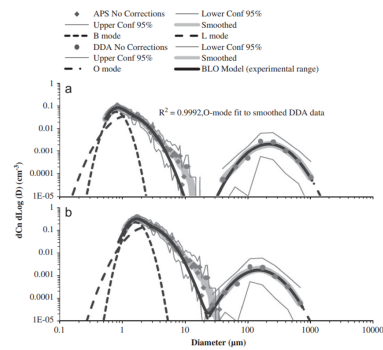


**Figure 10** Particle size distribution, where (a) is the uncorrected data and (b) is the corrected data [Johnson et al., 2011].

### Flow profile

This section will describe the flow profiles generated by different respiratory activities. Changes significantly depending on the activity. Violent respiratory activities such as coughing or sneezing do in general have high flow and velocity profiles when compared to breathing, however, studies show a very large variance in test subjects which should be considered.

#### Breathing

The flow profile from breathing can be represented by a sinusoidal function [Gupta et al., 2010]. The function is defined by the breathing frequency. The breathing frequency has been found to be between  $10\text{-}16\ \text{min}^{-1}$  depending on gender, height, weight and activity level [Gupta et al., 2010][Shimer et al., 1995]. The respiratory frequency is not the same for inhalation and exhalation. In other literature is often assumed to follow a sinusoidal function. The pulmonary rate can be described by equation (1). The

Simon Madsen

**Table 2** Droplets distribution for speech above 2  $\mu\text{m}$  [Chao et al., 2009]

Range [ $\mu\text{m}$ ]	Size class [ $\mu\text{m}$ ]	Average droplet number count	SD
2-4	3	1.7	1.62
4-8	6	26.8	8.94
8-16	12	9.2	4.67
16-24	20	4.8	4.07
24-32	28	3.2	2.36
32-40	36	1.6	1.03
40-50	45	1.7	0.90
50-75	62.5	1.8	0.98
75-100	87.5	1.3	0.65
100-125	112.5	1.7	1.01
125-150	137.5	1.6	1.03
150-200	175	1.7	1.01
200-250	225	1.5	0.82
250-500	375	1.4	0.50
500-1000	750	0.5	0.82
1000-2000	1500	0.0	0.00

factors can be found from Gupta et al. [2010]. of 1.4-4.15][Gupta et al., 2009][William G. Lindsley et al., 2010].

$$\text{Flow rate} = a \cdot \sin \beta t \quad (1)$$

By calculating the factors necessary factors in Gupta et al. [2010] the flow profile in figure 11 can be created with a peak flow of approximately 0.35 l/s.

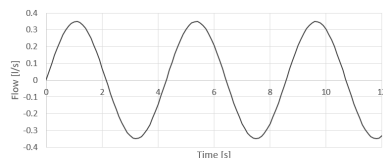


**Figure 11** Flow profile using the geometry of the thermal manikins used in this study [Gupta et al., 2010].

### Coughing

The flow profile for a cough can be found in equation (2)[Gupta et al., 2009]. The profile consists of a quick and rapid acceleration with a slower decay over time. The duration is rather short often only 0.5-1s and a total expelled volume

$$\bar{M} = \frac{a_1 \tau^{(b_1-1)} \exp\left(\frac{-\tau}{c_1}\right)}{\Gamma(b_1) c_1^{b_1}} + \frac{a_2 (\tau - 1.2)^{(b_2-1)} \exp\left(\frac{-(\tau-1.2)}{c_2}\right)}{\Gamma(b_2) c_2^{b_2}} \quad (2)$$

Using the appropriate factors based upon Gupta et al. [2009] and William G. Lindsley et al. [2010] the flow profile shown in figure 12 is found. The findings show conformity with velocity measurements using a PIV system, if the mouth opening area during coughing, that is suggested by Gupta et al. [2009] is used to convert the flow rate to a velocity [Tang et al., 2013][Kwon et al., 2012] [VanSciver et al., 2011][Zhu et al., 2006]. The maximum peak flow rate as suggested by William G. Lindsley et al. [2010] and Lindsley et al. [2013] is 10.5 l/S which is slightly higher than that reported by Gupta et al. [2009] which gives a maximum peak flow rate of 8.5 l/s. Lindsley et al. [2013] data is however based on influenza-positive test subjects which might influence the

flow rate. The equation for the flow profile as suggested by Lindsley et al. [2013] is however not as precise as that reported by Gupta et al. [2009] using a lognormal curve. The lognormal curve does not take the acceleration into account and the flow does not reduce close to 0 l/s, which means that the gamma-probability function suggested by Gupta et al. [2009] should be used.

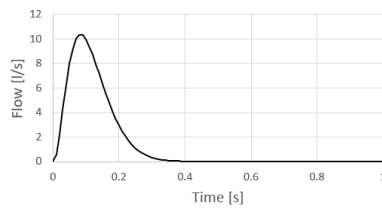


**Figure 12** Flow profile for a cough [Gupta et al., 2009].

### Sneezing

A flow profile was not found in the literature, however, multiple studies have investigated the airflow velocity from the mouth during a sneeze. If it is assumed that the mouth opening area of  $1.3 \text{ cm}^2$  can be used as a representative area, the velocities can be converted to a flow rate. In Han et al. [2021] it was found that the shape of the velocity profile for a sneeze was very similar to that of a cough. The found velocities and corresponding flow rates are shown in table 3 on 14. Through numerical studies, it was found that even though the shape of the flow is the same as a cough the total expelled air volume was significantly lower [Oh et al., 2022b]. The velocities reported by Han et al. [2021] was the airflow velocity as, during the PIV measurements stage fog particles were nebulized into the chamber. This is important as larger droplets can be propelled with

higher velocities than the airflow rate immediately at the mouth opening. The velocities found by Bourouiba [2020] shows a higher velocity range than Han et al. [2021].

Since the shape of the velocity profile from the mouth opening is similar to that of a cough it was found that a gamma-probability function could describe the velocity from a sneeze similar to the work done by Gupta et al. [2009] [Han et al., 2021]. The profile generated is shown in figure 13. The parameters used for the function are shown in table 4. The parameters found by Han et al. [2021] before the peak are identical to that found by Gupta et al. [2009] for a cough, suggesting that the period before the peak flow rate and velocity is reached is consistent between the two respiratory activities.

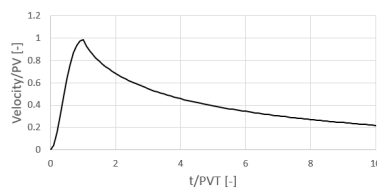


**Figure 13** Velocity profile for a sneeze.

**Table 4** Parameters used for gamma-probability distribution for a sneeze

Parameter	Value [-]
$a_1$	1.68
$b_1$	3.338
$c_1$	0.428
$a_2$	8.184
$b_2$	0.590
$c_2$	16.720

### Speech

The flow and velocity of during speech vary based upon previously mentioned

Simon Madsen

**Table 3** Peak velocities and flow rate

Source	Velocity range [m/s]	Velocity [m/s]	Flow rate [l/s]
Han et al. [2021]	4.64-19.0	11.7	1.52
Bourouiba [2020]	10-30	-	1.3-3.9

factors as well as physiological factors. The velocity of the airflow varies significantly based on the vocal uttered during speech. A study by [Han et al., 2021] investigated the velocity at the mouth opening. The velocity range for both different syllables and the time-averaged velocity is shown in figure 5 on page 15. Both Chao et al. [2009] and Kwon et al. [2012] found slightly lower velocities for speech.

As seen in table 5 there is a large variation from the subjects of the measurements. The large variation is both due to physiological factors but also the different syllables in the speech. The velocities found by Han [Han et al., 2021] correspond well with the results for the flow of a phrase found by Gupta [Gupta et al., 2010] but do give a slightly lower flow. The results achieved in the study are shown in figure 14 on page 15 and show the variation in velocity is also present in the flow rate. The previously mentioned variation for numbers is also present for different letters in the alphabet. The figure shows the flow profile for an uttered phrase. The flow during the phrase varies and supports the earlier statement, that the average value for all the vocals can be used as a representation of the flow during speech.

It can be argued that the flow from speech is almost continuous as the flow is only breaking up during inhalations and natural pauses during speech. The average flow rate is calculated based upon

Gupta et al. [2010] and is 0.131/s for a female subject based upon flow over a phrase. The results found by Han et al. [2013] suggest a lower flow rate for a phrase than Gupta et al. [2010] when converted from a velocity to a flow rate. However, both studies find that the time-averaged flow rate and velocities are significantly lower than instantaneous velocities for certain utterances. The flow rate is summarized in table ?? for letters, numbers, and the phrase.

**Table 6** Flow rate for speech for different patterns[Gupta et al., 2010]

Pattern	Flow Rate [l/s]
Letters	$0.432 \pm 0.115$
Numbers	$0.374 \pm 0.086$
Phrase	$0.128 \pm 0.014$

From the above-provided flow rate, a flow profile can be made assuming the flow rate is constant with individual breaks due to inhalation and natural breaks in speech. In order to determine how often a break occurs, the amount of inhalation in the flow profile provided by Gupta et al. [2010] for a phrase. Inhalation from both mouth and nose was included. The result gives a break roughly every 3 s but will vary significantly depending on the uttered phrase. The inhalation time during breathing last on average 0.5 s and is generally described as both short and fast inhalations[Rochet-Capellan and Fuchs, 2013]. The flow profile can be seen in figure 15

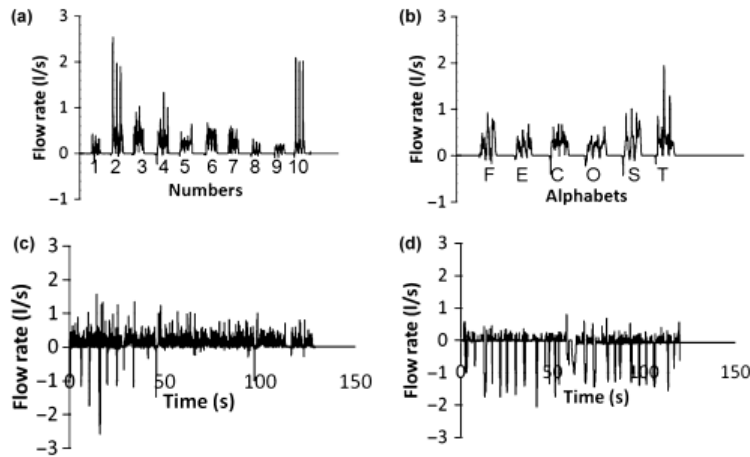


Figure 14 Flow for speech at the mouth opening. c) is the flow rate through the mouth during a phrase, d) is the flow rate through the nose for the same phrase [Gupta et al., 2010].

Direction of flow

This section will describe the direction of the flow generated by each respira-

tory activity. Often in both full-scale and numerical studies, the flow direction is often assumed to be horizontal as this can in many scenarios be considered the

Table 5 Velocity for speech at the mouth opening [Han et al., 2021]

Parameter		Male	Female
Maximum instantaneous velocity [l/s]	Range	1.23-25.3	2.63-11.6
	Ensemble-averaged value	6.65	5.94
Maximum time-averaged velocity [l/s]	Range	0.0771-0.511	0.0948-0.550
	Ensemble averaged value	0.206	0.1

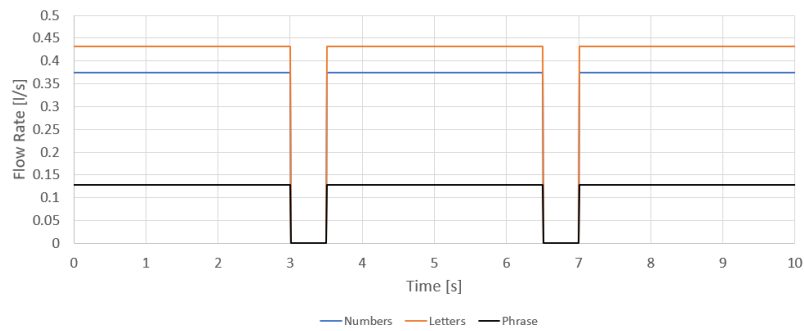


Figure 15 Flow profiles during speech based on different flow rates.

Simon Madsen

worst case. As this section will describe the flow direction differs significantly between activities and people.

### Breathing

For breathing the flow direction relies on whether breathing occurs through the mouth or the nose. Breathing through the nose is already angled due to the nostrils' position. The flow can be described by the spreading angle. The spreading angle can be described from the front, side, or top. According to Gupta et al. [2010] then the front spreading angle is  $21^\circ \pm 10^\circ$  and the spreading angle from the side is  $23^\circ \pm 14^\circ$  for 6 subjects. The spreading angle for breathing through the mouth was however only found for the side perspective where it was  $30^\circ$  on average. It was found that the angle of the flow varies significantly due to a multitude of factors such as the motion of teeth and lips and more, however, the flow could still be considered horizontal since the flow generally follows the centerline [Xu et al., 2015].

### Coughing

In the coughing scenario the cough the generated jet is downward. Gupta et al. [2009] found the direction based on the angle between the horizontal and the top and bottom part of the jet. The angle to the top part was found to be  $15^\circ \pm 5^\circ$ . The angle to the lower part of the jet is  $40^\circ \pm 4^\circ$ . The resulting spreading angle can be calculated too  $25^\circ$ . Assuming the cough is symmetrical around its centerline the angle of the centerline can be determined to be  $30^\circ$ . The centerline angle was found by Chen et al. [2014] was  $35.5^\circ$  for an uncovered cough showing similar results to Gupta et al. [2009]. Further-

more, the angles were investigated for covered coughs showing that the jet splits into two separate air flows.

### Sneezing

For sneezing a significantly smaller spread angle was found, meaning the airflow was more concentrated around the centerline. Both vertical and horizontal have been found by Han et al. [2013] to be  $15.1^\circ$  and  $15.4^\circ$  for vertical and horizontal spread angles respectively. A study by P. Bahl et al. [2021] found a significantly larger spread angle between  $11^\circ$  and  $127^\circ$  based on 5 subjects. It should, however, be noted that the spread angle found by P. Bahl et al. [2021] was based on the trajectories of the expelled droplets and not the airflow found using smoke such as Han et al. [2013] or Gupta et al. [2009] for coughs. P. Bahl et al. [2021] also investigated the mean direction of the flow which was found to be between  $7^\circ$  and  $33^\circ$  from horizontal.

### Speech

Speech is significantly different compared to the other respiratory activities when considering the flow direction and spread angles. During speech, the mouth constantly changes shape, size, and form which affects the flow direction and spread angles. Therefore the data for angle and direction is often based upon a single syllable or word. Han et al. [2013] found that the vertical and horizontal spread angles are different. The vertical spread angle varied between  $16.0^\circ$  and  $96.8^\circ$  and the horizontal spread angle varied between  $19.1^\circ$  and  $96.8^\circ$ . The averaged spread angles were  $52.9^\circ$  and  $42.9^\circ$  for the vertical and horizontal spread angles respectively. The data from Han

et al. [2013] is based on several different words spoken in a span of 10 s. Another study by Kwon et al. [2012] found the spread angles for speech using the words *Dul* for males and females. He found that the spread angle for females was significantly higher with an average spread angle of  $77.7^\circ$  based on 9 female subjects. The spread angle for males was on average  $49.3^\circ$  based on 17 male subjects.

**Summarized boundary conditions**

The boundary conditions for the different respiratory activities. The summarized boundary conditions from literature can be seen in table 7 on page 18 for breathing, table 8 on page 19 for coughing, table 9 on page 20 for sneezing and table 10 on page 21 for speaking.

**Table 7** Boundary conditions for breathing. The results are for both genders and the mean value unless different is stated. For the droplet distribution, the most common size is shown. The person used for the calculation of boundary conditions for articles that provides equations has a surface area of 1.44 m<sup>2</sup>. F/D Method=Methodology for measuring flow/velocity and droplet size/concentration, MFR=Minute Flow Rate, PV=Peak Velocity, RF=Respiratory Frequency, MOA=Mouth Opening Area, DD=Droplet Distribution, SM=Spirometer, AM=Anemometer, SI, Shadowgraph Imaging, RS=Respirometer, APS=Aerosols Particle Sizer, M=Male, F=Female, U=Unknown Gender, W=Weight, H=Height, and SD=Standard Deviation.

Source	Subjects	F/D Method	MFR [l/min]	PV [m/s]	RF [min <sup>-1</sup> ]	MOA [cm <sup>2</sup> ]	DD [µm]
Gupta et al. [2010]	M:13	SM	6.97-8.4	-	77.03-45.42H+0.2373W	1.20 ± 0.52	-
	F:12	SM	6.36-7.43	-	54.47-25.48H	1.16 ± 0.67	-
Xu et al. [2015]	M:15	AM	-	0.81 ± 0.40	-	-	-
	F:8	AM	-	1.03 ± 0.51	-	-	-
Ai et al. [2019]	U:5	AM	-	0.61-1.6	14-28	-	-
	M:10	SI	-	1.3	-	-	-
Tang et al. [2013]	F:10	SI	-	-	-	-	-
	U:160	RS	M: 10.65 F: 8.36	-	14.3 SD=4.3 15.0 SD=4.3	-	-
Shiner et al. [1995]	U:160	RS	-	-	-	-	-
	M:12	APS	-	-	-	0.6	-
Gregson et al. [2021]	F:13	APS	-	-	-	-	-
	M:6	APS	-	-	-	-	-
Johnson et al. [2011]	F:9	APS	-	-	-	≈ 0.8-0.9	-
	M:7	APS	-	-	-	-	-
Pan et al. [2022]	F:5	APS	-	-	-	-	80% < 2.642
	U:118 & U:33	APS	11.5	-	-	-	0.5-0.6
Archer et al. [2021]	U:118 & U:33	APS	-	-	-	-	-

**Table 8** Boundary conditions for coughing. The results are for both genders and the average value unless different is stated. For the droplet distribution, the most common size is shown. F/D Method=Methodology for measuring flow/velocity and droplet size/concentration, CPFR=Cough Peak Flow Rate, PV=Peak Velocity, T=Time/Duration, MOA=Month Opening Area, PVT=Peak Velocity Time, DD=Droplet Distribution, SM=Spirometer, AS=Aerosol sampler, SI=Schlieren Imaging, PIV=Particle Image Velocimetry, PTV=Particle Tracking Velocimetry, IMI=Interferometric Mie Imaging, SIMOP=Solid Impact Method using oil paper, DM=Direct Micrometry, OPC=Optical Particle Counter, AEM=Analytical Transmission Electron Microscope, APS=Aerodynamic Particle Size, SMPS=Scanning Mobility Particle Sizer, DDA=Droplet Deposition Analysis, M=Male, F=Female, U=Unknown gender, P=Influenza Positive, and N=Influenza Negative.

Source	Subjects	F/D Method	CPFR [l/s]	PV [m/s]	T [s]	MOA [cm <sup>2</sup> ]	PVT [ms]	DD [µm]
Gupta et al. [2009]	M: 13 F: 12 P: 47	SM	M: 3-8.5 F: 1.6-6 P: 7.1	-	0.5	M: 4.0±0.95 F: 3.37±1.4	M: 57-96 F: 57-110	-
William G. Lindsley et al. [2010]	N: 11	SM & AS	N: 7.6	-	0.9	-	-	-
Tang et al. [2012]	M: 10 F: 10	SI	-	M: 3.2-14 F: 2.2-5	0.2-0.35	-	-	-
Oh et al. [2022a]	M: 30 F: 30	PIV	-	M: 11.83 F: 10.08	M: 0.56±0.15 F: 0.53±0.13	-	M: 19±7 F: 18 ±6	-
Kwon et al. [2012]	M: 17 F: 9	PIV	-	M: 15.3 F: 10.6	-	-	-	-
Zhu et al. [2006]	M: 3 F: 0	PIV	-	11.2	-	-	-	-
Li et al. [2022]	U: 1	SM, PIV & PTV	7-8	-	1	-	-	-
Chao et al. [2009]	U: 11	IMI & PIV	-	11.7	-	-	-	4-8
Duguid [1946]	-	SIMOP & DM	-	-	-	-	-	4-8
Papinen and Rosenthal [1997]	U: 5	OPC & AEM	-	-	-	-	-	≤ 0.6
Yang et al. [2007]	M: 27 F: 27	APS & SMPS	-	-	-	-	-	82% 0.74-2.12
Johnson et al. [2011]	M: 6 and M: 2 F: 9 and F: 6	APS & DDA	-	-	-	-	-	B-mode: 1.6 L-Mode: 1.7 O-mode: 123

**Table 9** Boundary conditions for sneezing. The results are for both genders and the mean value unless different is stated. For the droplet distribution, the most common size is shown. F/D Method=Methodology for measuring flow/velocity and droplet size/concentration, PV=Peak Velocity, T=Time/Duration, PVT=Peak Velocity Time, MOA=Mouth Opening Area, DP=Droplet Distribution, PVI=Particle Image Velocimetry, SI=Shadowgraph Imaging, SIMOP=Solid Impact Method using oil-d paper, DM=Direct Micrometry, LPSA=Laser Particle Size Analyzer, M=Male, F=Female, U=Unknown Gender, GM=Geometric Mean.

Source	Subjects	F/D Method	PV [m/s]	T [s]	PVT [ms]	MOA [cm <sup>2</sup> ]	DD [µm]
Han et al. [2021]	M:5 F:5	PV	M:6.2 F:15.6	M:0.473 F:0.396	M:19 F:20	-	-
Bouroubba [2020]	F:1	-	10-30	-	-	1.29	-
Busco et al. [2020]	U:1	-	-	-	-	-	-
Tang et al. [2013]	M:10 F:10	SI	4.5 at 0.6 m	-	-	-	-
Cahramian [2023]	M:10 F:10	SI	M:31.2 ± 0.4 F:31.0 ± 0.4	-	-	-	-
Duguid [1946]	-	SIMOP & DM	-	-	-	-	4-8
Han et al. [2013]	M:10 F:10	LPSA	-	-	-	-	Unimodal: GM=360.1 Bimodal: GM1=386.2 and GM2=72.0

**Table 10** Boundary conditions for Speech. The results are for both genders and the average value unless different is stated. For the droplet distribution, the most common size is shown. F/D Method=Methodology for measuring flow/velocity and droplet size/concentration, AFR=Average Flow Rate, MOA=Mouth Opening Area,  $\theta/SD$ =Spread Angle/Standard Deviation DD=Droplet Distribution, PIV=Particle Image Velocimetry, PV=Peak Velocity, SM=Spirometer, IMI=Interferometric Mie Imaging, OPC=Optical Particle Counter, AEM=Analytical Transmission Electron Microscope, APS=Aerodynamic Particle Size, DDA=Droplet Deposition Analysis, SIMOP=Solid Impact Method using oiled paper, DM=Direct Micrometry, M=Male, F=Female, U=Unknown gender, V=Vertical, H=Horizontal, L=Letters, N=Numbers, and P=Phrase

Source	Subjects	F/D Method	AFR [l/s]	PV [m/s]	MOA [cm <sup>2</sup> ]	$\theta/SD$ [°]	DD [ $\mu$ m]
Han et al. [2013]	M: 5	PIV	-	M: 6.56	-	M: V=50.9/29.6	H=44.6/23.7
	F: 5			F: 5.94		F: V=54.9/23.7	H=41.2/22.4
Kwon et al. [2012]	M: 17	PIV	-	M: 4.07	-	M: 49	-
	F: 9			F: 2.31		F: 78	-
Gupta et al. [2010]	M: 13	SM	L: 0.432±0.115	-	-	-	-
	F: 12			N: 0.374±0.086		-	-
Chao et al. [2009]	U: 11	IMI & PIV	P: 0.128±0.014	3.9	1.8	-	4-8
Papineni and Rosenthal [1997]	U: 5	OPC & AEM	-	-	-	-	≤ 0.6
Johnson et al. [2011]	M: 6 and M: 2	APS & DDA	-	-	-	-	B-mode: 1.6
	F: 9 and F: 6			-	-	-	L-Mode: 2.5
Pan et al. [2022]	M: 7	APS	-	-	-	-	O-mode: 1.45
Duguid [1946]	F: 5	SIMOP & DM	-	-	-	-	50% ≤ 1.037
	-			-	-	-	90% ≤ 2.642
Asadi et al. [2019]	M: 26	APS	-	-	-	-	4-8
	F: 22			-	-	-	-

Simon Madsen

---

**Machines for simulation of respiratory activities**

To investigate how respiratory activities are affected by various parameters special equipment is needed in order to produce a consistent profile in order to investigate a single parameter at a time. To do so a machine for simulation of respiratory activities is often necessary. In the literature, a few different machines have been described. For breathing many machines have been developed in the form of artificial lungs. These machines consist normally of a controllable piston that can generate both inhalation and exhalation. Such a machine is available on the Aalborg University campus in the Indoor environment laboratory.

To simulate more violent respiratory activities fewer machines have been developed. Studies such as Lindsley et al. [2013] has created a machine for the simulation of coughing. The machine is based on a controllable piston as with breathing. Due to the nature of coughs, the piston has to accelerate move quicker than for breathing. The machine was supplied with an aerosol chamber to inject aerosols into the airflow.

Zhang et al. [2017] made a coughing machine based on another principle. Their machine used pressure from a gas canister and controlled it using a solenoid valve. The machine was used to investigate droplets. Their machine had therefore a nebulizer to generate fine droplets and a droplet ejector to create more course droplets.

These two studies demonstrate the principles of the two types of machines used in the literature, one based on piston flow

and another on pressure. For respiratory activities such as coughing or sneezing a high flow rate is produced. Due to the high flow rates a machine based on piston flow would require very high velocities and acceleration of the piston. For a machine based on pressure the peak flow would not be difficult to reach however it may be more difficult to control the flow after the initial peak. Both principles have been used in the literature with good results however as noted by Ai and Melikov [2018] the coughing machine should be able to follow the most important characteristics of a cough mainly the flow rate and mouth opening area. They argued that a good coughing machine should be able to change these parameters so multiple scenarios can be investigated.

**Conclusion**

The main conclusion from the literary review is that a lack of literature is present when discussing the boundary conditions for respiratory activities. More studies are needed to define and verify the boundary conditions.

A severe lack of literature is present on the mouth opening area during respiratory activities. Some studies such as Gupta et al. [2009] and Gupta et al. [2010] have made strives to give the mouth opening area for the investigated respiratory activities, however, no other studies have tried verifying the data. Further, the mouth opening area for sneezing could only be found in a single study and was based on only a single subject.

For sneezing a general lack of knowledge is present for the characteristics of the

airflow. Some studies have addressed it using PIV measurements, however little is known about the flow rate other than similarity with coughing. A lack of knowledge about the mouth opening area results in a scenario where a conversion between the velocity and flow rate is lacking.

When talking about cross-infection risk the exposure is well-defined for breathing in different scenarios. The parameters that influence the exposure are well-defined for breathing but little is known about the other respiratory activities. A few studies have tried investigating the exposure for other respiratory activities however the boundary conditions are not well defined. A focus on exposure to

other respiratory activities and how they can be influenced is needed. Most experimental studies have only investigated the near mouth scenario so what happens downstream from the mouth is not very well defined.

An effort to produce well-defined machines for simulation of different respiratory activities is also needed. Studies using a machine for simulation often have their own design specialized for the purpose of the study. The outcome becomes different machines being made for the same activity often built very differently resulting in uncertainty when comparing studies if the boundary conditions for these machines are not well defined and properly investigated and documented.

---

## Bibliography

---

- Ai et al., 2019.** Zhengtao Ai, Kaho Hashimoto and Arsen K. Melikov. *Influence of pulmonary ventilation rate and breathing cycle period on the risk of cross-infection*. Indoor Air, 29, 2019.
- Ai and Melikov, 2018.** Z.T. Ai and A.K. Melikov. *Airborne spread of expiratory droplet nuclei between occupants of indoor environments: A review*. Indoor Air, 28, p. 500–524, 2018.
- Archer et al., 2021.** Justice Archer, Lauren P. McCarthy, Henry E. Symons, Natalie A. Watson, Christopher M. Orton, William J. Browne, Joshua Harrison, Benjamin Moseley, Keir E. J. Philip, James D. Calder, Pallav L. Shah, Bryan R. Bzdek, Decal Costello and Jonathan P. Reid. *Comparing aerosol number and mass exhalation rates from children and adults during breathing, speaking and singing*. Interface Focus, 12, 2021.
- Asadi et al., 2019.** Sima Asadi, Anthony S. Wexler, Christopher D. Cappa, Santiago Barreda, Nicole M. Bourvier and William D. Ristenpart. *Aerosol emission and superemission during human speech increase with voice loudness*. Scientific Reports, 9, 2019.
- Bjørn and Nielsen, 2002.** E. Bjørn and P. V. Nielsen. *Dispersal of exhaled air and personal exposure in displacement ventilated rooms*. Indoor Air, 12, 2002.
- Bourouiba, 2020.** Lydia Bourouiba. *Turbulent Gas Clouds and Respiratory Pathogen Emissions, Potential Implications for reducing transmission of COVID-19*. JAMA Insights, 323, 2020.
- Bourouiba et al., 2014.** Lydia Bourouiba, Eline Dehandschiewercker and John W.M. Bush. *Violent expiratory events: on coughing and sneezing*. Journal of Fluid Mechanics, 745, 2014.
- Busco et al., 2020.** Giacomo Busco, Se Ro Yang, Joseph Seo and Yassin A. Hassan. *Sneezing and asymptomatic virus transmission*. Physics of Fluids, 32, 2020.
- Cahramian, 2023.** Alireza Cahramian. *Influence of indoor environmental conditions on airborne transmission and lifetime of sneeze droplets in a confined space: a way to reduce COVID-19 spread*. Environmental Science and Pollution Research, 30, 2023.
- Chao et al., 2009.** C.Y.H. Chao, M.P. Wan, L. Morawska, G.R. Johnson, Z.D. Ristovski, M. Hargreaves, K. Mengersen, S. Corbett, Y. Li, X. Xie and

- D. Katoshevski. *Characterization of expiration air jets and droplet size distributions immediately at the mouth opening*. *Aerosol Science*, 40, 2009.
- Chen et al., 2014.** C. Chen, C.-H. Lin, Z. Jiang and Q. Chen. *Simplified models for exhaled airflow from a cough with the mouth covered*. *Indoor Air*, 24, 2014.
- Craven and Settles, 2006.** Brent A. Craven and Gary S. Settles. *A Computational and Experimental Investigation of the Human Thermal Plume*. *Journal of Fluids Engineering*, 128, 2006.
- Ding et al., 2021.** Shirun Ding, Zhen Wei Teo, Man Pun Wan and Bing Feng Ng. *Aerosols from speaking can linger in the air for up to nine hours*. *Building and Environment*, 205, 2021.
- Duguid, 1946.** J.P. Duguid. *The size and the duration of air-carriage of respiratory droplets and droplet-nuclei*. *J Hyg (Lond)*, 44, 471–479, 1946.
- Fontana, 2008.** Giovanni A. Fontana. *Before we get started: What is a cough?* *Lung*, 186, 2008.
- Gralton et al., 2010.** Jan Gralton, Euan Tovey, Mary-Louise McLaws and Willian D. Rawlinson. *The role of particle size in aerosolised pathogen transmission: A review*. *Journal of Infection*, 62, 2010.
- Gregson et al., 2021.** Florence K. A. Gregson, Natalie A. Watson, Christopher M. Orton, Allen E. Harddrell, Lauren P. McCarthy, Thomas J. R. Finnie, Nick Gent, Gavin. C. Donaldson, Pallav L. Shah, James D. Calder, Bryan R. Bzdek, Declan Costello and Jonathan P. Reid. *Comparing aerosol concentrations and particle size distributions generated by singing, speaking and breathing*. *Aerosol Science and Technology*, 55, 2021.
- Gupta et al., 2009.** Jitendra K. Gupta, Chao-Hsin Lin and Qingyan Chen. *Flow Dynamics and Characterization of a Cough*. *Indoor Air*, 19, 517–525, 2009.
- Gupta et al., 2010.** Jitendra K. Gupta, Chao-Hsin Lin and Qingyan Chen. *Characterizing exhaled airflow from breathing and talking*. *Indoor Air*, 20, p. 31–39, 2010.
- Han et al., 2021.** Mengtao Han, Ryoza Ooka, Hideki Kikumoto, Wonseok Oh, Yunchen Bu and Shuyuan Hu. *Experimental measurements of airflow features and velocity distribution exhaled from sneeze and speech using particle image velocimetry*. *Building and environment*, 205, 2021.
- Han et al., 2013.** Z.Y. Han, W.G. Weng and Q.Y. Huang. *Characterizations of particle size distribution of the droplets exhaled by sneeze*. *Journal of the Royal Society Interface*, 10, 2013.
- Harrison et al., 2023.** Joshua Harrison, Brian Saccente-Kennedy, Christopher M. Orton, Lauren P. McCarthy, Justice Archer, Henry E. Symons, Alicja Szczepanska, Natalie A. Watson, William J. Browne, Benjamin Moseley,

- Keir E.J. Phillip, James H. Hull, James D. Calder, Declan Costello, Pallav L. Shah, Ruth Epstein, Jonathan P. Reid and Bryan R. Bzdek. *Emission rates, size distributions, and generation mechanism of oral respiratory droplets*. *Aerosol science and technology*, 57, 2023.
- Johnson et al., 2011.** G.R. Johnson, L. Morawska, Z.D. Ristovski, M. Hargreaves, K. Mengersen, C.Y.H. Chao, M.P. Wan, Y. Li, X. Xie, D. Katoshevski and S. Corbett. *Modality of human expired aerosol size distributions*. *Aerosol Science*, 42, 2011.
- Kwon et al., 2012.** Soon-Bark Kwon, Jaehyung Park, Jaeyoun Jang, Youngmin Cho, Duck-Shin Park, Changsoo Kim, Gwi-Nam Bae and Am Jang. *Study on the initial velocity distribution of exhaled air from coughing and speaking*. *Chemosphere*, 87, 2012.
- Li et al., 2022.** Mogeng Li, Kai Leong Chong, Chong Shen Ng, Prateek Bahl, Charitha M. de Silva, Roberto Verzicco, Con Doolan, C. Raina MacIntyre and Detlef Lohse. *Towards realistic simulations of human cough: Effect of droplet emission duration and spread angle*. *International Journal of Multiphase Flow*, 147, 2022.
- Licina et al., 2015.** D. Licina, A. Melikov, C. Sekhar and K.W. Tham. *Human convective boundary layer and its interaction with room ventilation flow*. *Indoor Air*, 25, 2015.
- Lindsley et al., 2013.** William G. Lindsley, Jeffrey S. Reynolds, Jonathan V. Szalajda, John D. Noti and Donald H. Beezhold. *A Cough Aerosol Simulator for the Study of Disease Transmission by Human Cough-Generated Aerosols*. *Aerosol Science and Technology*, 47, 937–944, 2013.
- Melikov, 2004.** A. K. Melikov. *Personalized ventilation*. *Indoor Air*, 14, 2004.
- Nielsen, 2009.** Peter V. Nielsen. *Control of airborne infectious diseases in ventilated spaces*. *Journal of the Royal Society interface*, 6, 2009.
- Nielsen and Xu, 2021.** Peter V. Nielsen and Chunwen Xu. *Multiple airflow patterns in human microenvironment and the influence on short-distance airborne cross-infection - A review*. *Indoor and Build Environment*, 31, 2021.
- Nielsen et al., 2022.** Peter V. Nielsen, Chen Zhang, Kirstine Meyer Frandsen, Rasmus Lund Jesen, Patrick Andersen Hundevad, Simon Madsen, Tonje Luckenwald, Najim Popalzai, Yuguo Li, Hua Qian, Chunwen Xu and Li Liu. *Cross-infection risk between two people in different temperature surroundings studied by aerosol dynamics*. 5th International Conference on Building Energy and Environment (COBEE 2022), 2022.
- Oh et al., 2022a.** Wonseok Oh, Ryoza Ooka and Hideki Kikumoto and Mengtao Han. *Numerical modeling of cough airflow: Establishment of*

- spatial-temporal experimental dataset and CFD simulation method*. Building and Environment, 207, 2022a.
- Oh et al., 2022b.** Wonseok Oh, Ryoza Ooka, Hideki Kikumoto and Mengtao Han. *Numerical modeling of sneeze airflow and its validation with an experimental dataset*. Indoor Air, 32, 2022b.
- P. Bahl et al., 2021.** C. de Silva P. Bahl, C.R. MacIntyre, S. Bhattacharjee, A.A. Chughtai and C. Doolan. *Flow dynamics of droplets expelled during sneezing*. Physics of Fluids, 33, 2021.
- Pan et al., 2022.** Shihai Pan, Chunwen Xu, Chuck Wah Francis Yu and Li Liu. *Characterization and size distribution of initial droplet concentration discharged from human breathing and speaking*. Indoor and Built Environment, 0, 2022.
- Papineni and Rosenthal, 1997.** Rao S. Papineni and Frank S. Rosenthal. *The Size Distribution of Droplets in the Exhaled Breath of Healthy Human Subjects*. Journal of Aerosol Medicine, 10, 1997.
- Riediker et al., 2022.** Michael Riediker, Leonardo Briceno-Ayala, Gaku Ichihara, Daniele Albani, Deyan Poffet, Dai-Hua Tsai, Samuel Iff and Christian Monn. *Higher viral load and infectivity increase risk of aerosol transmission for Delta and Omicron variants of SARS-CoV-2*. Swiss medical weekly, 152, 2022.
- Rochet-Capellan and Fuchs, 2013.** Amélie Rochet-Capellan and Susanne Fuchs. *Take a breath and take the turn: how breathing meets turns in spontaneous dialogue*. Philosophical Transactions of The Royal Society, 369, 2013.
- Seikel et al., 2019.** J. Anthony Seikel, David G. Drumright and Daniel Hudock. *Anatomy and Physiology for Speech, Language, and Hearing*. Hardback. San Diego: Plural Publishing, Incorporated, 2019. ISBN 1635502799.
- Shimer et al., 1995.** D.A. Shimer, P. L. Jenkins, S.P. Hui and W.C. Adams. *Measurement of breathing rate and volume in routinely performed daily activities*. Epidemiology, 6, 1995.
- Tang et al., 2012.** Julian W. Tang, Adre Nicolle, Jovan Pantelic, Koh Gerald C, Liang De Wang, Muhammad Amin, Christian A. Klettner, David K.W. Cheong, Chandra Sekhar and Kwok Wai Tham. *Airflow Dynamics of Coughing in Healthy Human Volunteers by Shadowgraph Imaging: An Aid to Aerosol Infection Control*. Plos One, 7, 2012.
- Tang et al., 2013.** Julian W. Tang, Andre D. Nicolle, Christian A. Klettner, Jovan Pantelic, Liangde Wang, Amin Bin Suhaimi, ASHlynn Y.L. Tan, Garrett W.X. Ong, Ruikun Su, Chandra Sekhar, David D.W. Cheong and Kwok Wai Tham. *Airflow Dynamics of Human Jets: Sneezing and Breathing - Potential Sources of Infectious Aerosols*. PLOS ONE, 8, 2013.

- Tang et al., 2006.** J.W. Tang, Y. Li, I. Eames, P.K.S. Chan and G.L. Ridgway. *Factors involved in the aerosol transmission of infection and control of ventilation in healthcare premises.* Journal of Hospital Infection, 64, 2006.
- Thomas et al., 2023.** Caroline Thomas, Gunchu Randhawa and Andrew S. Davies. *The Respiratory System: basic science and clinical conditions.* Hardback. Elsevier: Amsterdam, 2023. ISBN 9780702082849.
- VanSciver et al., 2011.** Meg VanSciver, Shelly Miller and Jean Hertzberg. *Particle Image Velocimetry of Human Cough.* Aerosol Science and Technology, 45, 2011.
- William G. Lindsley et al., 2010.** Francoise M. Blachere William G. Lindsley, Robert E. Thewlis, Abhishek Vishnu, Kristana A. Davis, Gang Cao, Jan E. Palmer, Karen E. Clark, Melanie A. Fisher, Rashida Khakoo and Donald H. Beezhold. *Measurements of Airborne Influenza Virus in Aerosol Particles from Human Coughs.* Plos One, 5, 2010.
- Xu et al., 2015.** C. Xu, Peter V. Nielsen, G. Gong, L. Liu and R.L. Jensen. *Measuring the exhaled breath of a manikin and human subjects.* Indoor Air, 25, 2015.
- Yang et al., 2007.** Shinhao Yang, Grace W. M. Lee, Cheng-Min Chen, Chih-Chen Wu and Kuo pin Yu. *The Size and Concentration of Droplets Generated by Coughing in Human Subjects.* Journal of Aerosol Medicine, 20, 2007.
- Zhang et al., 2017.** Bo Zhang, Chao Zhu, Zhiming Ji and Chao-Hsin Lin. *Design and characterization of a cough simulator.* Journal of Breath Research, 11, 2017.
- Zhu et al., 2006.** Shengwei Zhu, Shinsuke Kato and Jeong-Hoon Yang. *Investigation into Airborne Transport Characteristics of Airflow Due to Coughing in a Stagnant Indoor Environment.* Ashrae, 112, 2006.
- Özlem Önerci Celbi and Önerci, 2023.** Özlem Önerci Celbi and T. Metin Önerci. *Nasal Physiology and Pathophysiology of Nasal Disorders.* Hardback. Cham : Springer International Publishing : Imprint: Springer, 2023. ISBN 9783031123863.

# Calculation of boundary conditions for target manikin

## B

The boundary conditions are found for the target manikin. The manikins represent a female person and is closer described in chapter 1 and thus boundary conditions for a female person is used.

The manikin is 1.68 m tall with a surface area of 1.44 m<sup>2</sup> and the ability to be adjusted to multiple positions creating different scenarios such as sitting or laying down.

### B.1 Activity level

In order to calculate the boundary conditions a representative activity levels is selected. To coincide with previous studies the activity level is selected to be 1.4 met used previously in Zhang et al. [2022]. The mechanical lungs are based upon ASHRAE [2009] and the volumetric flow rate and the breathing frequency are found based on the activity level chosen for the lung. For easier understanding the activity level corresponds to standing which represent the current position of the manikin [Hyldgard et al., 1997].

### B.2 Respiration

The boundary conditions for the breathing of the manikin are found from the relation between activity level, volume flow and breathing frequency from the mechanical lungs based upon ASHRAE [2009]. Equation (B.1) gives the volume flow and equation (B.2) gives the breathing frequency. The results are shown in table B.1.

$$Q = 8.4767M - 1.3257 \quad (\text{B.1})$$

$$BF = 4.9023M + 9.7107 \quad (\text{B.2})$$

$Q$	Volumetric flow rate	[l/min]
$M$	Activity level	[met]
$BF$	Breathing frequency	[min <sup>-1</sup> ]

**Table B.1** Boundary conditions for breathing of thermal manikins. The breathing frequency is rounded down as the lung cannot give a frequency higher than 16 without overheating issues.

Parameter		Value
Q	[l/min]	10.54
$Q_{\max}$	[l/s]	0.576
BF	[min <sup>-1</sup> ]	16

A profile for the breathing process can be found using equation (B.3) assuming the breathing process follows a sine function. The amplitude of the sine function can be found from the minute volume as the artificial lung only provides this value.

$$Q(t) = Q_{\max} \cdot \sin(B \cdot t) \quad (\text{B.3})$$

B is determined by equation (B.4)

$$B = \frac{360}{BF \cdot 2\pi} \cdot \frac{1}{2} \quad (\text{B.4})$$

### B.3 Correction of manikin exhalation temperature

Figure B.1 shown below express the correction needed to account for the differences in air density due to humidity and gas concentration. The temperature of the exhalation is supposed to be 34 °C for normal human breathing, however as the target manikin exhales normal atmospheric air, without tracer gas, a correction is not needed. The figure shown that the density for atmospheric air and in human breathing coincide almost perfectly in the temperature interval of 32 °C to 34 °C.

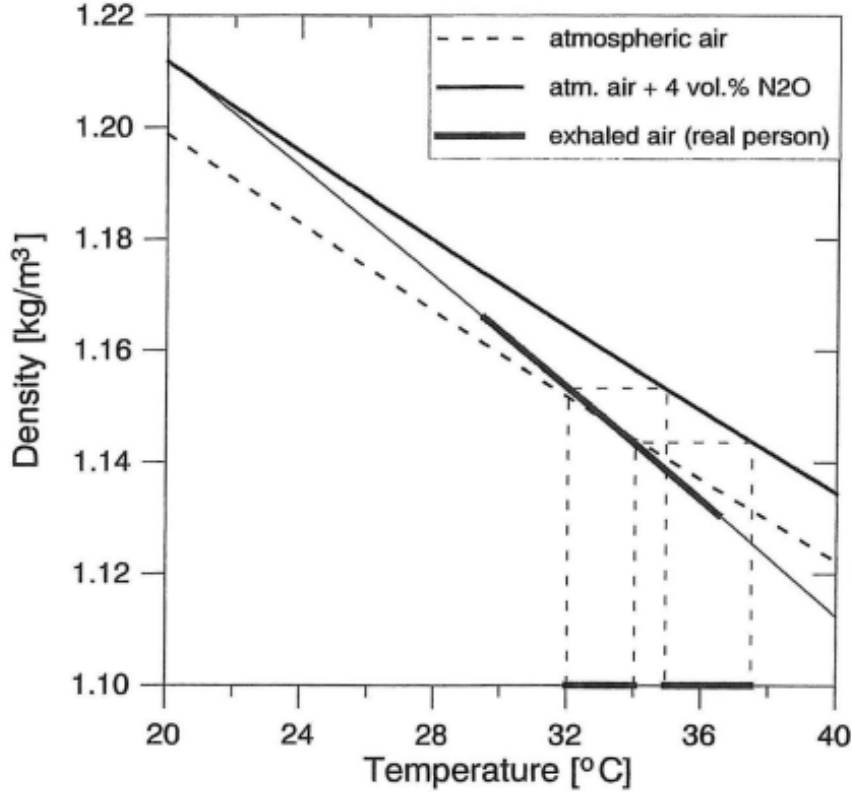


Figure B.1 Comparison in density for air with tracer gas and atmospheric air [Bjørn, 2000].

## B.4 Heat output by thermal manikins

The heat output for the thermal manikins depend on the activity level. When the activity level is 1.4 met the heat production in the body is  $81.4 \text{ W/m}^2$  [Hyldgard et al., 1997]. The heat production should be in other terms the heat loss from the body. The manikin can however not simulate the heat loss due to evaporation. To account for the evaporation the evaporation losses are subtracted from the heat production. The losses from evaporation are in three forms: diffusion of water vapour, respiratory heat output and evaporation of sweat. To determine the evaporation equations (B.5), (B.6) and (B.7) are used [Hansen et al., 2013].

$$E_{dif} = 0.31 \cdot (2.56 \cdot t_{sk} - 33.7 - 0.01P_{da}) \quad (\text{B.5})$$

$$E_{res} = 0.0017 \cdot H \cdot (58.7 - 0.01 \cdot P_{da}) \quad (\text{B.6})$$

$$E_{sw} = 0.42 \cdot (H - 58) \quad (\text{B.7})$$

$E_{dif}$	Heat loss caused by diffusion of water vapour	$[\text{W/m}^2]$
$E_{res}$	Heat loss caused by evaporation in respiration	$[\text{W/m}^2]$
$E_{sw}$	Heat loss caused by evaporation of sweat	$[\text{W/m}^2]$
$t_{sk}$	Surface temperature of manikin	$[\text{°C}]$
$P_{da}$	Water vapour partial pressure	$[\text{Pa}]$
$H$	Total produced heat	$[\text{W/m}^2]$

To determine the heat losses the water vapour partial pressure is calculated assuming an ambient temperature of 23 °C and a relative humidity of 50 %. The water vapour partial pressure is found to be 1,500 Pa [Group, 2018]. The surface temperature of the manikin is calculated using Fanger's comfort equation shown in equation (B.8) [Hyldgard et al., 1997].

$$t_{cl} = 35.7 - 0.028 \frac{M}{A_{Du}} - 0.155 I_{cl} \cdot \left[ \frac{M}{A_{Du}} - 2.6 \cdot 10^{-3} (5770 - 7.16 \frac{M}{A_{Du}} - P_{da}) \right. \\ \left. - 0.42 \left( \frac{M}{A_{Du}} - 58 \right) - 1.72 \cdot 10^{-5} \cdot (5800 - P_{da}) - 0.0012 \frac{M}{A_{Du}} (34 - T) \right] \quad (\text{B.8})$$

$t_{cl}$	Temperature on clothing	[°C]
$M$	Activity level	[met]
$A_{Du}$	Body surface area	[m <sup>2</sup> ]
$I_{cl}$	Heat resistance of clothing	[clo]
$P_{da}$	Water vapour partial pressure	[Pa]
$T$	Ambient temperature	[°C]

To be comparable with previous studies a heat resistance of 1 clo is chosen and represents medium office clothing. Examples for different types of clothing combinations resulting in 1 clo is shown in [Hyldgard et al., 1997]. 1 clo is chosen to be comparable to previous studies [Zhang et al., 2022]. The resulting comfortable surface temperature is 33.5 °C. The heat loss from evaporation can then be calculated to determine the heat output of the manikins. Using equation (B.5), (B.6) and (B.7) the heat losses shown in table are found B.2.

**Table B.2** Boundary conditions for breathing of thermal manikins

Parameter	Value [W/m <sup>2</sup> ]
$E_{dif}$	11.5
$E_{res}$	6.0
$E_{sw}$	9.8
$E_{latent}$	27.3

Using the calculated evaporation and the total heat production the heat output of the manikin should be 54.0 W/m<sup>2</sup>. Using the known body surface area the total heat output is 77.8 W.

# Calibration of temperature sensors



---

This appendix revolves around the calibration of the temperature sensors used in the setup. The temperature sensors used are PT100 RTD's (Platinum 100 Ohm Resistance Temperature detector) and thermocouples. This appendix is based upon [Artman et al., 2008] and [Johra, 2020] unless otherwise stated. In total 6 PT100 RTD's was used together with 30 thermocouples. The thermocouples was connected to a compensation box which in turn is connected to a Fluke Helios datalogger.

## C.1 PT100 RTD

This section will explain in detail how the PT100 RTD's was calibrated.

### C.1.1 Equipment

The following equipment was used for the calibration and will subsequently be explained.

1. F200 Precision Thermometer
2. Isocal-6
3. NI 9216 module
4. PC with Labview
5. Pt 100 temperature probes

The F200 Precision Thermometer is made by ASL. It has a measuring range of  $-200^{\circ}\text{C}$  to  $850^{\circ}\text{C}$ . The F200 has a traceable calibration from January 2022. The calibration was done with a range of  $-20^{\circ}\text{C}$  to  $100^{\circ}\text{C}$  which makes it eligible for the calibration. The thermometer has an accuracy of  $0.01^{\circ}\text{C}$  and has a resolution of  $0.001^{\circ}\text{C}$  [ASL, 2022].

The Isocal-6 is a temperature well and is used to generate an environment with specific temperatures. The Isocal does not maintain a precise temperature which is why the F200 is used as reference [Isotech, 2022].

The NI 9216 module works as a datalogger. The instrument is made by national instruments and is used to log the data from the temperature probes. The module is an RTD input module The module has a range of  $-200^{\circ}\text{C}$  to  $850^{\circ}\text{C}$ . The module has an accuracy of  $\pm 0.15^{\circ}\text{C}$  in the range  $-200^{\circ}\text{C}$  to  $150^{\circ}\text{C}$  and an accuracy of  $\pm 0.20^{\circ}\text{C}$  in the range  $150^{\circ}\text{C}$  to  $850^{\circ}\text{C}$  [Instruments, 2022].

The PT100 probes is the subject of this calibration. They are used for two main purposes. 4 of them are calibrated to measure the temperature in the compensation box

for the thermocouples. The remaining 2 are used to control and validate the exhalation temperatures due to their high precision and quick response time. The PT100 used for these measurement can sample data every 65 ms roughly. The PT100 used in these measurements are the 4-wire PT100's as they are considered the most accurate [Johra, 2020].

### C.1.2 Calibration setup

The Isocal-6 is used to generate temperatures at which data can be collected for the calibration. These setpoints are measured by the PT100's and preciously by the F200. For each temperature point an average is made over a 10 min period after the Isocal has reached the setpoint. The temperature setpoints used in the Isocal is shown in table C.1.

**Table C.1** Coefficients for PT100's first order calibration curve.

Compensation box [°C]	Exhalation [°C]
10	25
18	30
20	35
22	40
24	45
30	-

Meanwhile point measurements are done every 30 s on the F200. During the measurements the software uses a specific pre-calibration type which must remain consistent throughout the measurements. Finally a linear regression is made using Least Squares method is performed for each of the probes. A principle sketch of the setup is shown on figure C.1.

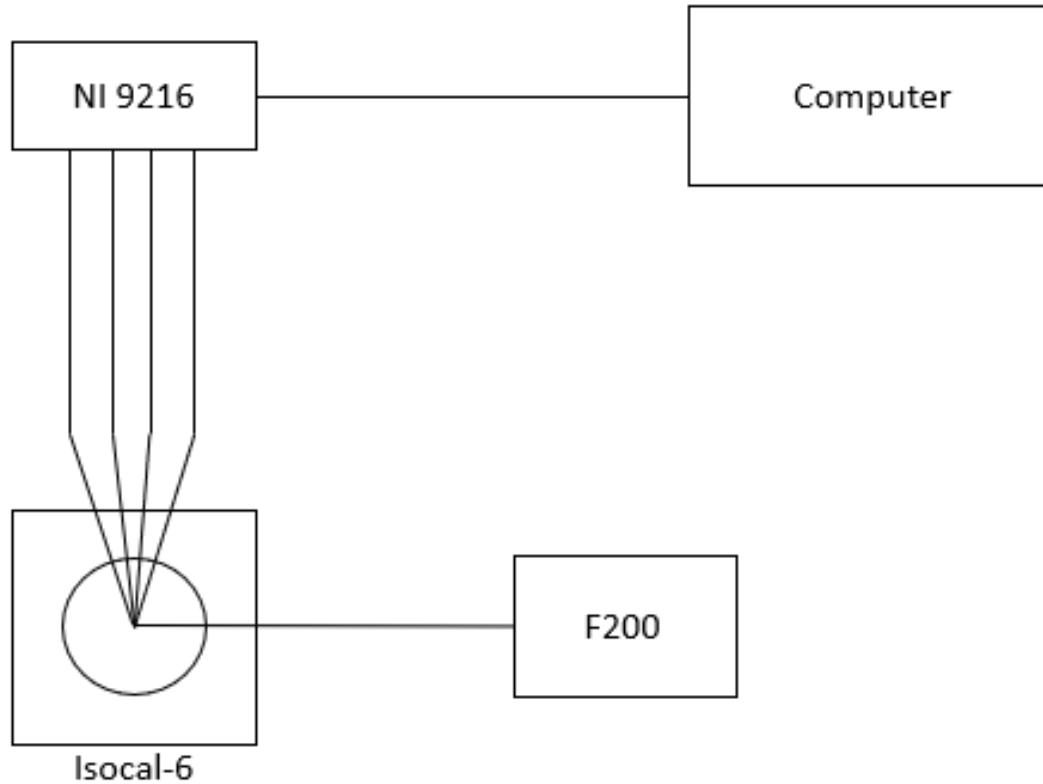


Figure C.1 Principle sketch of the calibration setup.

### C.1.3 Results

This section will show the results of the calibration and will include the calibration curve for a single PT100 while the coefficients for the remaining PT100's are shown in table. The calibration curve is shown for the PT100 in the first channel (channel 1) for the compensation box. A first order polynomial is used for the calibration. The calibration curve is shown on figure C.2.

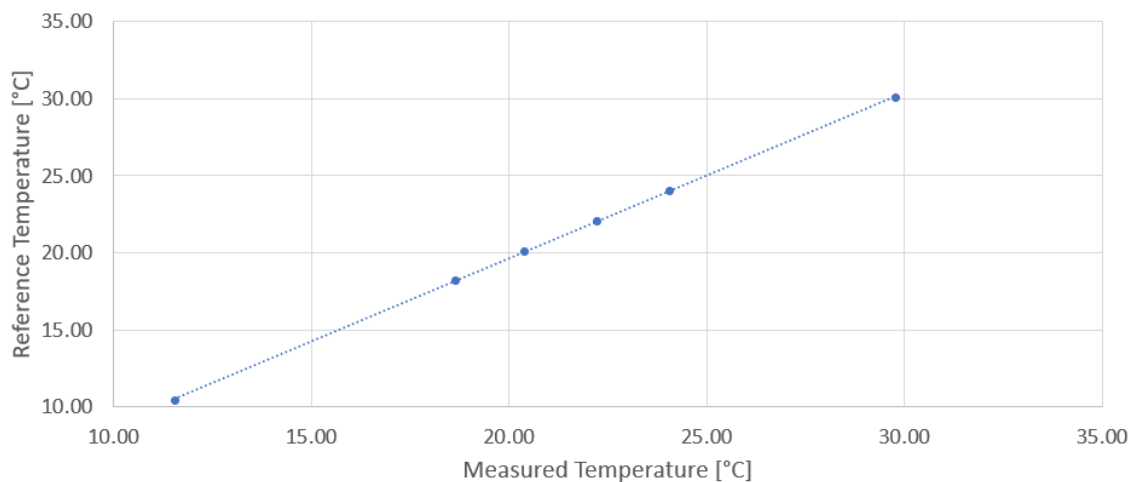


Figure C.2 Calibration curve for PT100 in Channel 1

The remaining PT100's coefficient is shown in table C.2 and is complying with a first order polynomial,  $y = Ax + B$ .

**Table C.2** Coefficients for PT100's first order calibration curve.

	Channel	A	B	$R^2$
Compensation box	1	1.08	-1.95	1.00
	2	1.10	-2.57	1.00
	3	1.05	-0.91	1.00
	4	1.13	-3.25	1.00
Exhalation	2	1.01	-0.32	1.00
	3	1.02	-0.30	1.00

### C.1.4 Validation of calibration

In order to verify the calibration and if the probes measures correctly. The PT100's should be comparable with the readings from the F200. An error plot has been made to show the deviation of the calibration from the reference values. The probes used in the exhalation as an increased range compared with the probes in the compensation box. The error plot can be seen on figure C.3.

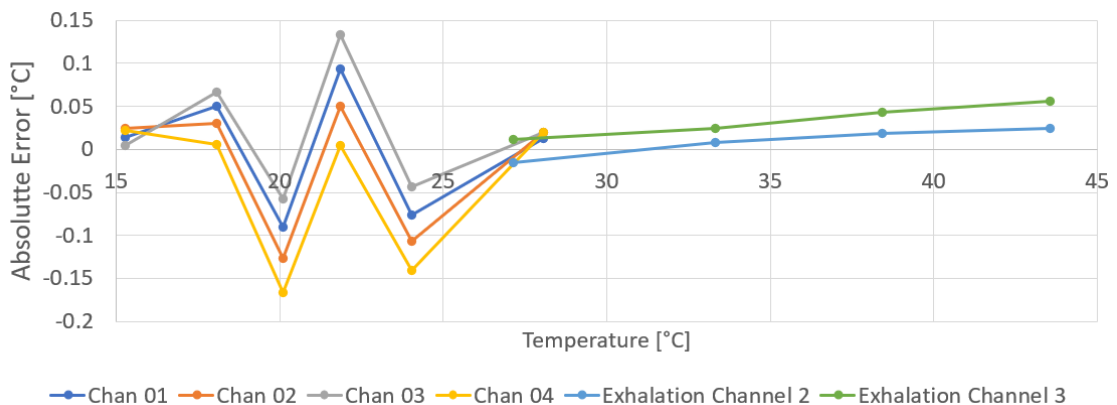


**Figure C.3** The absolute error for the PT100's for both compensation box and exhalation.

The error is less than  $\pm 0.01$  °C in most scenarios and only for 3 PT100's. The error is deemed acceptable however it will cause some uncertainty in the measurements.

For the exhalation flow an error of  $\pm 0.01$  °C is irrelevant and will not have any significant impact on the measurements as it is mainly used to control the correct setting on the equipment and will not be used to retrieve data from.

The PT100's used in the compensation box may cause some uncertainties however as mentioned before are deemed acceptable.

## C.2 Thermocouples

This section will describe the calibration of the thermocouples. The calibration is similar to that for the PT100's described in section C.1.

### C.2.1 Equipment

1. Type K thermocouple
2. Helios datalogger
3. Compensation box
4. Copper cables
5. F200 Precision Thermometer
6. Isocal-6
7. NI 9216 module
8. PC with Labview
9. Pt 100 temperature probes

The thermocouple is type K which means that it consists of two different nickel alloys namely Chromel and Alumel. The thermocouples used in these measurements have an accuracy of approximately  $\pm 1$  V depending on deviations in the alloys. The range is from  $-200$  °C to  $1,260$  °C [Engineering, 2022]. The thermocouples are connected from the measuring point to the compensation box.

The Helios datalogger of the variant 2680A is a data acquisition system which can have up to 120 channels in total or 6 modules with 20 channels each. Depending on the module it can use analog or digital signals. The two types of analog modules are PAI (precision analog module) and FAI (fast analog module). The PAI has a resolution of  $5\frac{1}{2}$  digits with an accuracy of 0.02%. The FAI has a resolution of  $4\frac{1}{2}$  digits and an accuracy of 0.04%, however the FAI module can only withstand up to 50 V. The logger have different modes however the DC volt measurement mode is used to get the difference between the two ends of the thermocouple. During calibration and measurements the Helios has a logging interval of 3.5 s. The mode and settings used reduce fluctuations however reduces the logging speed resulting in the previous mentioned logging interval.

The compensation box consist of terminal blocks and the wires are shielded from radiation by a metal casing. To avoid deviations due to fluctuating temperatures around the terminal blocks the box is covered with expanded polystyrene to insulate against fluctuating temperatures. Inside the box the terminal blocks connects one end of the thermocouples with the copper cables connected to the Helios datalogger. Inside the compensation box 4 PT100's are placed to provide a precise temperature as reference for the thermocouples.

The copper cables are used to connect the compensation box and the Helios datalogger.

Item 5-9 are described in section C.1

### C.2.2 Calibration setup

The calibration consists of the Isocal-6 generating multiple temperature setpoints at which the thermocouples measured value is compared to the reference value of the F200. The thermocouples are inserted into the wells outer ring in pairs of 5 to insure the same conditions on all of them. The F200 is also placed in one of the wells outer ring. The thermocouples ends are taped to avoid any disturbances by conductive metal or other thermocouples. The Isocal is insulated to make the process quicker and provide more stable temperature setpoints.

The compensation box is insulated to prevent most of the air movement into the box. The air movement might affect the readings and the box is therefore insulated extensively. The insulation is made of paper towels, the same as the insulation of the Isocal.

On figure C.4 a principle sketch of the calibration is shown.

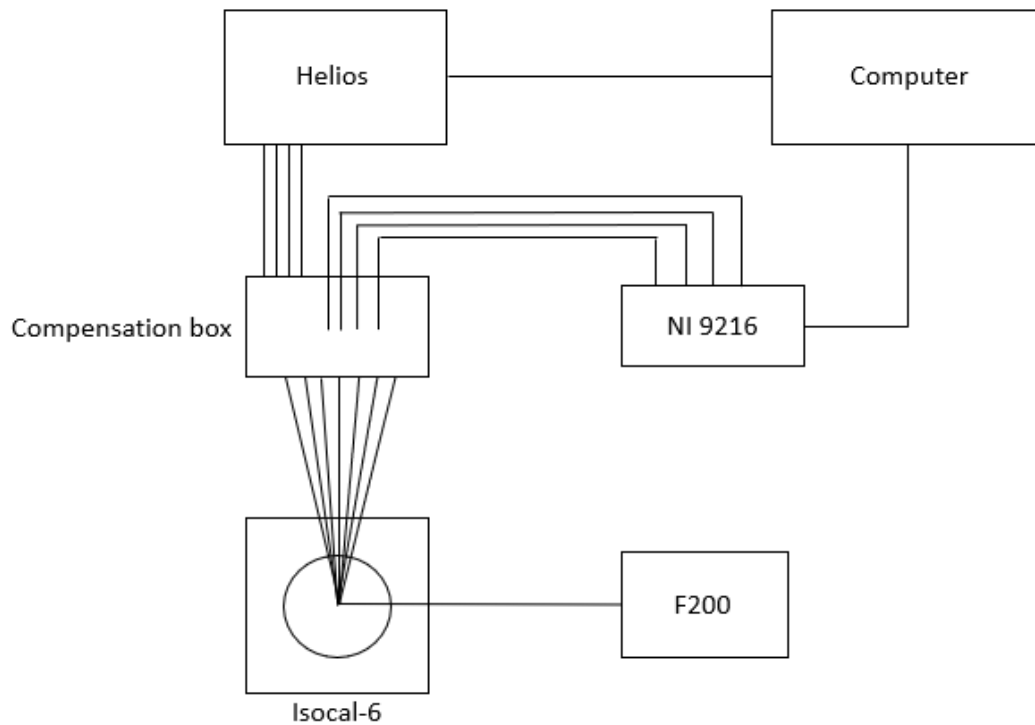


**Figure C.4** Principle sketch of the calibration setup.

### C.2.3 Results

The thermo-electric effect that is between the Chromel and Alumel alloys is temperature dependent. For this reason a third order polynomial is used in the calibration. An example of a calibration curve for a thermocouple is shown on figure C.5.

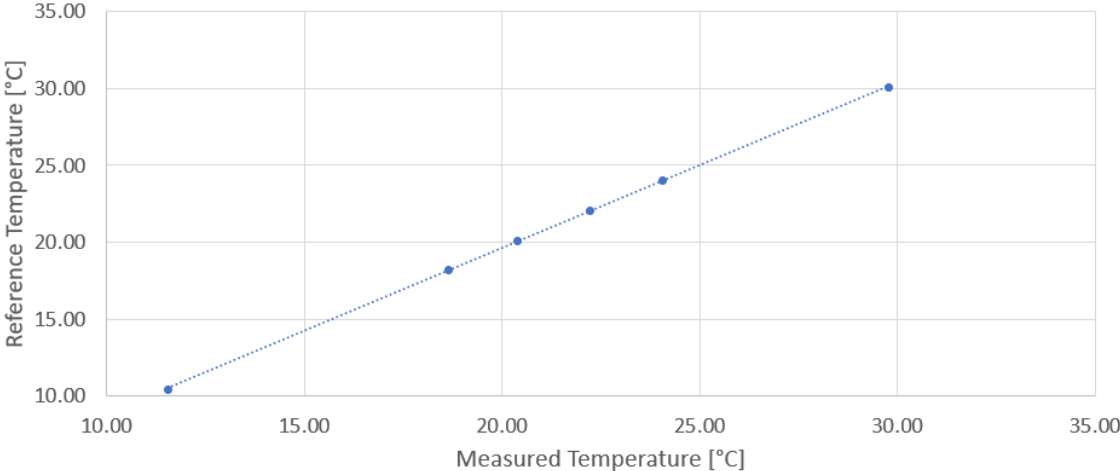


**Figure C.5** Calibration for thermocouple in channel 1

The shown calibration curve has the function  $y = 3.54 \cdot 10^8 x^3 - 6.35 \cdot 10^5 x^2 + 2.50 \cdot 10^4 x + 2.35 \cdot 10^{-1}$  with an  $R^2$ -value of 1.00. To avoid clutter on the graphs the coefficient for all the thermocouples are provided in table C.3 shown below.

**Table C.3** Coefficients for thermocouple third order calibration curve.

Channel	$U_1$ [ $10^7$ ]	$U_2$ [ $10^5$ ]	$U_3$ [ $10^4$ ]	$U_4$ [ $10^{-1}$ ]	$R^2$ [-]
1	35.4	-6.35	2.50	2.35	1.00
3	3.41	-3.57	2.48	1.15	1.00
4	-1.12	-4.05	2.51	1.18	1.00
5	-13.99	-3.12	2.52	1.07	1.00
7	-0.69	-3.00	2.48	1.10	1.00
8	-1.81	-3.83	2.51	1.48	1.00
9	-0.53	-3.29	2.48	1.44	1.00
10	-3.93	-2.77	2.49	1.40	1.00
11	-3.83	-2.55	2.48	1.23	1.00
12	-5.01	-2.84	2.50	1.57	1.00
13	-3.01	-3.03	2.50	1.56	1.00
14	-2.36	-3.78	2.51	1.44	1.00
15	-3.91	-2.92	2.51	1.39	1.00
16	-9.47	-1.60	2.49	1.58	1.00
17	-10.18	-1.76	2.48	1.66	1.00
18	-13.70	-1.85	2.52	1.58	1.00
19	-10.13	-1.52	2.49	1.58	1.00
20	-23.69	-0.55	2.49	1.61	1.00
21	-10.61	-1.65	2.49	1.64	1.00
23	-13.61	-1.61	2.49	0.95	1.00
24	-6.90	-1.34	2.50	1.18	1.00
25	-8.10	-1.97	2.48	1.08	1.00
26	-5.49	-2.83	2.49	1.21	1.00
27	-3.20	-3.89	2.51	1.00	1.00
28	-4.03	-3.51	2.51	1.49	1.00
29	-5.16	-2.97	2.48	1.35	1.00
30	-6.33	-2.66	2.48	1.37	1.00
31	-5.19	-2.83	2.48	1.56	1.00
32	-6.18	-2.67	2.49	1.65	1.00
33	-4.70	-2.77	2.50	1.54	1.00
34	-7.04	-2.67	2.48	1.44	1.00
35	-4.68	-2.40	2.49	1.61	1.00

### C.2.4 Validation of calibration

To verify the calibration a validation has been performed for all the sensors and the absolute error has been calculated. The validation was done in the same manner as the calibration but at different temperatures within its range. The F200 was used as reference value. The absolute error for the thermocouples is shown on figure C.6 which shows that highest expected error is  $\pm 0.5^\circ\text{C}$ . This error is deemed acceptable since thermocouples monitors the temperatures and ensures they are stable, however it is not the main parameter that is investigated. Furthermore the temperatures of the exhalation which is the most important is controlled by PT100's beforehand due to the slow logging interval of the thermocouples.

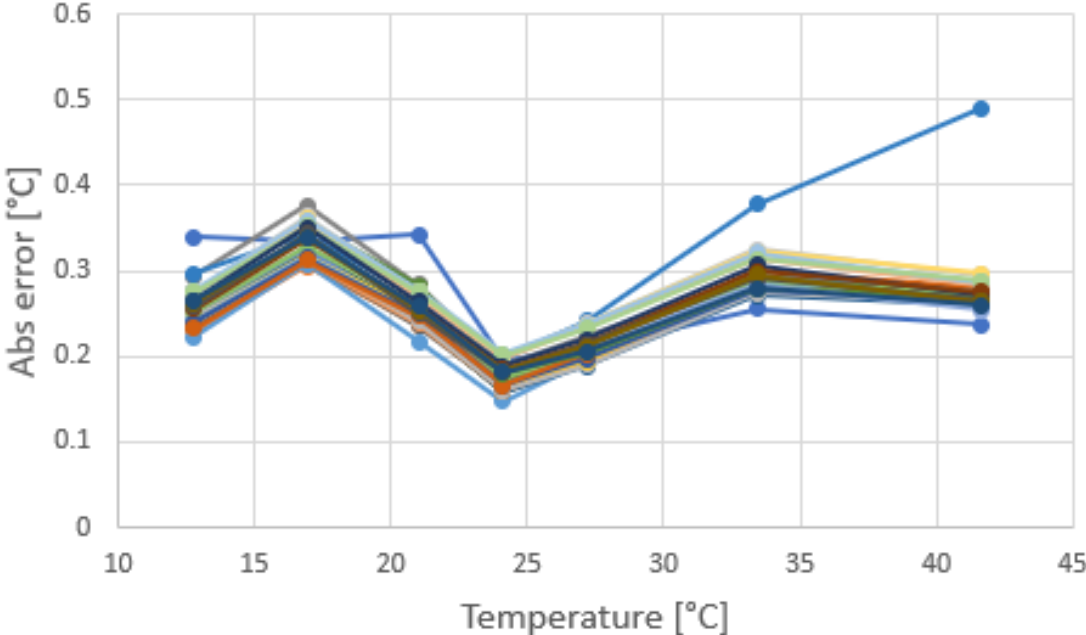


Figure C.6 Absolute error for the thermocouples.

# **F200 Calibration** D

**TEKNOLOGISK  
INSTITUT**

Teknologiparken  
Kongsvang Allé 29  
Bygning 14  
8000 Aarhus C  
Tlf. +45 72 20 20 00  
info@teknologisk.dk  
www.teknologisk.dk

**KALIBRERINGS CERTIFIKAT**

CERTIFIKATNR.:

**200-T-23460**

Side 1 af 3  
Antal bilag: 0  
Init: DDS/JNN

**Rekvirent:** Aalborg Universitet, Institut for Byggeri, By og Miljø (Build)  
Thomas Manns Vej 23  
9220 Aalborg Øst

**Emne: Termometer**

Fabrikat:	ASL	Model:	F200
Serienr.:	<b>000031/74</b>	Kundemærke:	<b>Inst. 6/54192</b>
Område:	-20 - +100 °C	Type:	Digital
Inddeling:	0,001 °C		
Tilbehør:	1 stk. Pt100 føler mærket "Føler 1".		

**Periode:** Modtaget: 21-01-2022      Kalibreret: **26-01-2022**

**Procedure:** D1-2.2

**Bemærkninger:** Kalibreringen af føler er foretaget i væskebade ved sammenligning med referenceføler. Ved 0 °C er kalibreringen udført i ispunkt. Føleren er kort ift. diameteren af sensorkappen, men har været neddyppet ca. 9 cm, tilsvarende 15 gange diameteren.

**Vilkår:** Kalibreringen er udført akkrediteret i henhold til internationale krav (DS/EN ISO/IEC 17025:2017) og i henhold til Teknologisk Instituts almindelige vilkår. Kalibreringsresultater gælder udelukkende for det kalibrerede emne. Kalibreringscertifikatet må kun gengives i uddrag, hvis Teknologisk Institut skriftligt har godkendt uddraget.

**Kalibreret af:** Dennis Dam Sørensen, 72 20 32 27, dds@teknologisk.dk

Godkendt og  
digitalt signeret  
28-01-2022 af:

  
Jan Nielsen  
Cand. Scient



Dette PDF dokument er kun gyldigt, hvis det er digitalt signeret med OCES digitalsignaturen for Jan Nielsen, Teknologisk Institut.



**DANAK**  
CAL Reg.nr. 200

TEMPERATURLABORATORIET  
TEKNOLOGISK INSTITUT

Certifikat nr.: 200-T-23460

Side 2 af 3

KALIBRERINGS CERTIFIKAT  
Resultater

Føler mærket: Føler 1

Reference- værdi °C	Aflæsning °C	Fejl °C	Usikkerhed °C	Note
-20,0467	-20,0620	-0,0153	0,0065	
-10,0290	-10,0360	-0,0070	0,0063	
0,0001	-0,0050	-0,0051	0,0027	
9,9945	9,9990	0,0045	0,0053	
19,9957	20,0050	0,0093	0,0058	
29,9948	30,0080	0,0132	0,0053	
40,0542	40,0630	0,0088	0,0064	
50,0393	50,0470	0,0077	0,0036	
60,0263	60,0320	0,0057	0,0037	
70,0175	70,0240	0,0065	0,0039	
80,0099	80,0190	0,0091	0,0040	
90,0065	90,0130	0,0065	0,0041	
100,0047	100,0090	0,0043	0,0043	

**Bemærkninger:**

Aflæsning er middelværdien af flere aflæsninger på det kalibrerede måleinstrument.  
Fejl = Aflæsning - referenceværdi.

Temperatur - 20211011

## TEMPERATURLABORATORIET

## TEKNOLOGISK INSTITUT

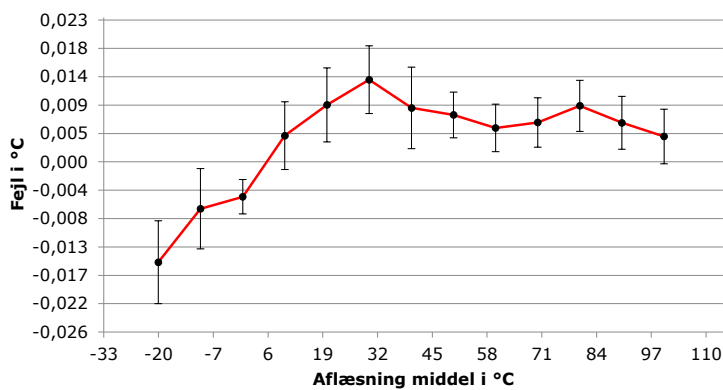
Certifikat nr.: 200-T-23460

Side 3 af 3

## KALIBRERINGS CERTIFIKAT

## Fejlkurve

Føler mærket: Føler 1

**Kun de markerede punkter er målt.****Bemærkninger:**

Aflæsning er middelværdien af flere aflæsninger på det kalibrerede måleinstrument.  
Fejl = Aflæsning - referenceværdi.

Den rapporterede ekspanderede usikkerhed er angivet som standardusikkerheden af målingen multipliceret med dækningsfaktoren  $k=2$ , således at dæknings sandsynligheden svarer til ca. 95 %.

Alle temperaturer er i henhold til ITS90

**Kalibreringsforhold:**

Rumtemperatur: 23,1 °C ± 1,1 °C  
Relativ fugtighed: 33,5 %rh ± 5,0 %rh  
Barometerstand: 1017,4 mbar ± 2,4 mbar

**Sporbarhed:**

Dette kalibreringscertifikat er omfattet af DANAK akkreditering og EA's og ILAC's multilaterale aftaler for kalibrering, hvilket sikrer, at målingerne er sporbare til SI enhedssystemet.

Temperatur - 20211011

# Calibration of anemometers E

---

This appendix revolves around the calibration and validation of the anemometers and describes the procedure and setup for the calibration. The calibration is done by making a comparison between the measured voltage from the anemometers and a measured reference air velocity.

## E.1 Equipment

The following equipment was used for the calibration and will subsequently be explained

1. Dantec 54R102 thermal comfort probes
2. Dantec Comfort Sense 16-port
3. Jet wind tunnel
4. Micromanometer
5. Orifice plates
6. Digital pressure gauge
7. Sensirion EK-H4

The Dantec 54R102 is a hot wire anemometer. The anemometer is of the type 54R102 and is used to measure the air velocity. The anemometers have a range of 0-5 m/s and can therefore be used in measurements for the room conditions and heavy breathing. It has a precision of  $\pm 2\%$  in the range of 0.05 to 1.0 m/s and a precision of  $\pm 5\%$  in the range of 1.0 to 5.0 m/s [Kristensen et al., 2015]. In total 10 anemometers are calibrated and used during the measurements.

The Dantec Comfort Sense is used to log the data from the anemometers. It has 16 ports so only 1 is needed.

The Jet wind tunnel is used to create and maintain the air flows needed for the calibration. The Jet wind tunnel is fitted with a ventilator to achieve this.

The micromanometer is used to measure the pressure drop through the orifice plate. It is of the type Min2P from Debro. It has a range of  $\pm 20$  mbar and an uncertainty of  $\pm 0.02$  mmH<sub>2</sub>O [Engen, 1985].

The orifice plates are used to generate pressure drop. The orifice plates have corresponding calibration curves which makes it possible to determine the air velocity. To calibrate the full range of the anemometers a orifice plate with a diameter of 10 mm, 23 mm and 46 mm is needed.

The digital pressure gauge is a barometer and is used to make a correction in the air density due to atmospheric pressure. It is how the type 2104 from Mensor and has a compensated temperature range of 15-45 °C. When readings are within this range the precision of the barometer is 0.01 % of the reading [Mensor.com, 2005].

The Sensirion EK-H4 is an evaluation kit for humidity and temperature sensors. For the calibration only the temperature sensors are used. The sensors are used for correction of the air density due to temperature fluctuations. The sensor has a range of  $-20\text{ }^{\circ}\text{C}$  to  $70\text{ }^{\circ}\text{C}$ . It can measure in an interval of 1 s to 1,440 s [Sensirion, 2015].

## E.2 Calculation of reference air velocity

Since a calibration curve is available for the orifice plates the air velocity can be calculated from the pressure drop through the orifice. The pressure drop is used to calculate the air velocity based upon the specific orifice plates pressure drop. The orifice plates calibration formula is shown in table E.1.

**Table E.1** Equations for calculations of velocity from orifice plates. The pressure is given in mbar.

Inner diameter [mm]	Range [m/s]	Criterion	Equation
10	0-0.11	$\Delta p < 0.5\text{mbar}$	$v = 0.14663\Delta p^{0.3878}$
	0.11-0.42	$\Delta p > 0.5\text{mbar}$	$v = 0.157\Delta p^{0.485}$
23	0.25-1.1	-	$v = 0.744\Delta p^{0.4516}$
46	1-5	-	$v = 2.886\Delta p^{0.49}$

The equations for the orifice plates are made assuming a air density of  $\rho_{\text{air}} = 1.2\text{ kg/m}^3$ . Since the calibration of the anemometers is performed under different conditions a correction needs to be made. The correction is calculated using equation E.1 which is the Ideal Gas Law.

$$\rho_{\text{air,corr}} = \frac{MP_{\text{baro}}}{RT} \quad (\text{E.1})$$

Where:

$\rho_{\text{air,corr}}$	Density of air after correction	[kg/m <sup>3</sup> ]
$M$	Molar mass	[kg/mol]
$P_{\text{bar}}$	Barometric pressure	[Pa]
$R$	Gas constant	[J/(molK)]
$T$	Temperature	[K]

Both the temperature and barometric pressure is measured during the calibration. The gas constant is 8.314,5 J/(molK) [Toolbox, 2023a] and the molar mass of atmospheric air is found to be 28.97 g/mol [Toolbox, 2023b]. The reference velocity can be calculated using equation with density correction from equation E.1 and velocity from E.1.

$$v_{\text{ref}} = v_{\text{measured}} \sqrt{\frac{1.2 \text{ kg/m}^3}{\rho_{\text{air,corr}}}} \quad (\text{E.2})$$

Where:

$v_{\text{ref}}$	Reference velocity	[m/s]
$v_{\text{measured}}$	Air velocity from orifice plates	[m/s]
$\rho_{\text{air,corr}}$	Density of air after correction	[kg/m <sup>3</sup> ]

### E.3 Calibration setup

Firstly the barometric pressure is measured as a point value for each anemometer. The measurement is performed during the beginning of each anemometers calibration.

The temperature is measured as a point value for each setting of the jet wind tunnel. Because of uncontrollable variations in the temperature as they are performed in a large laboratory a measurement of the temperature is performed for each new setting on the jet wind tunnel.

The anemometer is placed in the jet wind tunnel. The direction and orientation of the jet wind tunnel and anemometers is important as it will influence the measurements. The anemometers is placed perpendicular to the airflow since the the direction of the air flow is not necessarily known. The orientation of the jet wind tunnel is however important. The jet wind tunnel is orientated vertical. This means that the anemometers have a horizontal orientation.

For the calibration the anemometers the velocity was averaged over a 180 s period. In total 14 measurement points were made in order to calibrate for the full range of the anemometer. A guideline of points was made to ensure a even distribution of measurement points and ensure that the entire range was covered. The guidelines is shown in table E.2.

**Table E.2** Guideline for ensuring calibration of anemometers full range

Orifice plate [mm]	Guideline [mbar]
10	0
10	2
10	8
10	15
10	23
10	62
23	2
23	14
23	30
23	60
46	4
46	8
46	16
46	30
46	max

The guideline refers to the pressure measured with the Debro micromanometer. The measurement is done after the pressure drop across the orifice plate has reached steady-state. The orifice plate is switched according to the guidelines as 62 mbar is near the limit.

## E.4 Results

This section shows the results of the calibration. The calibration graph for one anemometers is selected out to be shown. For each anemometer a calibration file is generated to be used with the corresponding Labview program. The calibration curve is shown on figure E.1

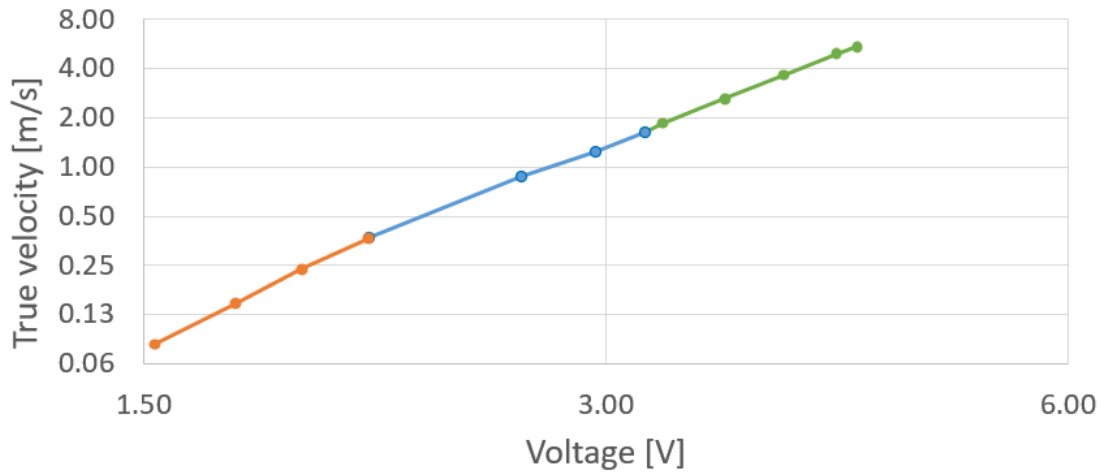


**Figure E.1** Calibration curve for anemometer 11 in channel 11. The colour of points represents the orifice plate, orange is 10 mm, blue is 23 mm and green is 46 mm. The results is shown on logarithmic scale.

## E.5 Validation

A validation of the anemometers is performed to verify that the measurement is correct. The validation is done for six measurement points to find the error of the calibrations. The relative error is shown on figure E.2. On the figure 10 anemometers is shown. All the anemometers have around a 6 % or lower relative error which is deemed acceptable for the measurements. The largest fluctuations are seen at lower velocities where the air flow is in the transitional period between laminar and turbulent flow.

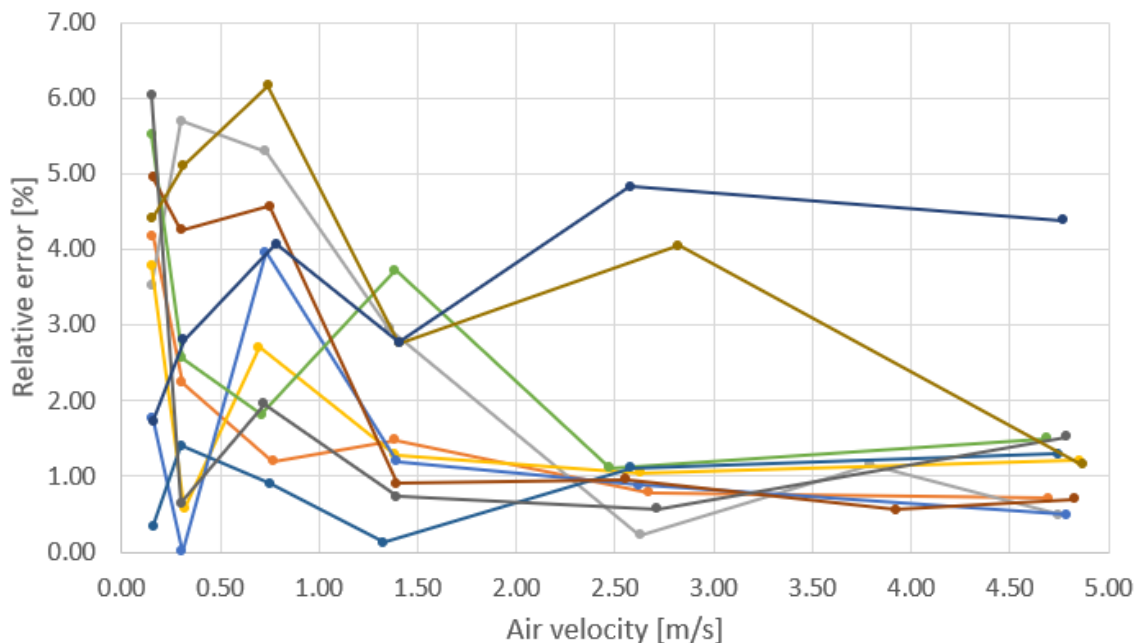


**Figure E.2** Relative error for all anemometers. In total 10 anemometers is shown.

# Calibration of tracer gas monitor and sampler F

---

This appendix revolves around the calibration of the tracer gas monitor and sampler. The appendix is based upon the monitor and samplers technical documentation including field guides[LumaSense, 2016].

The calibration consist of four parts one listing the equipment needed for the calibrations the remaining three are each about a specific calibration. The three calibrations are: zero point calibration, humidity calibration and gas span calibration.

The tracer gas monitor use the Innova software so result of the calibration is kept in the software. This chapter will instead clarify how it was calibrated.

## F.1 Equipment

The following equipment was used for the calibration.

1. 1303 Multipoint Sampler and Doser
2. 1412 Photoacoustic Field Gas-Monitor.
3. 1302 Multi-Gas monitor
4. PC with Innova software 7620 and Windows XP
5. 3 mm Teflon tubing
6. 3-way fitting for tubing
7. Outer filter
8. Flow meter
9. Water bath
10. Clean, dry 100 %  $N_2$  gas
11. 1,000 ppm  $CO_2$  gas
12. 3,000 ppm  $CO_2$  gas

The 1303 Multipoint Sampler and Doser is used to monitor multiple points using the Photoacoustic Field gas-monitor. The sampler can connect up to 6 measuring points with a cable length of 50 m each. The schematic of the sampler can be seen on figure F.1.

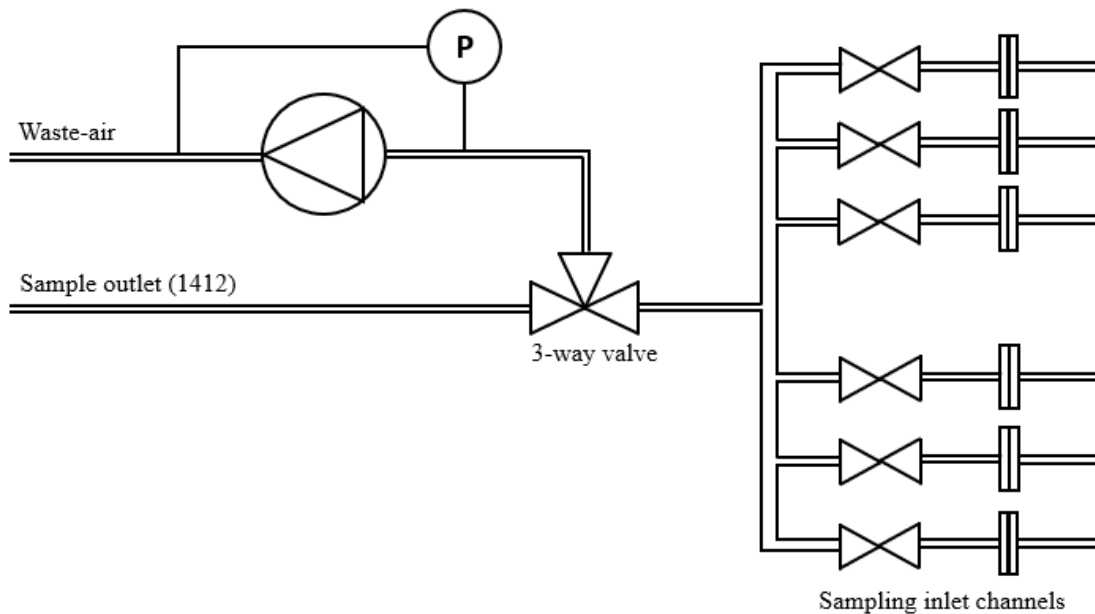


**Figure F.1** The 1303 multipoint sampler [LumaSense, 2008].

The 1412 Photoacoustic Field Gas-Monitor and 1302 Multi-Gas monitor is the equipment that measures the concentration of the tracer gas. Both pieces of equipment uses the same principle for measurements. Two pieces of equipment are calibrated due to problems with the 1412 later on during measurements. A schematic for the Gas-Monitor is shown on figure F.2. It draws air from the sampler by the use of a pump to get a new measurement point and flush out the old measurement. The sample is then led to a sealed analyses cell. Infrared light is then reflected through a chopper, which makes it pulsate, and then through an optical filter. The infrared light that passes through the filter then heats the gas, which equally cools because its pulsating. Because the temperature increase and decrease the pressure of the gas does as well which makes an acoustic signal. Two microphones mounted in the analyses cell this measures the signal which is proportional to the gas concentration. The optical filters change depending on the chosen gas to be monitored in a sample. The analyser has a response time of approximately 13 s up to 26 s if 5 gasses and water vapour is measured. To protect the equipment the system cannot be exposed to a pressure greater than 0.1 bar.

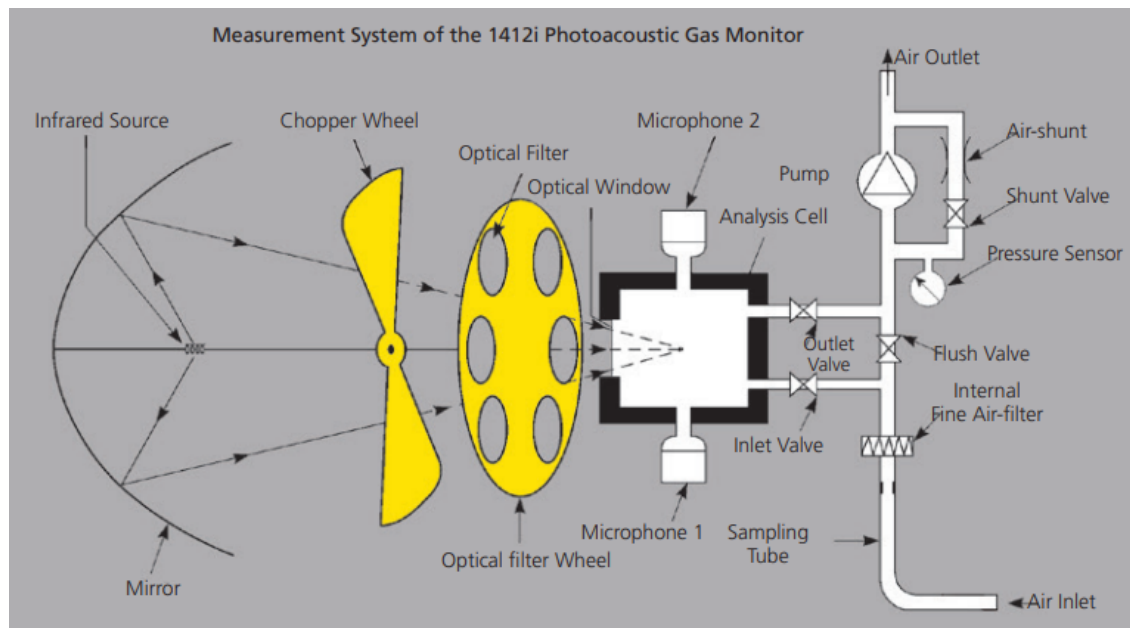


**Figure F.2** The 1412 Photoacoustic Field Gas-Monitor [LumaSense, 2017].

To get data from the measurements and to set up the monitor a PC with Innova software 7620 is needed.

The Teflon tubing is to transport the sample while reducing the absorption of the sample to its environment as much as possible.

The 3-way fitting is needed to attach a flow meter to the setup.

The outer filter is set on each tube that is sampling. The filter is to avoid dust and other particles from influencing the measurements.

The flow meter acts as a safety valve in the system if the pressure gets to high. It also makes it easier to adjust the correct pressure on the gas when doing the calibrations.

The water bath is used during the calibration for humidity. Because all the supplied gas available is dry the humidity of the gas needs to be increased in order perform the calibration.

The dry clean 100 %  $N_2$  gas is used in the zero point calibration. The 1,000 ppm and 3,000 ppm gasses are used for the gas span calibration.

## F.2 Zero point calibration

The zero point calibration is a necessary step and should be done first. The calibration is performed to filter out cell noise and noise from other gasses. The calibration is illustrated on figure F.3. A dry clean 100 %  $N_2$  gas is supplied to the system because we are calibrating for  $CO_2$ . Since there are no  $CO_2$  in the gas any concentration measured for  $CO_2$  is due to noise which can then be compensated for. As discussed earlier the flow meter is an important part of the setup and ensures the safety of the gas monitor and ensures that

the supply of gas is not too low. The "flow ball" in the flow meter should never sit on the bottom nor should it be at the top.

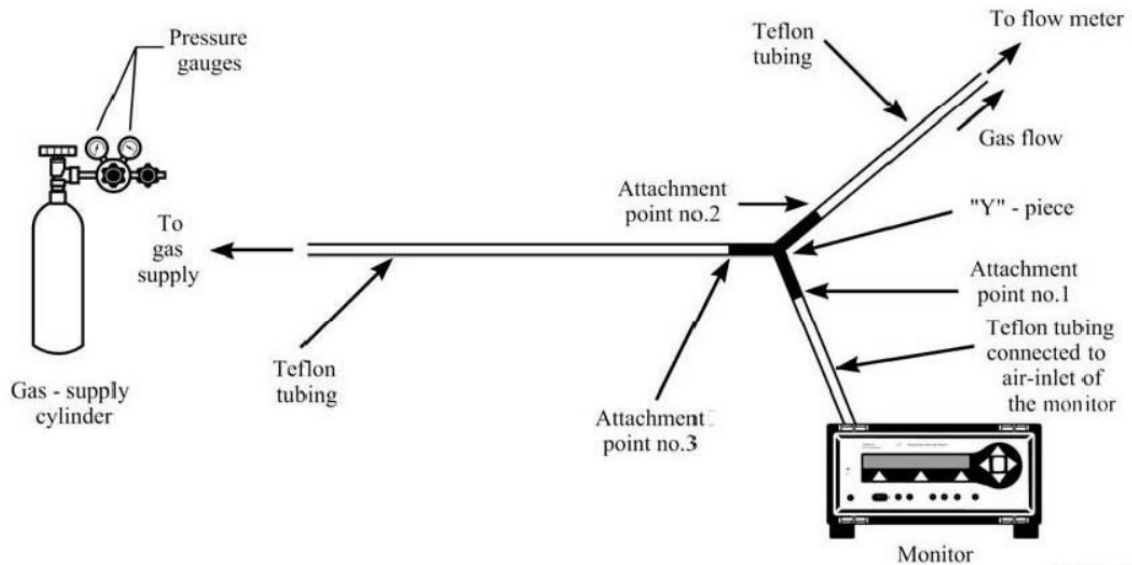


**Figure F.3** The setup for the Zero Point Calibration [LumaSense, 2017].

### F.3 Humidity calibration

The humidity calibration is performed remove any interference that the humidity might have on the measurements. The setup for the calibration is shown on figure F.4. The gas used for this calibration is the same as for the Zero Point Calibration, however the gas has to be wet. To ensure the gas is humidified the gas is filtered through a water bath twice to ensure no water droplets get into the system. It is important that there is no condensation. To ensure this the water bath should be 2 °C lower than the ambient temperature and the gas monitor must be warmed up.

To perform the calibration the software needs the value for the water concentration. The water concentration is found by only having the gas and flow meter connected to the water bath. By measuring the weight of the water before the gas is turned on the total weight absorbed by the gas can be found using the total volume of air found using the flow meter by adjusting the flow of gas to a specific flow rate.

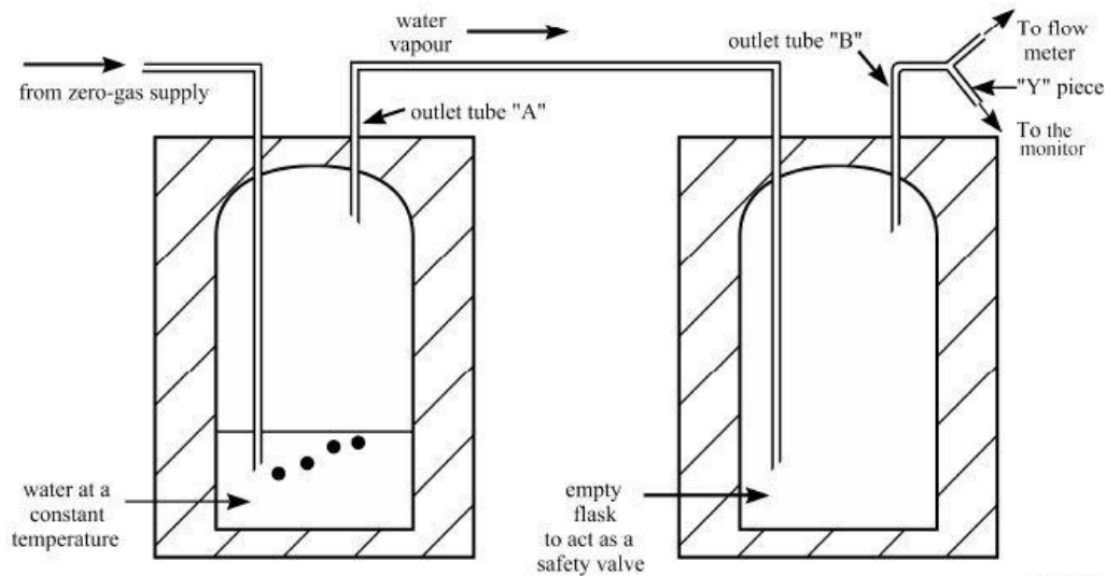
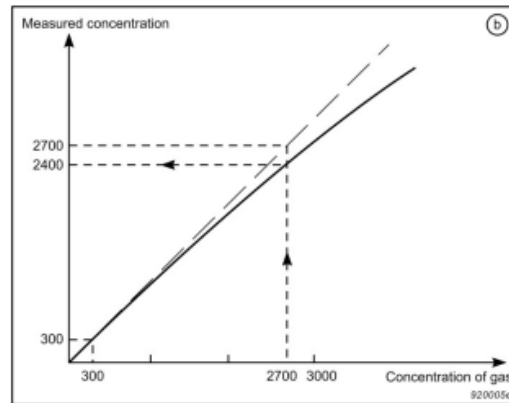


Figure F.4 The setup for the Humidity Calibration [LumaSense, 2017].

## F.4 Gas Span Calibration

The Gas Span Calibration is performed with the same setup as the Zero Point Calibration however the gas is different. Both a single point and two point calibration can be performed. The detection range of the monitor for  $CO_2$  is 1.5 ppm. A single point calibration is enough if the expected concentrations is within  $10^4$  times the detection range, meaning within a concentration of 1.5-15,000 ppm. The range can be expanded to  $10^5$  times the detection range if a two point calibration is performed. The calibration gasses used should be at least 100 times the detection range. The two point calibration requires a "low" and "high" gas in terms of concentration. The "low" gas should be around 10% to 30% of the expected measured gas concentration. The "high" gas should be between 75% and 100% of the expected maximum measured gas concentration. As some measurements are expected to be around or above 40,000 ppm to control the concentration from the coughing machine a two point calibration is appropriate. A two point calibration is however not possible due to limitations in available gas. The laboratory does only have calibration gasses with a concentration of 1,000 ppm and 3,000 ppm. A single point calibration is therefore performed on the 3,000 ppm gas. This influence of this error will increase as the gas concentration increases. The influence should be considered as rather significant when the concentration gets above 15,000 ppm. An example of this is shown on figure F.5 for an unknown gas[LumaSense, 2017].



**Figure F.5** Difference between linear and dynamic calibration curve for optical filters [LumaSense, 2017].

# **Compensation for electrical noise generated by Air Handling Unit**

---



During initial measurements it was found that when the AHU was turned on the temperatures changed rapidly despite the ventilation not being connected and/or the flow was 0. The issue was investigated and it was found to be due to the electrical consumption of the AHU that disturbed the Helios datalogger. To eliminate the noise a compensation was made. The ventilation duct was detached from the room so no air was supplied. Everything except the manikins heating was turned off. The ventilation dampers was also shut to ensure no disturbance of the room. A measurement of the temperature was then made as normal for a 5 min period. The AHU was then turned on and a new measurement of 5 min was done. To ensure that both measurements was for the same conditions the measurement period was kept short. The mean difference between the two measurements was then calculated and used to compensate for the noise. The disturbance is shown in table G.1 for all channels.

**Table G.1** Noise generated by electrical noise for AHU.

Channel	Disturbance [V] [ $10^{-5}$ ]
1	1.735
3	1.815
4	1.807
5	1.719
7	1.767
8	1.815
9	1.857
10	1.769
11	2.477
12	2.514
13	2.675
14	2.529
15	2.360
16	2.526
17	2.504
18	2.381
19	2.781
20	2.610
21	1.045
23	1.089
24	0.964
25	0.919
26	0.973
27	0.896
28	0.979
29	0.991
30	1.034
31	1.438
32	1.614
33	1.493
34	1.458
35	1.502

# Control of tracer gas concentration in initial cough

## H

---

This appendix will detail how the tracer gas concentration was measured for a cough from the coughing machine. The measured concentration is not for a real cough but a cough generated by the coughing machine supplied with 6l/min of pure CO<sub>2</sub>.

### H.1 Methodology

The measurements was performed with the target manikins exhalation turned off to avoid disturbance created by the its breathing function. The room was ventilated to avoid build up of tracer gas to ensure it was the concentration of the flow that was found. The concentration is measured as the main experiments. The same equipment is used and the principle behind the calibration is shown in appendix F.

The concentration are measured at two different points, just outside the pipe, and inside the pipe. The reasoning is to investigate if the measurements just outside the opening are appropriate to measure the concentration. The measurement inside the pipe have a large variance as it was impossible to properly fastened the sampling tube and the tube may therefore have moved during measurements inside the pipe. The difference in maximum concentrations between the two positions was negligible. It measurement point outside the pipe opening is shown on figure H.1 from the side and figure H.2 from the front. The measurement point was in the middle of the flow this was not guaranteed for measurements inside the pipe which may have been a contributing factor to the large variance in those measurements.

The average concentration was calculated for a period of 5 minutes. Measurements of the concentration was observed over a longer period of 15 minutes to ensure stable conditions. The total amount of coughs in this period was 35



**Figure H.1** Measurement point seen from the side



**Figure H.2** Measurement point seen from the front

## H.2 Results

The average concentration was 73,608 ppm which is significantly higher than the 40,000 ppm in normal human exhalation Bjørn [2000]. It is however not possible to lower the tracer gas concentration significantly as the only available pressure gauge fitting the gas canisters has a minimum flow of 5 l/min. However due to the pressure in the tank the flow rate of gas will vary which will affect the concentration in the room. The change in concentration would normally affect the direction of the flow and may in that way create disturbance between measurements. It can however be argued that the exposure should not vary significantly as the concentration of all the sampling points will change accordingly. The measured value however should not be considered a precise value as a two point calibration was not performed the actual concentration will be lower. The reasoning behind this is given in appendix F.

# Control test of exhalation temperature

# I

This appendix will detail how the exhalation temperature was measured as a control value before the experiments described in chapter 1 was performed.

## I.1 Methodology

The control test was performed under the same conditions as the measurements described in chapter 1. For the test a pair of PT100 probes was used and placed immediately at the mouth opening. The PT100 probes was used as the sampling rate made is possible to capture the temperature development during the entire exhalation which was not possible using the Helios datalogger. The sampling rate is 5 Hz. The calibration of the PT100 probes can be found in appendix C. The test was performed for both the manikin and the coughing machine. The measurement location is shown on figure I.1 for the coughing machine and figure I.2 for the manikin.

The temperatures was measured how several hours as the temperature had to stabilise between each adjustment. The temperature average was calculated for a 5 minute period.

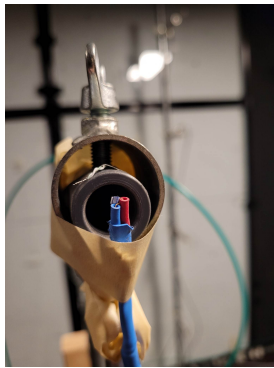


**Figure I.1** Measurement point for the coughing machine



**Figure I.2** Measurement point for the manikin

## I.2 Results

The temperature of the flow generated by the coughing machine was to be the ambient temperature in the laboratory and was thus turned off soon after as to avoid any disturbance on the measurement of the exhalation temperature of the manikin. The manikins exhalation temperature was on average 33.90 °C. The average was taken for

over the all registered temperatures over  $33.55\text{ }^{\circ}\text{C}$ . This ensures that the average found is for the exhalation only. The values used to calculate the average is thus all temperatures above 98 % of the maximum observed temperature which was  $34.23\text{ }^{\circ}\text{C}$ . A graph of the temperature development is shown on figure I.3. The figure shows that the peak is always above  $34\text{ }^{\circ}\text{C}$ .

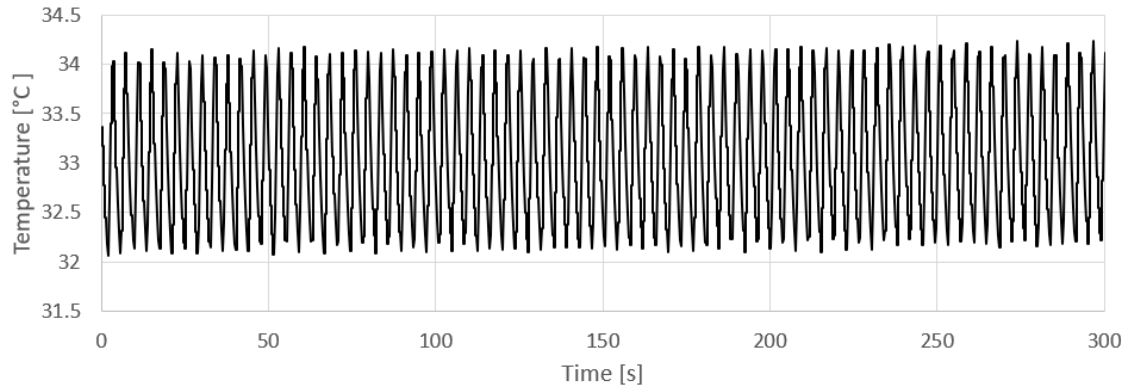


**Figure I.3** Temperature development of the exhalation flow from the manikin.

# Technical drawing of coughing machine



This chapter provides technical drawings of the coughing machine. All measurements are in millimeters.

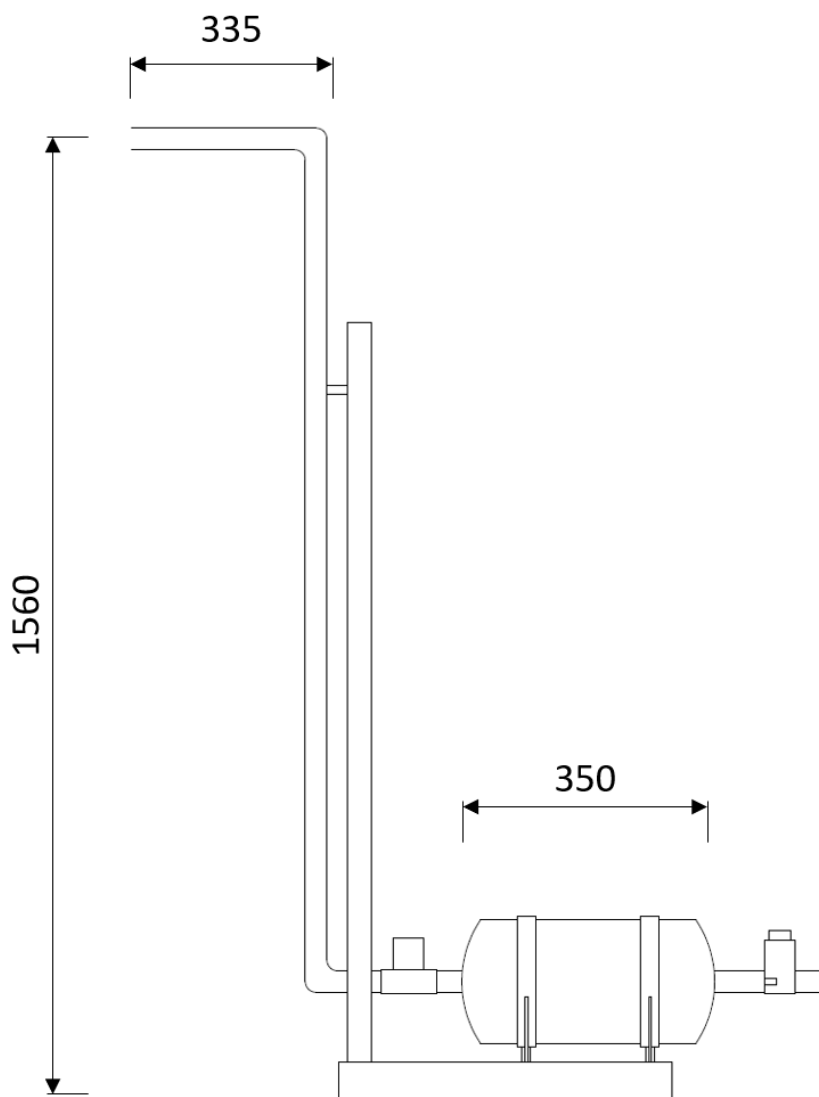


**Figure J.1** Technical drawing of the coughing machine as seen from the side.

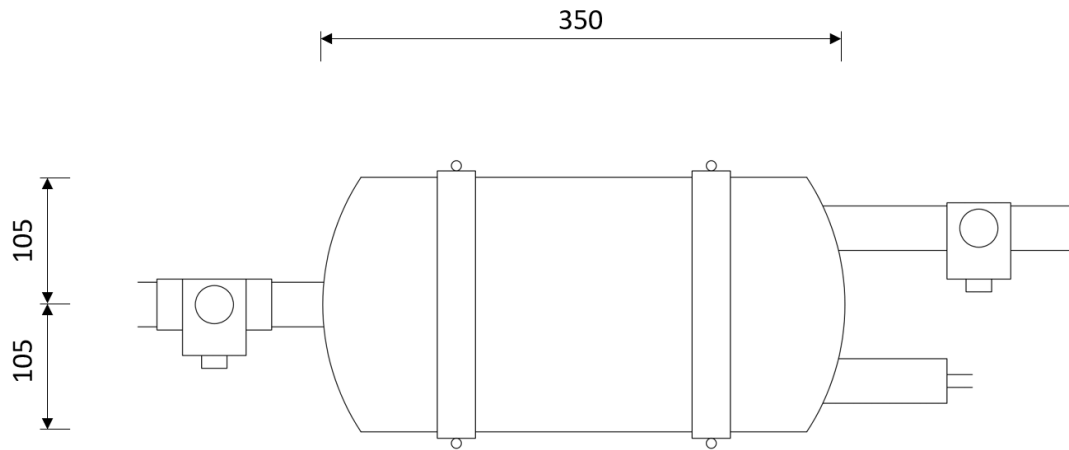


**Figure J.2** Technical drawing of the coughing machine tank.

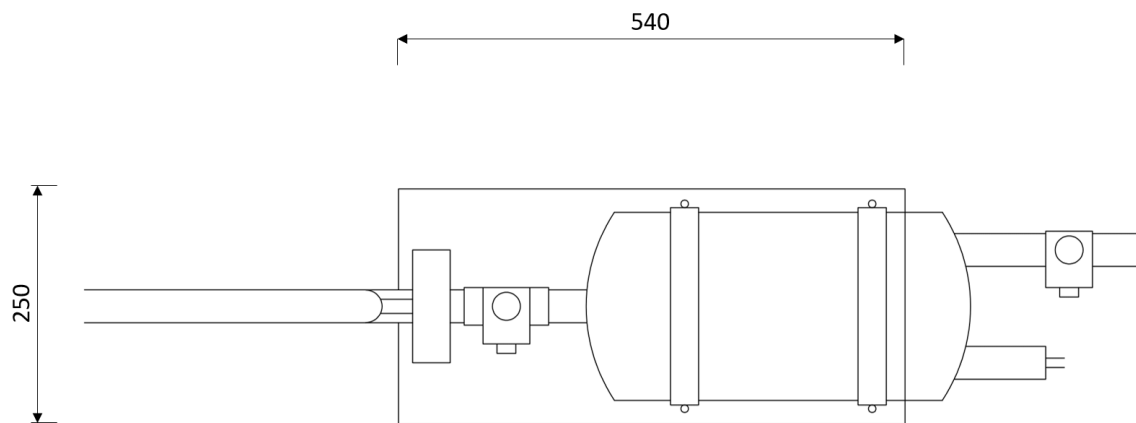


**Figure J.3** Technical drawing of the coughing machine as seen from the top.

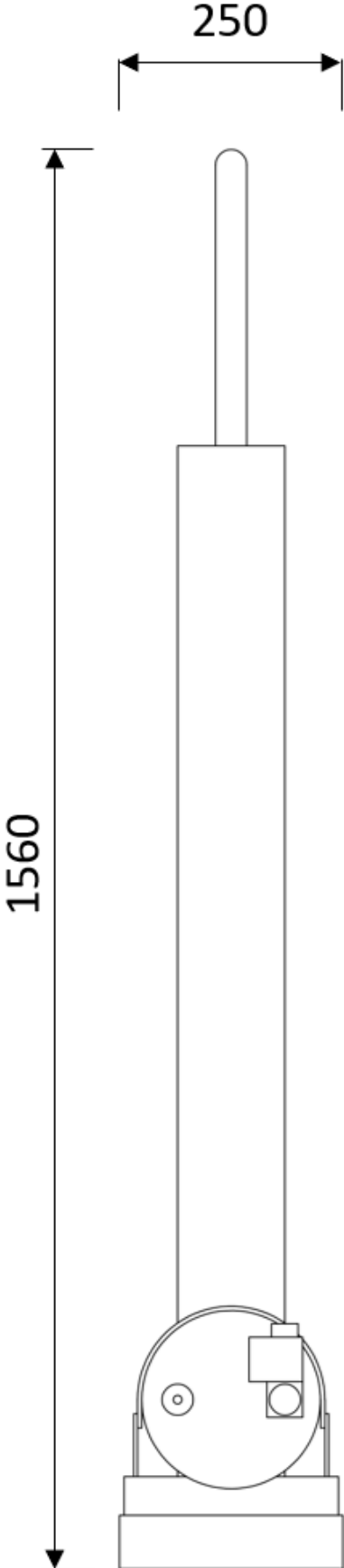
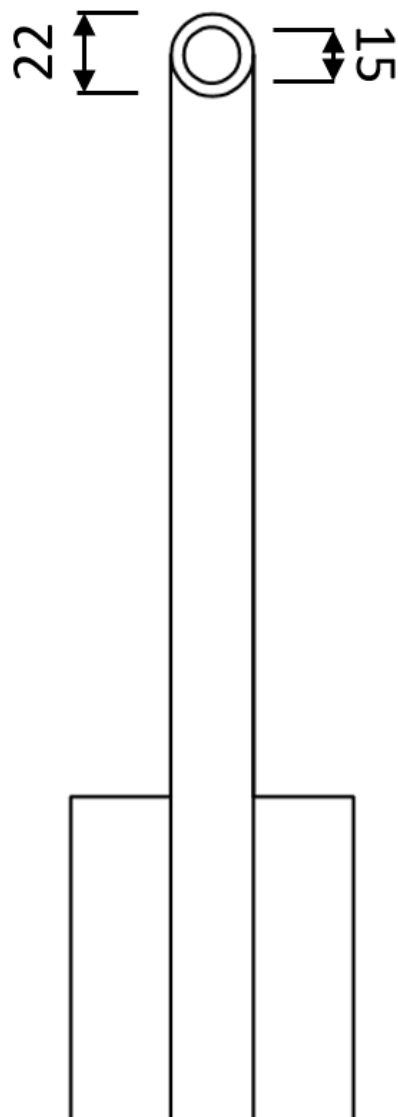


Figure J.4 Technical drawing of the coughing machine as seen from the back.



**Figure J.5** Technical drawing of the coughing machine zoomed in on the mouth opening from as seen from the front.

# Determination of needed measurement period for stable results



This appendix will describe how long the measuring period needs to be for more stable results. The need for a significant measuring period was shown by Nielsen et al. [2011]. The tracer gas measurement have peak and it is important to have a large enough data set so the calculation is precise. If the measuring period is not sufficient the results may be disturbed by the timing of the equipment and respiratory activity. This is shown on figure K.1.

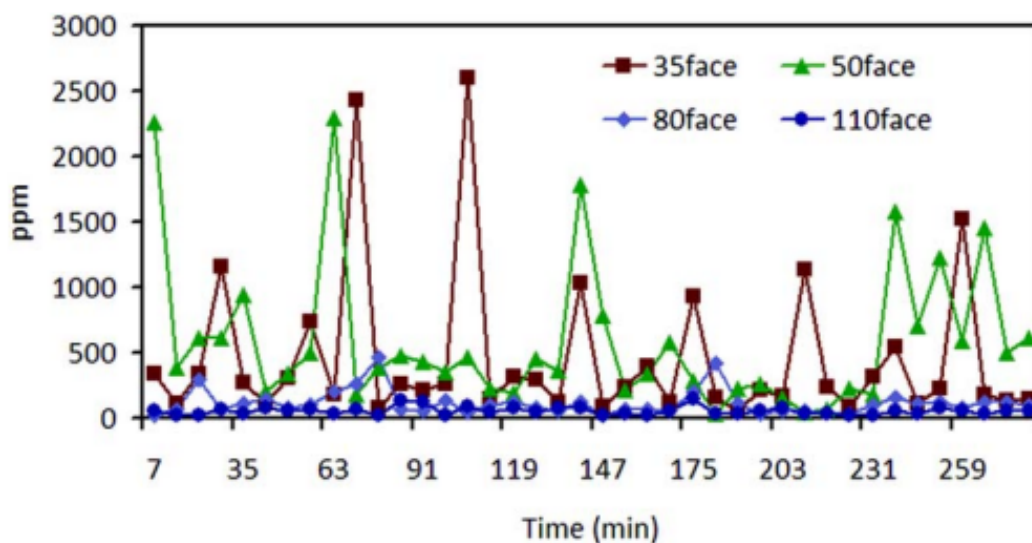


**Figure K.1** Tracer gas data over time. Few peaks affects the calculated average significantly. [Nielsen et al., 2011]

A measurement was done over a 4 hour period to investigate the relative error due to the influence of the peak. For this measurement the average over the entire data set of 4 hours was assumed to be the 'true value'. The relative error was calculated and is shown in figure K.2. The relative error is calculated based upon the exposure. The data shows that after 2 hours the expected error is around 10%. The error is calculated for each channel. The measurement used is at a distance of 1 m. The channel with the largest variance and error was channel 3 which is shown in figure K.2. The other channels had an error of around 5% after 1 hour at the same distance from the coughing machine. It is likely that

which channel is worst changes depending on distance. It is assumed that the channel with largest error are more directly in the flow from the cough.

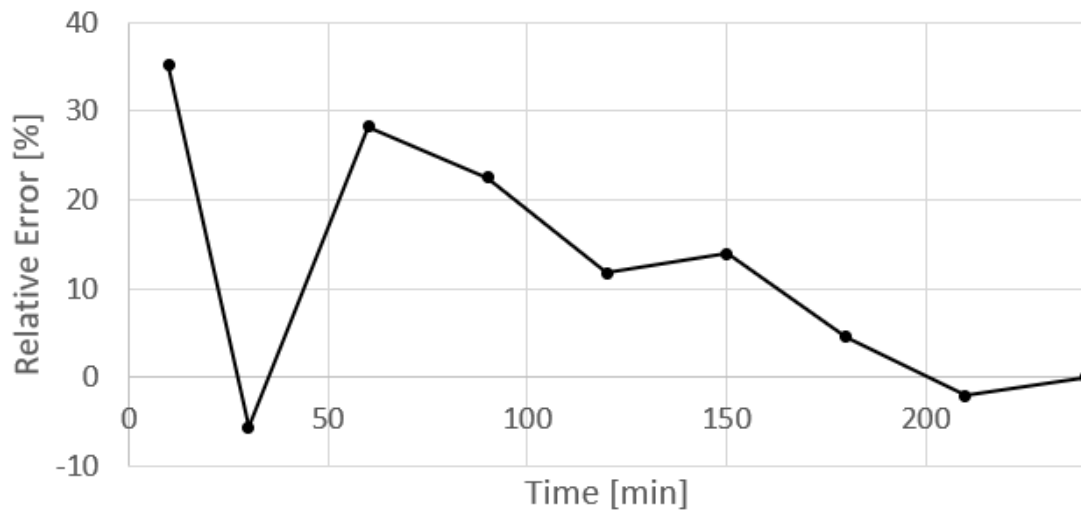


**Figure K.2** The relative error when calculating the exposure based upon a 4 hour measurement period.